AFWAL-TR-86-3091   **AD–A211 086**

MISSILE DATCOM
VOLUME I – FINAL REPORT

STEVEN R. VUKELICH
STAN L. STOY
KEITH A. BURNS
JOSEPH A. CASTILLO
MARVIN E. MOORF

McDonnell Douglas Missile Systems Company

Saint Louis, Missouri 63133

DTIC
ELECTE
JUL 12 1989
S E D

89   7   13
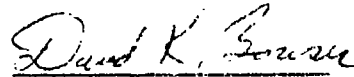
NOTICE

This technical report has been reviewed and is approved for publication.

JERRY E. JENKINS
Project Engineer
Control Dynamics Branch
Flight Control Division

DAVID K. BOWSER, Chief
Control Dynamics Branch
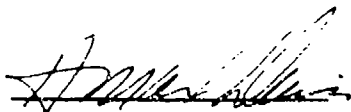Flight Control Division

FOR THE COMMANDER

H. MAX DAVIS, Assistant for
Research and Technology
Flight Control Division
Flight Dynamics Laboratory

REPORT DOCUMENTATION PAGE

1a. REPORT SECURITY CLASSIFICATION UNCLASSIFIED		1b. RESTRICTIVE MARKINGS			
2a. SECURITY CLASSIFICATION AUTHORITY		3. DISTRIBUTION / AVAILABILITY OF REPORT Approved for public release; distribution unlimited.			
2b. DECLASSIFICATION / DOWNGRADING SCHEDULE					
4. PERFORMING ORGANIZATION REPORT NUMBER(S)		5. MONITORING ORGANIZATION REPORT NUMBER(S) AFWAL-TR-86-3091, Vol 1			
6a. NAME OF PERFORMING ORGANIZATION McDonnell Douglas Missile Systems Company	6b OFFICE SYMBOL (If applicable)	7a. NAME OF MONITORING ORGANIZATION Flight Dynamics Laboratory (AFWAL/FIGC) Air Force Wright Aeronautical Laboratories			
6c. ADDRESS (City, State, and ZIP Code) P.O. Box 516 St. Louis, MO 63166		7b ADDRESS (City, State, and ZIP Code) Air Force Systems Command Wright Patterson AFB, OH 45433-6553			
8a. NAME OF FUNDING/SPONSORING ORGANIZATION	8b. OFFICE SYMBOL (if applicable)	9. PROCUREMENT INSTRUMENT IDENTIFICATION NUMBER F33615-81-C-3617			
8c. ADDRESS (City, State, and ZIP Code)		10. SOURCE OF FUNDING NUMBERS			
		PROGRAM ELEMENT NO. 62201F	PROJECT NO. 2403	TASK NO. 05	WORK UNIT ACCESSION NO. 50

11 TITLE (Include Security Classification)

MISSILE DATCOM VOLUME I - FINAL REPORT

12. PERSONAL AUTHOR(S)
S. R. Vukelich, S. L. Stoy, K. A. Burns, J. A. Castillo, M. E. Moore

13a. TYPE OF REPORT Final Technical	13b. TIME COVERED FROM 09/81 TO 12/85	14. DATE OF REPORT (Year, Month, Day) 88 December	15. PAGE COUNT 134

16. SUPPLEMENTARY NOTATION

$(KR) \leftarrow$

17. COSATI CODES			18 SUBJECT TERMS (Continue on reverse if necessary and identify by block number)
FIELD	GROUP	SUB-GROUP	Computer Program Supersonic Missiles
			Subsonic Hypersonic Dynamic Derivatives
			Transonic Aerodynamics Arbitrary Bodies

19 ABSTRACT (Continue on reverse if necessary and identify by block number)

Development of a Missile DATCOM handbook and computer program is described. The type of methods investigated as well as a method selection rationale is discussed. Methods were selected for predicting the aerodynamics of missile configurations made up of circular, elliptic or arbitrary bodies with or without fins and inlets. These methods predict static and dynamic stability derivatives and are suitable for preliminary design. A summary of the comparisons of many results with experimental data is included.

20. DISTRIBUTION / AVAILABILITY OF ABSTRACT ☒ UNCLASSIFIED/UNLIMITED ☐ SAME AS RPT ☐ DTIC USERS	21 ABSTRACT SECURITY CLASSIFICATION UNCLASSIFIED	
22a NAME OF RESPONSIBLE INDIVIDUAL William Blake	22b TELEPHONE (Include Area Code) (513) 255-8485	22c OFFICE SYMBOL AFWAL/FIGC

DD FORM 1473, 84 MAR   83 APR edition may be used until exhausted.   SECURITY CLASSIFICATION OF THIS PAGE
All other editions are obsolete.

PREFACE

This report was prepared for the Flight Dynamics Laboratory of the Air Force Wright Aeronautical Laboratories, Wright-Patterson AFB, Ohio, under Contract F33615-81-C-3617. The work was performed by McDonnell Douglas Astronautics Company, St Louis, Missouri (MDAC-STL), a division of McDonnell Douglas Corporation. The initial development of Missile Datcom was initiated in September 1981 and completed in December 1985. Mr. Jerry E. Jenkins (AFWAL/FIGC) was the Air Force project engineer. Mr. Steven R. Vukelich was the principal investigator for the period September 1981 to February 1985. Mr. Stanley L. Stoy assumed the responsibilities of Principal Investigator in February 1985.

The authors gratefully acknowledge the contributions of the AFWAL/FIGC staff, whose guidance was instrumental for the successful completion of the study. The encouragement and support from numerous professionals from the aerospace community were significant to the effort.

AFWAL is committed to the continuing development of Missile Datcom. This development is dependent to a large extent on user feedback. Questions about the program or suggestions for future improvements to the program should be directed to the current Air Force project engineer, Mr. William Blake, at (513) 255-6764.

Volume I of this report summarizes the method selection philosophy and method selection criteria for the Missile Datcom development program. Volume II is the program User's Manual.

Accession For	
NTIS GRA&I	☒
DTIC TAB	☐
Unannounced	☐
Justification	
By	
Distribution/	
Availability Codes	
Dist	Avail and/or Special
A-1	

iii

TABLE OF CONTENTS

TABLE OF CONTENTS (CONTINUED)

LIST OF ILLUSTRATIONS

LIST OF ILLUSTRATIONS (CONTINUED)

LIST OF TABLES

NOMENCLATURE

SYMBOL	DEFINITION

Lower Case

d	Body diameter
f	Fineness ratio
l	Body length, length
p	Roll rate
q	Pitch rate
r_{eq}	Equivalent radius
x	Longitudinal distance
x_c	Body planform area centroid

Upper Case

A'	Apparent area
AR	Aspect ratio
L_{Ref}	Reference length
M	Mach number
RN	Reynolds number per foot
Sp	Body planform area
S_{Ref}	Reference area

Coefficients

C_A	Axial force coefficient
C_{Af}	Total (average) skin friction coefficient
C_{Ap}	Axial force due to pressure drag
C_{Aw}	Axial force due to wave drag
C_D	Drag coefficient
C_{dc}	Cross flow drag coefficient
C_L	Lift coefficient
C_l	Section lift coefficient
C_m	Pitching moment coefficient
$C_{m\alpha}$	Pitching moment curve-slope
C_N	Normal force coefficient
$C_{N\alpha}$	Normal force-curve-slope
$C_{N\alpha\alpha}$	Second derivative of normal force curve with angle of attack
C_n	Yawing moment coefficient
$C_{n\beta}$	Derivative of yawing moment due to sideslip angle
C_Y	Side force coefficient
$C_{Y\beta}$	Derivative of side force due to sideslip angle
C_{mq}	Pitching moment due to pitch rate
$C_{m\dot{\alpha}}$	Pitching moment due to rate of change of angle of attack

NOMENCLATURE (Continued)

COEFFICIENTS	DEFINITION
C_{Nq}	Normal force due to pitch rate
$C_{N\alpha}$	Normal force due to rate of change of angle of attack
C_{Yp}	Side force due to roll rate
C_{np}	Yawing moment due to roll rate
C_{lp}	Rolling moment due to roll rate

Greek

α	Angle of attack
α_{eq}	Equivalent angle of attack
$\dot{\alpha}$	Rate of change of angle of attack
	Angle of yaw, Mach similarity parameters
δ	Fin deflection/incidence angle
$\dot{\delta}$	fin deflection rate
η	Cross flow drag proportionality factor
ϕ	Roll angle
ϕ'	Aerodynamic bank angle

General Subscript

A	Afterbody
AC	Aerodynamic center
CG	Center of gravity
N	Nose
NT	Newtonian theory
O	Zero lift condition
P	Potential
SB	Slender body theory
V	Viscous

Nondimensional Factors - All forces and moments are nondimensionalized by the free-stream dynamic pressure and the reference area. The reference area is the maximum cross-sectional area of the body. In addition, the moments are nondimensionalized by the body maximum diameter. The reference area and length are constant for both longitudinal and lateral-directional aerodynamic coefficients.

The dynamic derivatives are nondimensionalized by the free-stream dynamic pressure, the reference area and the reference length. In addition, the rate derivatives are non-dimensionalized using the free-stream velocity and the reference length. For example, the dynamic derivative C_{mq} is nondimensionalized using

$$\frac{q L_{ref}}{V_\infty}$$

1.0 INTRODUCTION

This report summarizes the methods selected for use in Missile DATCOM. Since the preliminary design of missiles requires the use of rapid and accurate methods, it became clear from the Feasibility Study (Reference 1) that extremely sophisticated paneling codes would be incompatible with the design environment. Although codes exist which provide the quick and inexpensive tool desired, each has major limitations which reduce design productivity.

Every effort was made to produce a method collection which encompasses a wide range of configuration geometries and flight conditions, however, there remain many areas which cannot be addressed with a preliminary design code. These limitations result from the lack of applicable methodology and are identified throughout this report. The lack of applicable methods may be due to either a lack of any known accurate methods or to a lack of sufficiently simple methods to fit the preliminary design environment.

2.0 METHOD SELECTION PROCEDURE

The methods for Missile DATCOM were selected in four stages:

Stage 1: Feasibility Study methods screening
Stage 2: Development Study preselection
Stage 3: Method incorporation and validation
Stage 4: Method usage in a Handbook or computer code

These four stages permitted a wide range of method types to be evaluated and allowed the methods being evaluated to be selected based upon range of applicability (Stage 1), ease of use and automation (Stage 2), accuracy when compared to experiment (Stage 3), and computational time (Stage 4).

The following paragraphs summarize the types of analysis performed during each stage.

2.1 FEASIBILITY STUDY SCREENING

The purpose of the Feasibility Study (Reference 1) was to:

(a) Determine the range of geometric and flight conditions for which methodology should be specified,

(b) Survey the literature for applicable methodology and determine those areas lacking in appropriate methods and needing further development,

(c) Det.rmine the structure of a Handbook and/or computer program which allows rapid and accurate use of the available methodology in the missile design environment, and

(d) Assess the feasibility, or probability of success, of developing a Missile DATCOM and recommend a Handbook and/or computer program format.

3

The ranges of geometric and flight conditions were determined from analysis of existing experimental data and existing operational missiles worldwide. The results, shown in Figure 1, were categorized by Priority. Priority 1 were the ranges of which at least 75 percent of the configurations and their corresponding flight conditions would be placed; Priority 2 encompasses more than 90 percent of the total configurations studied.

The available methods were assessed using the eight criteria given in Figure 2. Generally, methods were sought which were:

(a) Theoretical or semi-empirical, so that the more "unusual" geometries could be accurately evaluated and, hence, limit empirical data base extrapolations,

(b) Require minimum geometry detail,

(c) Demonstrated to be accurate for the design environment,

(d) Currently used in industry and thought to be good, reliable techniques,

(e) Applicable to a wide range of geometries and flight conditions, and

(f) Generally traceable in origin and compatible with other selected techniques.

After studying more than 315 individual methods, it became clear that component build-up methods were better suited to fulfilling the eight selection criteria. It was also demonstrated that in spite of deficiencies in some areas, sufficient "good" methodology existed to develop a design tool applicable to preliminary design.

A qualitative assessment of the two approaches (component build-up and panel methods) is shown in Figure 3. In general, the cost of using component

PARAMETER	SYMBOL	PRIORITY 1	PRIORITY 2	SOURCE
ANGLE OF ATTACK, DEG.	α	$-20 \leq \alpha \leq 30$	$-180 \leq \alpha \leq 180$	AEROMECHANICS
ANGLE OF YAW, DEG.	β	$-20 \leq \beta \leq 20$	$-180 \leq \beta \leq 180$	SURVEY AND
AERODYNAMIC ROLL, DEG.	ϕ	$0 \leq |\phi| \leq 45$	$0 \leq |\phi| \leq 180$	WORLD'S
MACH NUMBER	M	$0 \leq M \leq 6$	$0 \leq M \leq 10$	MISSILE
BODY FINENESS RATIO	$(l/d)_B$	$6 \leq (l/d)_B \leq 20$	$1 \leq (l/d)_B \leq 30$	SYSTEMS
NOSE FINENESS RATIO	$(l/d)_N$	$.5 \leq (l/d)_N \leq 5$	$0 \leq (l/d)_N \leq 7$	
FIN EXPOSED SPAN TO DIAMETER	b/d	$1 \leq b/d \leq 6$	$0 \leq b/d \leq 10$	
FIN ASPECT RATIO	AR	$0.6 \leq AR \leq 4$	$0.1 \leq AR \leq 10$	
FIN PLANFORM		TRIANGULAR TRAPEZOIDAL	ALL	
WING/TAIL ORIENTATION		IN-LINE	ALL	
CONTROL METHOD		ALL MOVEABLE FIN	ALL	
REYNOLDS NUMBER/FT	R_N	$3 \times 10^5 \leq R_N \leq 2 \times 10^7$	$10^3 \leq R_N \leq 3 \times 10^7$	MACH-ALTITUDE
FIN DEFLECTION/INCIDENCE, DEG.	δ	$0 \leq \delta \leq 30$	$0 \leq \delta \leq 60$	BOUNDARY
ROLL RATE, RAD/SEC.	p	$0 \leq |p| \leq 1$	$0 \leq |p| \leq 8$	MISSILE SYSTEM
PITCH RATE, RAD/SEC.	q	$0 \leq |q| \leq 1.5$	$0 \leq |q| \leq 3$	ANALYSIS
YAW RATE, RAD/SEC.	r	$0 \leq |r| \leq 1.5$	$0 \leq |r| \leq 3$	
FIN DEFLECTION RATE, RAD/SEC.	δ	$0 \leq |\delta| \leq 10$	$0 \leq |\delta| \leq 28$	

FIGURE 1   RANGE OF GEOMETRIC/FLIGHT CONDITIONS

1. METHOD APPROACH

- Theoretical
- Semi-Empirical
- Empirical

2. EFFICIENCY (HANDBOOK, COMPUTER)

- Number Computations
- Complexity of Logic
- Number, Type of Inputs
- Iterative
- Detail of Geometry Required

3. ACCURACY

- Existing Validation
- Compatibility with Accuracy Requirements
- Sensitivity of Output to Input Accuracy
- Derivation Assumptions — Theoretical
- Range of Data — Empirical
- Geometric Model

4. STATUS

- Current Use in Industry
- Handbook Method Available
- Method Coded and Used Locally
- Does it Need Modification
- Is Modification State-of-the-Art

5. RANGE OF APPLICABILITY

- Flight Conditions (Mach, α, β, ϕ)
- Geometry

6. UTILITY OF OUTPUT PARAMETERS

- Compatibility with Other Methods
- Thoroughness

7. GENERAL UTILITY

- Understandability
- Traceability
- Modifiability

8. VALIDATION STATUS

- Existing Validation
- Data Base Available
  to Complete Validation

FIGURE 2 ASSESSMENT CRITERIA

6

	COMPONENT BUILD-UP	PANELING
COST	LOW	HIGH
GEOMETRY	CONVENTIONAL	ARBITRARY
ACCURACY	GOOD	VARIES
PARAMETRICS	EASY	DIFFICULT
TEST DATA USE	YES	NO
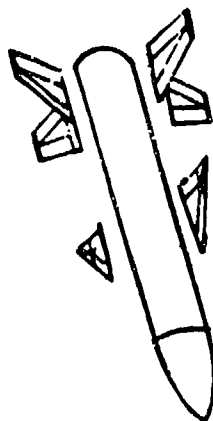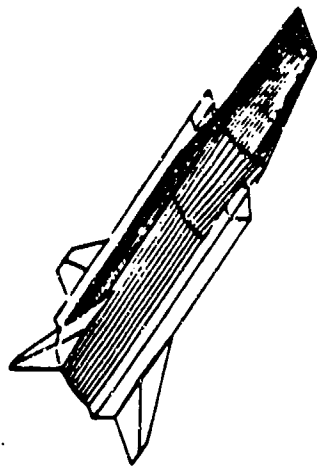
✔ COMPONENT BUILD-UP MORE VERSATILE, COST EFFECTIVE

FIGURE 3 APPROACHES TO AERODYNAMIC PREDICTION

7

build-up methods are far less than panel type methods, due to the increase in required configuration detail for panel methods. Although computer costs can be a factor in selection, the cost in labor hours is far more significant; paneling codes can require as much as ten times more labor for the same configuration shape.

Paneling-type methods are better suited for more arbitrary configurations. The majority of component build-up methods have been developed for conventional missile shapes (circular or elliptical bodies with straight-tapered fins, and planar or cruciform fin arrangements. Component build-up methods are fairly accurate for conventional configurations and easily lend themselves to parametric analysis. For these reasons and because most near term missiles will continue to have conventional shapes, component build-up methods are the best choice. Another plus is that with the build-up approach it is easier to substitute experimental data which allows for more detailed analysis.

The development of Missile DATCOM was found to be feasible and methodology available to perform preliminary or conceptual missile design. No comprehensive collection of missile design methods is available, and the assembly of a methods Handbook would fill this important void.

Existing computer programs were available, but were often limited in applicability, poorly programmed, too complex, or substantially undocumented. To overcome these problems, Missile DATCOM was to be developed as follows:

(a) A Handbook and its companion computer program were to be developed in parallel. The Handbook would include: (1) a brief but thorough discussion of the physical phenomena being modeled, (2) a description of the selected method, including all equations, tables, and charts necessary for its use, and (3) a bibliography.

8

(b) The computer program, developed concurrently with the Handbook, would reflect, as a minimum, the same capability as the Handbook. The program was to be written with the following characteristics: (1) to conform with American National Standards Institute (ANSI) standard FORTRAN language for ease of use on a wide variety of computer systems, (2) structured code using the concept of structured programming for code readability, (3) liberal internal documentation to aid code development and increase its utility, (4) modular method subroutines, so that they can be easily exchanged for better techniques in the future without the need for extensive code revisions, (5) inputs were to be structured to minimize the number and type of inputs required, (6) designed to minimize computer execution time and memory, and (7) a User's Manual which defines the inputs required and the outputs available.

2.2 DEVELOPMENT STUDY PRESELECTION

In many cases, the Feasibility Study showed that more than one technique was available to compute a particular aerodynamic parameter. Hence, it was necessary to select one for use. One way of accomplishing this task was the use of a methods development tree where the assumptions made in deriving the techniques could be directly compared, and a method with the least simplifying assumptions could be given more weight in the selection process.

Preselection also considered the currently available status of the methods. Since the primary analysis tool was expected to be the computer code, the availability of a well coded and documented procedure was important for overall development efficiency and future code maintenance.

2.3 METHOD INCORPORATION AND VALIDATION

This third stage of method selection is meant to automate the selected methods, verify they provide accurate results, and then compare their accuracy to experimental data or theory, whichever is most appropriate. In many cases

the selected methods already existed in automated form, making conversion into the Missile DATCOM code simply one of interfacing the inputs and outputs. In other cases, new code had to be written.

Whenever computer code is used to represent an analytical technique, it typically takes months of testing to reduce programming error. In order to shorten the time needed to make this code operational, a "Top-Down Design" and "Structured Programming" technique was used. In addition, to make the code as transportable between machines as possible, ANSI standard FORTRAN-66 language (ABSI X38,01966) was selected.

The concept of "Top-Down Design" means that the code is designed in a tree structure, where the main program is the root, and each task is assigned to a separate branch. Each branch, or task, is independent of others; that is, the type of method incorporated has no bearing on the type of method selected for other tasks in the system. Hence, individual methods can be replaced at will without influencing the remainder of the code. The basic tree structure of the code is illustrated in Figure 4. A significant by-product of this tree structure is well defined tasks which can be overlayed to reduce the needed computer core required for execution.

The second concept, Structured Programming, defines the way the code is to be written, with emphasis on internal documentation. A large number of comment cards are incorporated in the program to determine the logic and func-ional processes.

Both concepts resulted in the successful development of the code. Over 40,000 lines of code were implemented in less than three years, with few maintenance tasks identified. As mentioned earlier, a method must be verified as being coded correctly before its accu ay can be correctly determined. This was performed by parametrically varying the method Subroutine inputs and plot-ting the outputs as a function of the parametric variable. By comparing these results with theory, or experiment, each method was verified as being an analytical model of the method selected.
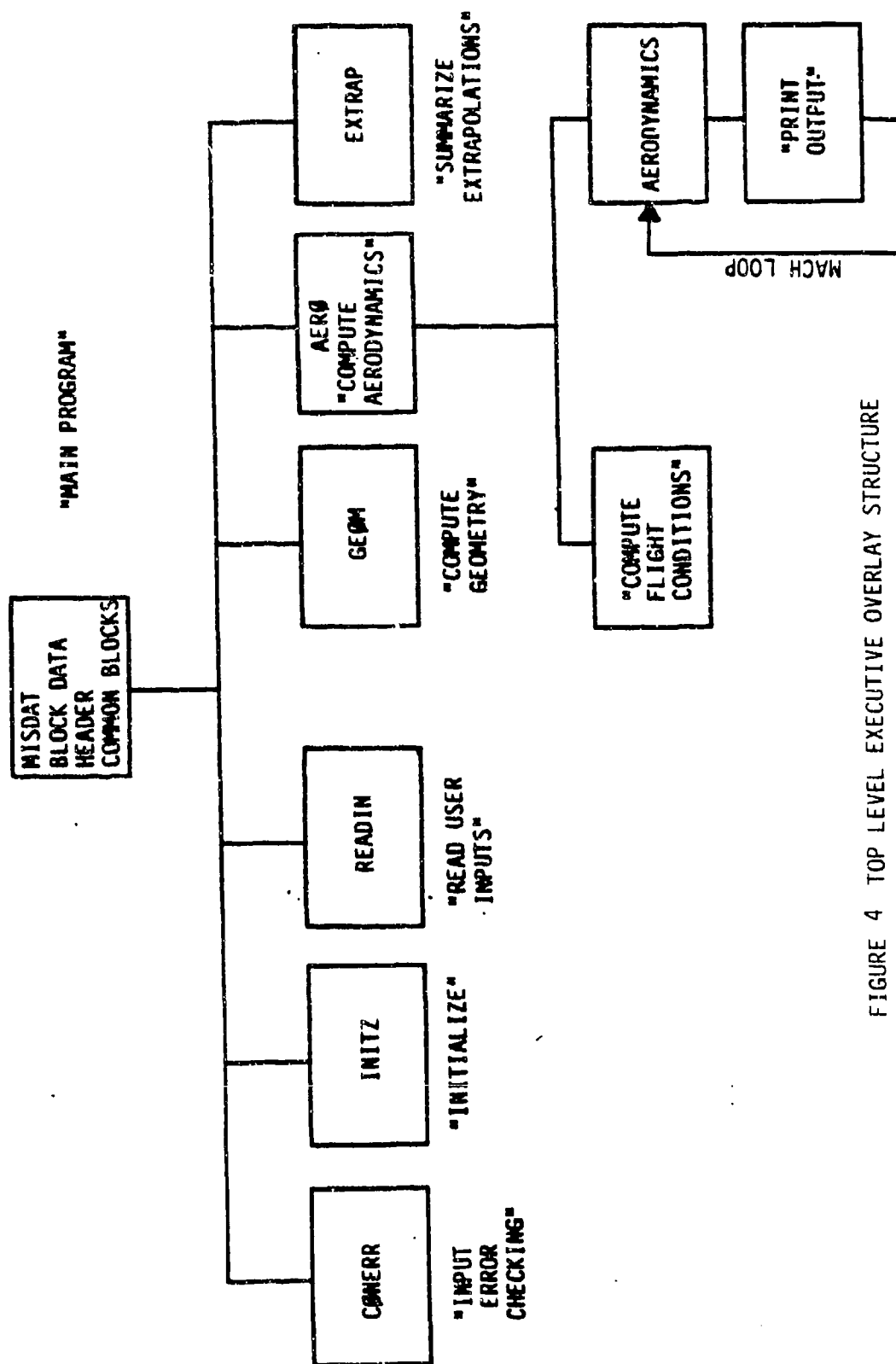
FIGURE 4 TOP LEVEL EXECUTIVE OVERLAY STRUCTURE

11

To evaluate the accuracy of the individual methods an accepted accuracy criteria was employed. The accuracy criteria selected was the one developed by Krieger and Williams (Reference 2). It is based on the idea that the accuracy to which an aerodynamic coefficient needs to be predicted should be a function of what the coefficient is going to be used to compute. If it is used to compute obtainable load factor then it may not be required to be as accurate as if it was being used to compute the range. Therefore, the uses to be made of the different aerodynamic coefficients must be determined followed by a determination of accuracy required for the performance parameters. The accuracy required in the prediction of the aerodynamic coefficients is then backed out of the equations for the performance parameters. This process is outlined for the longitudinal coefficients C_N, C_m and C_A in Figure 5. From this accuracy criteria it is found that it is acceptable to predict C_N and C_m within ± 20 percent while C_A is often required to be predicted to within ± 10 percent. Application of this method allowed for a quantitative assessment of the accuracy of the individual methods.

In addition to individual method accuracy, it was necessary to insure that they were compatible as a function of Mach number. As illustrated in Figure 6, it was desirable that there be no predictive discontinuities at the limits of method applicability. Even though this was not practical, the differences at method switchover were kept at a minimum. Method switchover occurred at the following conditions:

CONFIGURATION	MACH NUMBER	COEFFICIENTS
BODY	1.2	ALL
	2.0	ALL
FINS	0.8	ALL
	1.4	ALL

The reasons for the switchover are defined in the method selections described in Section 3 and Section 4.

12

DESIGN PARAMETER	ERROR ALLOWED
RANGE	± 10%
TURN RADIUS	± 20%
TURN RATE	± 20%
LOAD FACTOR	± 20%
SPECIFIC EXCESS POWER	± 100 FPS
FIN PANEL AREA	± 20%
MANEUVER DECELERATION	± 20%
CRUISE ALTITUDE	± 1000 FT
RESPONSE TIME	± 20%
CENTER OF GRAVITY	± 2% BODY LENGTH
STATIC STABILITY/ CROSS COUPLING PARAMETERS	± 25%

COEFFICIENT	ERROR ALLOWED	DESIGN PARAMETER
C_N	± 20%	RANGE, LOAD FACTOR
C_m	± 20% OR ± 2% L	FIN SIZE OR STATIC MARGIN
C_A	± 10% OR ± .2 C_D/($C_A \cos \alpha$)	COAST RANGE OR TURN DECELERATION

FIGURE 5   DERIVATION OF ACCURACY CRITERIA
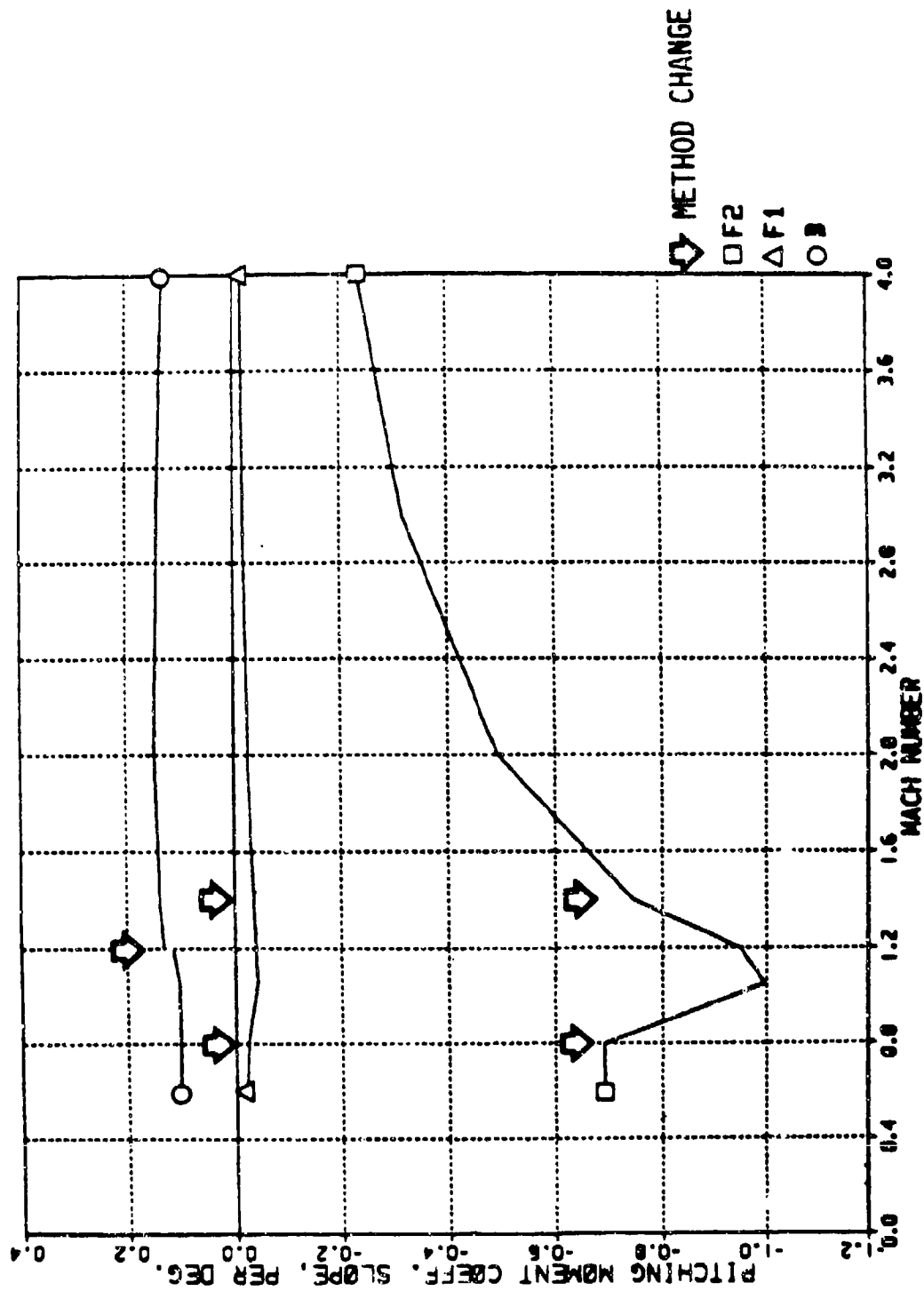
FIGURE 6 MACH SWEEP CHECKS METHODS COMPATIBILITY

14

2.4 CODE AND HANDBOOK METHOD SELECTION

The goals for the Missile DATCOM program were to have the computer code and the Handbook complement each other, yet be independent so that either could be used without requiring the use of the other. In some cases, the "best" methodology could be efficiently used on computer equipment and not be easily solved by hand in a methods Handbook. It would have been possible to use the code to generate Handbook design charts, which was ultimately done for the skin friction calculation method, but this approach was avoided since it does not lend itself to a thorough understanding of the method. By avoiding this, the Handbook and code methods are independent checks of one another, and in some instances are from different method sources, so the methods in the Handbook could be kept as simple as possible.

Where there are method differences between the Handbook and the computer code, those differences are described in the method description sections of this report.

3.0 BODY ALONE METHOD SELECTIONS

This section summarizes the methods selected for body alone aerodynamics. It is divided into two sections: bodies with circular cross sections (axisymmetric bodies) and bodies with noncircular cross sections. Each section is further subdivided by aerodynamic coefficient.

It should be noted that a significant number of "easy to apply" methods for noncircular bodies have been used for bodies with elliptically-shaped cross sections. Although methods can be extended to handle more arbitrary shapes, this has not been done due to the limited amount of information available for extending these techniques. The method used in the computer code for bodies with arbitrary cross sections is numerically intensive, therefore no hand calculation methods are presented.

3.1 BODIES WITH CIRCULAR CROSS SECTIONS

This section summarizes the body alone methods investigated for inclusion into the Missile DATCOM methods compendium. Approximately 108 individual methods were identified during the Missile DATCOM Feasibility Study as either recommendations or alternates

Method selection began with the Feasibility Study results. Each of the recommended techniques were again studied using the assessment criteria shown in Figure 2. The final selections are given in Figure 7, and a summary comparison with the Feasibility Study recommendations is given in Table 1. In nearly all cases, the Feasibility Study recommendations were the final method selections.

As shown in Figure 8, component build-up methods remain questionable for some configurations. For example, the subsonic/transonic axisymmetric methods included are only applicable to conical or tangent ogive nose shapes attached to cylindrical bodies, whose lengths are at least six body diameters. The reasons for the configuration limitations are as follows:

17

	SUBSONIC	TRANSONIC	SUPERSONIC
	$M < 0.8$	$0.8 \leq M \leq 1.2$	$M > 1.2$
C_{N_α} (NOSE-CYLINDER) c_{m_a}	MBB TN WE 2-97/69 AND WE 12-88/70 ▲ (20)		
C_{N_α} (BOATTAILS) c_{m_a}	NSWC TR-81 156 ▲ (21)		NSWC TR-81-156 (HYBRID/SOSE)
C_{N_α} (FLARES) c_{m_a}	AMCP 70x 280 ▲ (13)		(21)
η	"MODERN DEVELOPMENTS IN FLUID DYNAMICS" (GOLDSTEIN) ▲ (22)	AEDC TR-75-124 ▲ (23)	(VALUE OF UNITY ASSUMED) (15)
c_{d_c}	NASA TN-D-6986 AND AEDC TR-75-124 ▲ (23,18)		
SKIN FRICTION	BLASIUS + TRANSITION ▲ + VAN DRIEST II (4,5,3)		
PRESSURE DRAG - NOSE-CYLINDER	"FLUID DYNAMIC DRAG" (HOERNER) (6)		
PRESSURE DRAG - BOATTAILS	DTNSRDC/ASED-80/10 ▲ (11)		(NOT APPLICABLE)
PRESSURE DRAG - FLARES	AMCP 706-280 ▲ (13)		
WAVE DRAG NOSE - CYLINDER	(NOT APPLICABLE)	NSWC TR-80-346 (8)	NSWC TR-81-156 (HYBRID/SOSE)
WAVE DRAG - BOATTAILS		DTNSRDC/ASED-80/10 ▲ (11)	
WAVE DRAG - FLARES		AMCP 706-280 ▲ (13)	(21)
BASE DRAG CYLINDERS	NASA TR-R100 ▲ (14)		
BASE DRAG - BOATTAILS	NSWC TR-81-156 ▲ (21)		
BASE DRAG - FLARES	AMCP 706-280 ▲ (13)		

▲ EMPIRICAL METHOD
( ) REF. NUMBER

FIGURE 7 AXISYMMETRIC BODY ALONE AERODYNAMICS

TABLE 1 BODY ALONE METHODS

	FEASIBILITY RECOMMENDATION	METHOD SELECTED	REASON FOR CHANGE
C_{A_f}	Van Driest II (Ref. 3)	Van Driest II	(No change)
C_{A_p}	Hoerner (form factor)(Ref. 5)	Hoerner (form factor)	(No change)
$C_{A_{P,W}}$ (nose-cylinder)	Chaussee (ogives) (Ref. 7) MDAC-HB (cones)(Ref. 24)	Devan (ogives)(Ref. 8) Devan (cones)(Ref. 8)	Better accuracy Data Proprietary
C_{A_W} (nose-cylinder)	SOSE (Ref. 25)	Modified SOSE(Ref. 21) Van Dyke Hybrid	Better accuracy Better at low supersonic speeds
$C_{A_{P,W}}$ (boattails)	Payne correlation (Ref. 11)	Payne correlation	(No change)
C_{A_W} (boattails)	SOSE	Modified SOSE Van Dyke Hybrid	Better accuracy Better at low supersonic speeds
$C_{A_{P,W}}$ (flares)	(Not identified)	AMCP-706-280	Only available method
C_{A_b}	NACA-TN-3819	NASA-TR-R100 (AMCP-706-280)	Previously automated
$C_{A_{jet}}$	Payne method (Ref. 26)	(None)	Insufficient data to quantify
$C_{A_{protuberance}}$	Hoerner	(None)	Too general, not automated
$C_{A(\alpha)}$	Allen and Perkins(Ref. 27)	Allen and Perkins	(No change)

19

TABLE 1 (CONTINUED)

	FEASIBILITY RECOMMENDATION	METHOD SELECTED	REASON FOR CHANGE
C_{N_α}, C_{m_α} (subsonic/transonic)	Baker, Klopfer/Chausse (Ref. 23, 28)	MBB[1] (Ref. 20)	Wider range of fineness ratios
C_{N_α}, C_{m_α} (supersonic)	SOSE	Modified SOSE Van Dyke Hybrid	Better accuracy Better at low supersonic speeds
C_{N_α} (boattails, subsonic/transonic)	Moore (Ref. 21)	Moore	(No change)
C_{N_α} (flares, subsonic/transonic)	(Not identified)	AMCP-706-280	Only available method
η	Goldstein, Baker(Ref. 22, 23)	Goldstein, Baker	(No change)
C_{d_C}	Baker (Ref. 23)	Baker (w/corrections) (Ref. 23, 15)	Better accuracy

1 Messersmitt-Bölkow-Blohm

	SUBSONIC M $\leqslant$ 0.8	TRANSONIC 0.8 $<$ M $\leqslant$ 1.2	SUPERSONIC M $\geqslant$ 1.2
NOSE SHAPE			
CONE	$\checkmark$	$\checkmark$	$\checkmark$
TANGENT OGIVES	$\checkmark$	$\checkmark$	$\checkmark$
OTHER	?	?	$\checkmark$
NOSE BLUNTNESS			
SHARP	$\checkmark$, ?[1]	$\checkmark$, ?[1]	$\checkmark$
SPHERICAL BLUNTNESS	?[1]	?[1]	$\checkmark$
TRUNCATED	X	X	$\checkmark$
OTHER	X	X	$\checkmark$
CONFIGURATION			
NOSE – CYLINDER	$\checkmark$	$\checkmark$	$\checkmark$
NOSE – BOATTAIL	?	?	$\checkmark$
NOSE – FLARE	?	?	$\checkmark$
NOSE – CYLINDER – BOATTAIL	$\checkmark$	$\checkmark$	$\checkmark$
NOSE – CYLINDER FLARE	?	?	$\checkmark$
FINENESS RATIO			
2 $\leqslant$ ℓ/d $\leqslant$ 28	$\checkmark$	$\checkmark$	$\checkmark$
ANGLE OF ATTACK			
$0 \leqslant \alpha \leqslant$ 30	$\checkmark$	$\checkmark$	$\checkmark$

$\checkmark$ APPLICATION SUITABLE
? APPLICATION QUESTIONABLE/LIMITED
X DOES NOT APPLY

1 TANGENT OGIVES: $\checkmark$

FIGURE 8   COMPONENT BUILD-UP APPLICABILITY

(a) In the subsonic and transonic Mach regimes no easy to apply method is available to analyze general nose shape contours. Although design charts exist for selected nose shapes, the methods require substantial input description and user intervention. Therefore they are not included in the Missile DATCOM code. Parametric results in the form of design charts have not been published and are therefore unavailable for incorporation.

(b) Methods to compute the effect of spherical nose bluntness is only available for C_A at zero angle of attack. The blunted cone method used is weak. (Design charts are available for blunted cones, but are not in the public domain.)

(c) Elliptically shaped nose bluntness was not addressed in any literature sources searched.

21

(d) The extreme dependency of the nose flow field on the afterbody for short cylindrical afterbodies prohibits the generalization of a method for arbitrary afterbody shape or nose-flare geometries.

(e) The existing flare methodology at subsonic and transonic speeds is limited to conical flares whose surface slope angle is small.

The following paragraphs detail each of the aerodynamic coefficient methods selected and their limitations.

3.1.1 Axial Force Coefficient

In general, the methods recommended during the Feasibility Study were found to be acceptable during method selection. Each of the following paragraphs summarize the results observed during the method implementation and validation.

3.1.1.1 <u>Skin Friction</u> – The method of Van Driest (referred to as Van Driest II) was found to produce acceptable skin friction drag characteristics for turbulent boundary layers at all speeds (Reference 3). The method of Blasius, for laminar boundary layers, and the MDAC method for laminar boundary layer transition completed the scope of the skin friction calculations (References 4 and 5 respectively). Since skin friction is difficult to extract from a majority of experimental results for bodies, the absolute magnitude of the method's predictive accuracy cannot be determined. However, based upon total drag comparisons with experimental data, it was deduced that the skin friction calculations are quite adequate for preliminary design purposes.

Since the Van Driest II method is iterative, it cannot be easily computed by hand using a methods handbook. However, since it includes the effects of wall temperature, Mach number, Reynolds number, and surface roughness it far surpasses the available simple techniques. Hence, the production of design charts for the methods handbook was considered the best compromise; an example is shown in Figure 9. In the computer code the free stream temperature is used as the wall temperature.

22
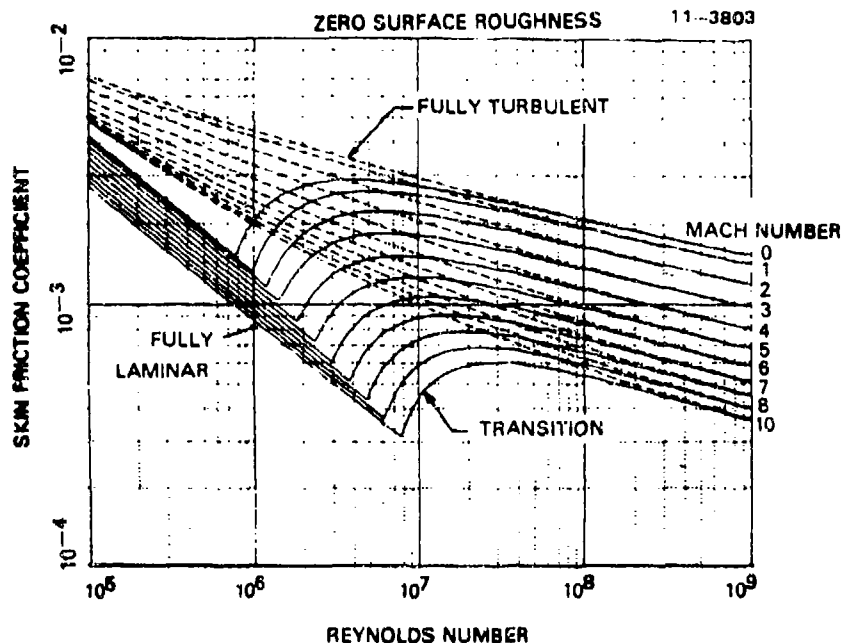
FIGURE 9   SKIN FRICTION METHOD RESULTS

3.1.1.2 **Subsonic Pressure Drag** - The method of Hoerner, which correlates pressure drag to skin friction drag was retained from the Feasibility Study results (Reference 6). There were no subsonic (Mach numbers less than 0.6) predictive comparisons which demonstrated that this approach is inappropriate.

3.1.1.3 **Transonic Pressure/Wave Drag** - For ogive-cylinder configurations the method of Chaussee (Reference 7) was initially selected because of its basis in transonic flow theory. However, after the Feasibility Study was completed, it was determined that the Chaussee results were substantially in error for selected nose fineness ratio combinations. These discrepancies were corrected by Devan (Reference 8) and form the basis of the final method selected. Comparison with experiment has shown that this technique gives excellent results (Figure 10), although it was required to be coded as a multivariable table lookup. The original Lagrange interpolation was replaced with a linear interpolation to reduce interpolation error.

23
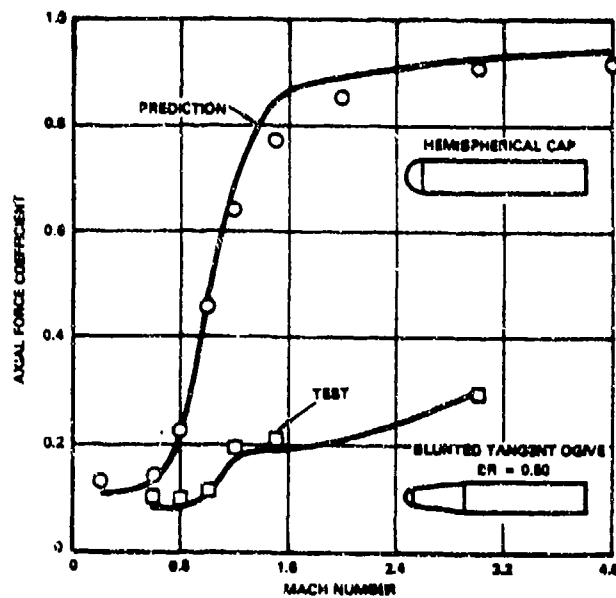
FIGURE 10   SPHERICALLY BLUNTED NOSE DRAG RESULTS
USING DEVAN'S METHOD

The recommended approach for cone-cylinder pressure/wave drag was develop-
ed by MDAC.   It covered a wide range of cone fineness ratios and nose blunt-
ness ratios.   Although this technique is probably one of the better approach-
es, the method is considered propietary and was not used.   The alternative
approach was one derived by Devan from experimental observations, which indi-
cated a very small effect of nose bluntness. Since this approach is not en-
tirely accurate, nor does it cover a sufficiently wide range of nose fineness
ratios, it is recommended that it be replaced with a better technique when
available.   The coded method's limitations are summarized in Figure 11.

3.1.1.4   Supersonic Wave Drag - Two techniques were selected for body wave
drag, the Modified Second Order Shock Expansion (SOSE) method of DeJarnette
(Reference 9), and the Van Dyke hybrid theory method as automated by NSWC for
the Aeroprediction Code (Reference 10).   Both techniques were selected so that
the entire supersonic Mach regime could be adequately covered.

24

TRANSONIC SPEEDS

OGIVES

BLUNTNESS IGNORED
$0.5 \leq L_N \leq 3.5$
$6 \leq L_C \leq 20$

BLUNTNESS ACCOUNTED FOR
USING RAXBOD/EULER CODE
$0.5 \leq L_N \leq 5$

CONES
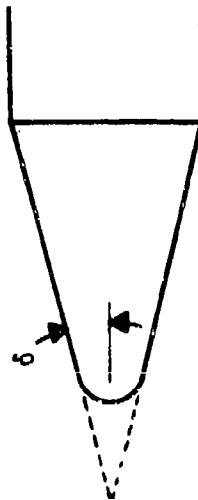
BLUNTNESS IGNORED
$0 \leq L_N \leq 2.5$
$6 \leq L_C \leq 15$

BLUNTNESS IGNORED
(VALID FOR MODERATE BLUNTNESS)
$0 \leq \delta \leq 25$ DEG.

C_N, C_M:

C_A:

FIGURE 11 NOSE-CYLINDER GEOMETRY LIMITATIONS

25

At Mach numbers below approximately 2.0, there is a tendency for SOSE to overpredict wave drag by approximately 20 percent (See Figure 12). Since this approach models geometry as a series of cone frustrums, this type of error can be expected at low supersonic speeds for some shapes. At a Mach number of approximately 1.4 or less, the SOSE code will compute subsonic flow behind the shock, with large nose tip pressures being a result; hence, the axial force will climb to extremely high values. The flow expands to supersonic speeds with no noticeable effect on C_N and C_m curve slope near zero angle of attack.

To avoid this problem at low supersonic speeds, the Van Dyke Hybrid method was incorporated. Its use eliminated the large wave drag characteristic of SOSE, but at the expense of computational time. Although Hybrid Theory improved the prediction accuracy at lower speeds, it does not compute the effects of spherical nose bluntness accurately, and for this reason is not recommended for blunted noses at any speed. The effect of nose bluntness at low supersonic speeds is a noticable methods problem area. It is recommended that a new method be incorporated in the Mach range from 1.2 to 1.5 for blunted noses. The easiest approach would be to extend the transonic methods from the current Mach 1.2 to Mach 1.5; sufficient data exists in the transonic method data tables to permit this extension.

3.1.1.5 <u>Boattail Pressure/Wave Drag</u> – The Payne correlation of boattail drag at subsonic and transonic speeds is comprehensive and is restricted only by the limitations detailed in Figure 13 (Reference 11). It was found to be sufficiently accurate for preliminary design. However, it does assume that sufficient distance exists between the nose and the boattail to minimize nose flow field coupling (approximately six calibers). Shorter cylindrical afterbodies should not be investigated using this technique, and no other method is available that can be substituted. Hence, the derivation of a new subsonic/transonic boattail drag model is required. A recommended approach would be to use the code RAXBOD to generate parametric results which could be interpolated for the computer code, and used to create a design chart for the methods handbook (Reference 12).
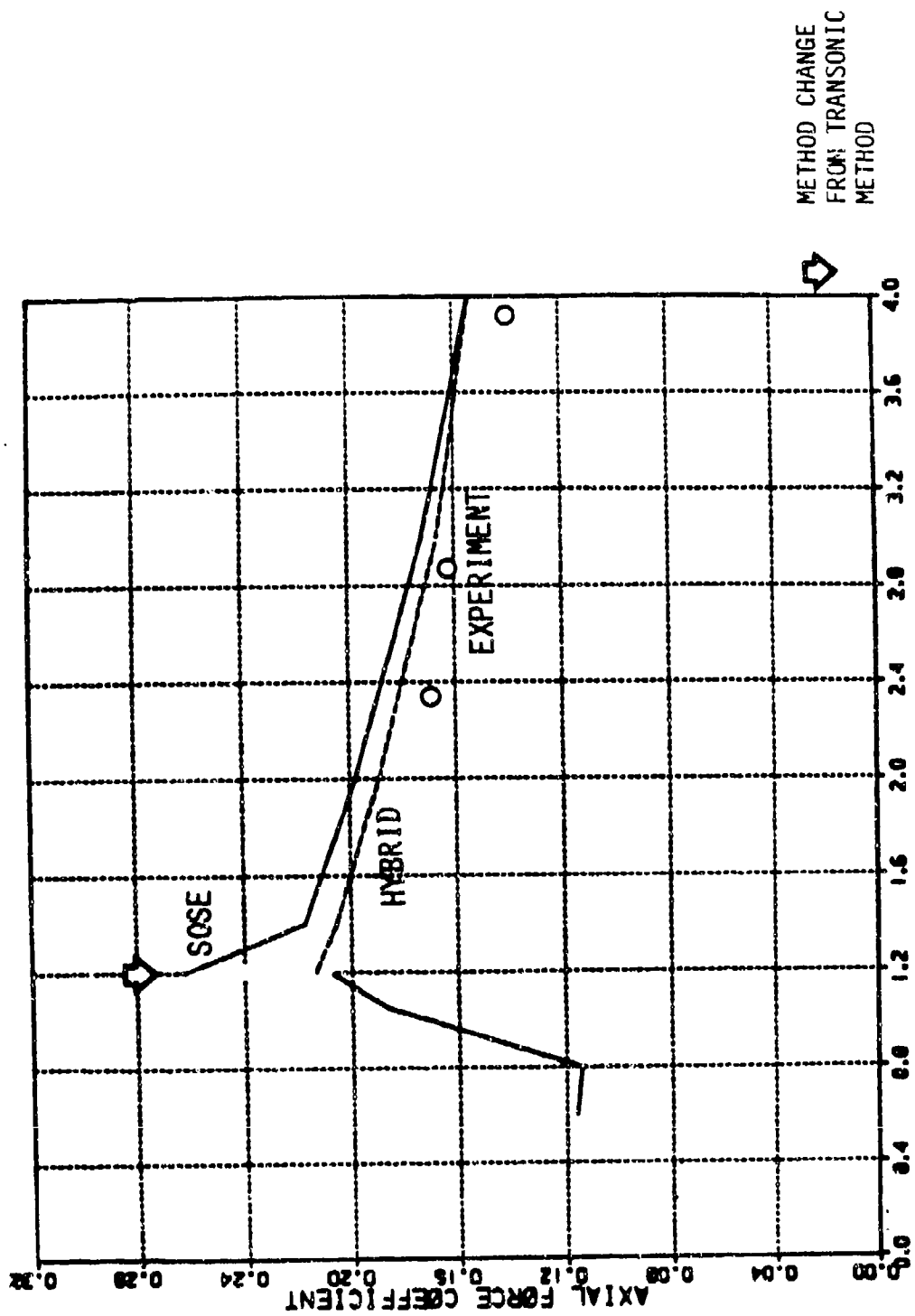
FIGURE 12   SOSE DOES POORLY AT LOW SUPERSONIC MACH NUMBERS.

CONICAL

OGIVAL

β_{MAX} = 16 DEG.

β_{MAX} = 28 DEG.
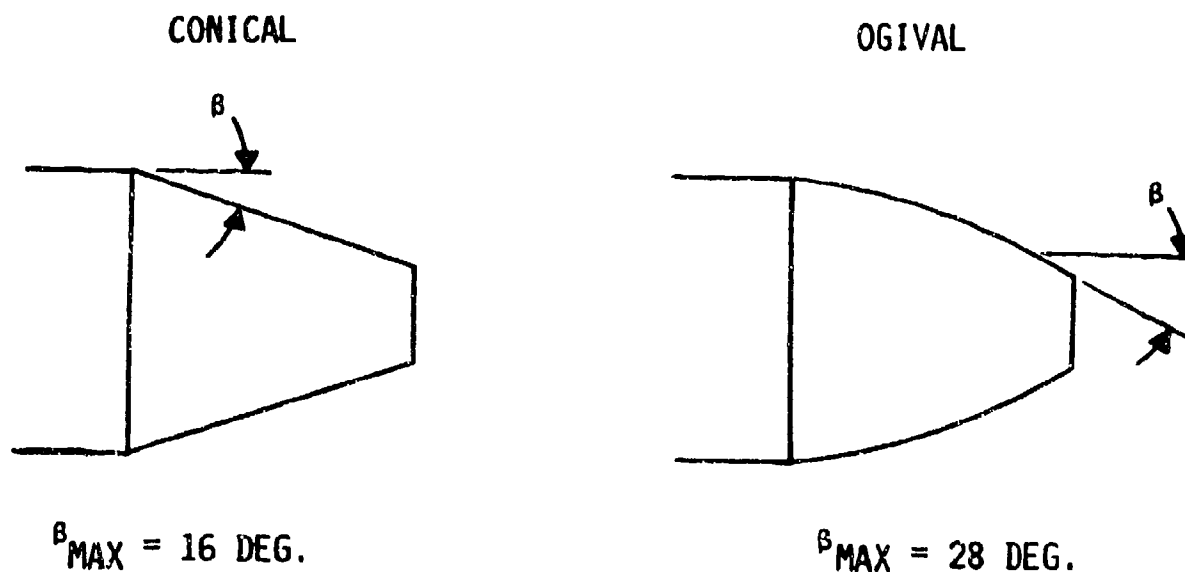
FIGURE 13 BOATTAIL GEOMETRY LIMITATIONS

Comparisons with experimental data at supersonic speeds have shown that the SOSE and/or Hybrid methods are sufficiently accurate for preliminary design since they inherently include nose/afterbody coupling.

3.1.1.6 **Flare Pressure/Wave Drag** - The Feasibility Study did not identify a method for flares in the subsonic/transonic regime since it was thought that their usage was limited to projectile shapes. Subsequent information revealed that there exists much more interest than first believed, so two methods were later selected for stuty. The first was an empirical data base of a wide variety of flare fineness ratios; it was rejected because of the extremely short cylindrical centerbody separating it from the nose. The second, a U.S. Army correlation, seemed to be a reasonable alternative although it only addressed conical flares (Reference 13). The limitations placed on the geometry are described in Figure 14. Since no other method exists it was selected. It is recommended that an improved new technique be developed.

CONICAL   OGIVAL

$^\beta$MAX = 10 DEG. $^\beta$MAX = 10 DEG.
                                                 (USING CONICAL DATA)
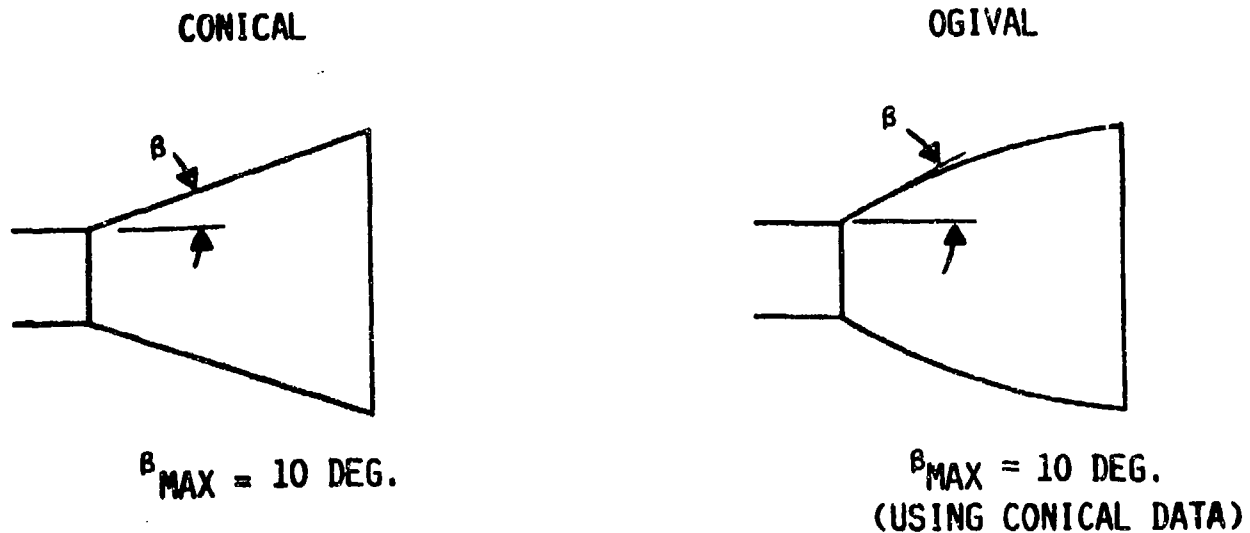
FIGURE 14 FLARE GEOMETRY LIMITATIONS

At supersonic speeds, flares can be analyzed quite easily using either the
SOSE or Hybrid methods described above. Comparison with experiment has shown
the pressure distributions calculated to be quite accurate at lower angles of
attack (less than eight degrees).

3.1.1.7 General Nose Shape Pressure/Wave Drag - The only nose shapes cur-
rently being addressed at subsonic/transonic speeds are tangent ogives and
cones. There is an urgent need to develop methods for other shapes, such as
Haack series, power-law, and secant ogive noses. The approach recommended
is to use the code RAXBCD and parametrically vary the nose fineness ratio to
develop design charts. The supersonic speed regime is once again adequately
covered by the SOSE/Hybrid combination.

3.1.1.8 __Base Drag__ - The method selected by the Feasibility Report was slightly changed simply due to automation convenience. The use of NASA-TR-R-100 is thought to be slightly more advantageous due to the wide range of flight test results used in derivation of the method (Reference 14). The method was modified using a U. S. Army method so that the base drag due to boattails and flares could be accommodated (Reference 13).

3.1.1.9 __Jet Exhaust and Protuberance Effects__ - Although methods were identified in the Feasibility Study for the effects of jet exhaust and protuberances, they proved to be too limited in application or too general to be useful. Hence, neither set of techniques were incorporated.

3.1.1.10 __Angle-of-Attack Effect__ - The recommended Allen and Perkins plus Jorgensen method was incorporated (Reference 15). Prediction comparisons showed that the techniques were adequate to approximately 30 degree angle of attack.

However, in the transonic Mach regime the discrepancy with experiment was largest between 15 degrees and 60 degrees angle of attack. Some predictions followed the experimental results quite accurately, while others were significantly in error. It is not known whether this effect is Reynolds number, nose shape, or total body fineness ratio dependent. Analyses which are more dependent upon results in this angle of attack range will require a significantly improved axial force due to angle of attack model.

3.1.2 Normal Force and Pitching Moment Coefficient

The methods selected for configuration normal force and pitching moment are far superior to those originally recommended in the Feasibility Study. This is due to the discovery of methods not previously available in the open literature and the improvement of the selected supersonic techniques.

It is assumed that the normal force and pitching moment coefficients can be approximated as the sum of potential and viscous contributions:

$$C_N = C_{Np} + C_{NV}$$

$$C_m = C_{mp} + C_{mV}$$

where,

$$C_{Np} = 0.5 \ C_{N\alpha} \ \sin(S\alpha) \cos(\alpha/2)$$

$$C_{NV} = \eta \ C_{dc} \ S_p \ \sin^2(\alpha)/S_{ref}$$

$$C_{mp} = 0.5 \ C_{m\alpha} \ \sin(2\alpha) \cos(\alpha/2)$$

$$C_{mv} = \eta \ C_{dc} \ S_p \ \sin^2(\alpha)/S_{ref}(X_{cg}-X_c)L_{ref}$$

3.1.2.1 Potential Normal Force and Pitching Moment

Two separate methods were implemented: the Second Order Shock Expansion (SOSE) method and the Van Dyke Hybrid Theory. As illustrated in Figure 15, a significant methods overlap region exists for the most commonly used noses. It would appear advantageous to include only the SOSE method at all supersonic speeds and simplify the code. At Mach 2.3, the SOSE pressure coefficient distributions over a 3:1 tangent ogive at eight degrees angle-of-attack, compare favorably to the more complex Hybrid and Shock Capturing codes, Figure 16. Other SOSE comparisons to the configurations shown in Figure 17 were also quite satisfactory (Figures 18 through 24).

Using a large data base of experimental results, the accuracy of the SOSE method was assessed. The results, shown in Figures 25 and 26, divided by nose shape, shows that a large percentage of the configurations (over 65 percent) can be predicted with 10 percent error or less, and over 75 percent can be predicted with less than 15% error. The average error on normal force and pitching moment coefficient slope, summarized in Figure 27, is far below the $\pm$ 20 percent allowable using the accuracy criteria developed in Section 2.
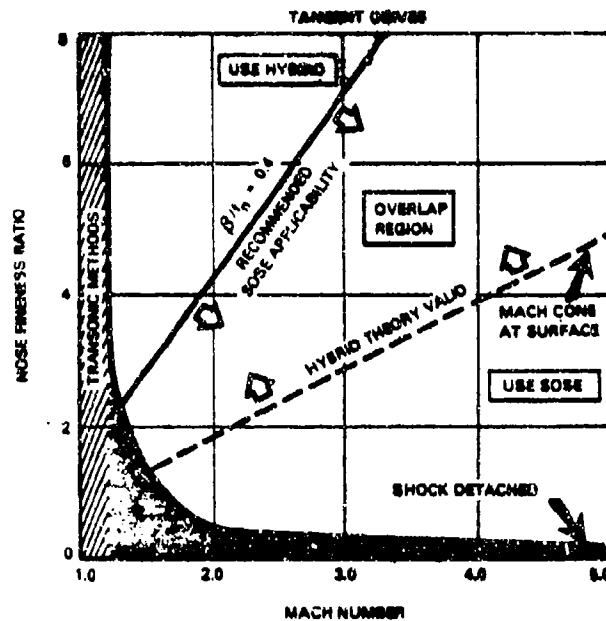
FIGURE 15 REGIONS OF APPLICABILITY--SUPERSONIC THEORIES

In Figure 28 these results were divided by the most common geometry criteria:

(1) $\beta/f_N < 0.4$ – an assumed poor SOSE application region,

(2) $M < 2$ – an assumed lower Mach limit for SOSE,

(3) $f_A = 0$ – no cylinder added to the nose, and

(4) $M \geq 2$, $f_A > 0$ – the best SOSE application region.

As assumed, criteria 4 was the best demonstrated operating region for SOSE. However, the average error for the other regions was a scant 2.0 percent to 3.4 percent greater.

32
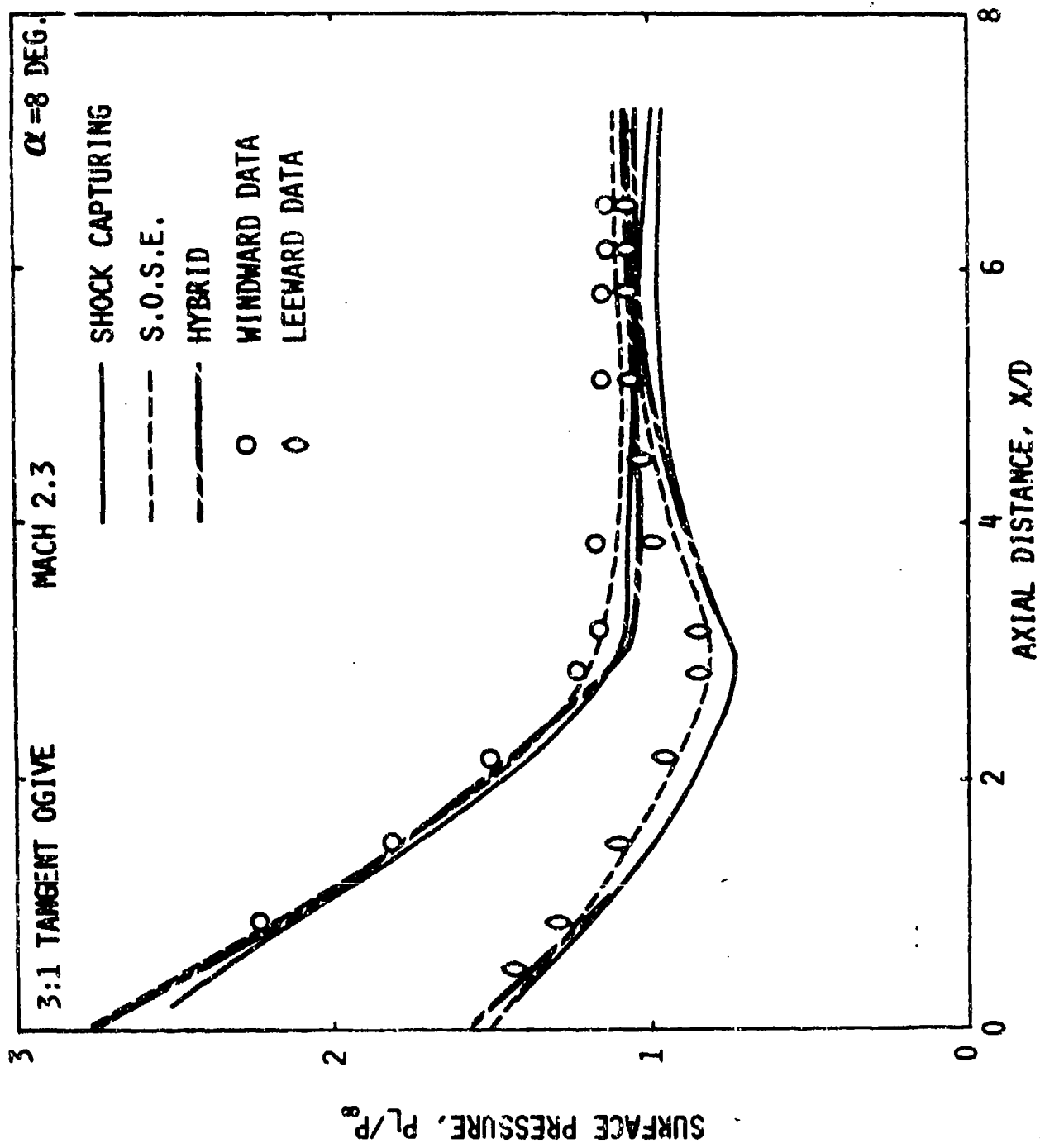
FIGURE 16 MISSILE DATCOM COMPUTED PRESSURE COMPARISONS

2. Circular-arc—cylinder

4. Circular-arc—circular-arc

6. Circular-arc—cylinder—flare

1. Cone—cylinder

3. Blunt-nose—cylinder

5. Circular-arc—cylinder—boattail

FIGURE 17. CONFIGURATIONS TESTED BY LANDRUM

34

MACH=1.6 ALPHA=0. PHI=0.

LONGITUDINAL STATION

PRESSURE COEFFICIENT

FIGURE 18 SOSE PRESSURE COEFFICIENT DISTRIBUTIONS OVER A CONE-CYLINDER

MACH=1.6 ALPHA=0. PHI=0.

FIGURE 19 SOSE PRESSURE COEFFICIENT DISTRIBUTION OVER AN OGIVE-CYLINDER

MACH=1.6 ALPHA=8.0 PHI=0.

FIGURE 20 SOSE PRESSURE COEFFICIENT DISTRIBUTION OVER AN OGIVE CYLINDER AT ANGLE OF ATTACK

37

MACH=1.6 ALPHA=8.0 PHI=0.

PRESSURE COEFFICIENT
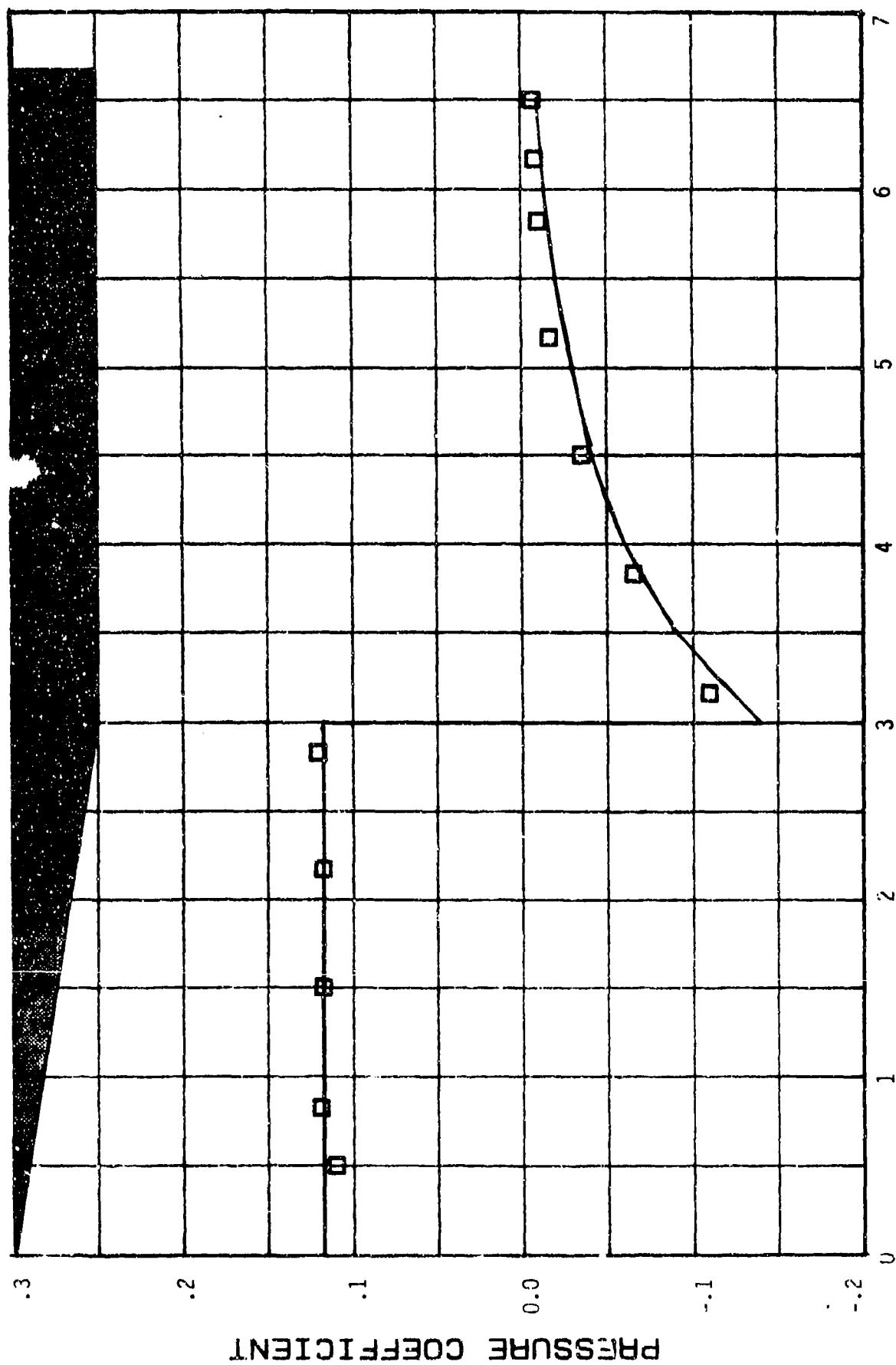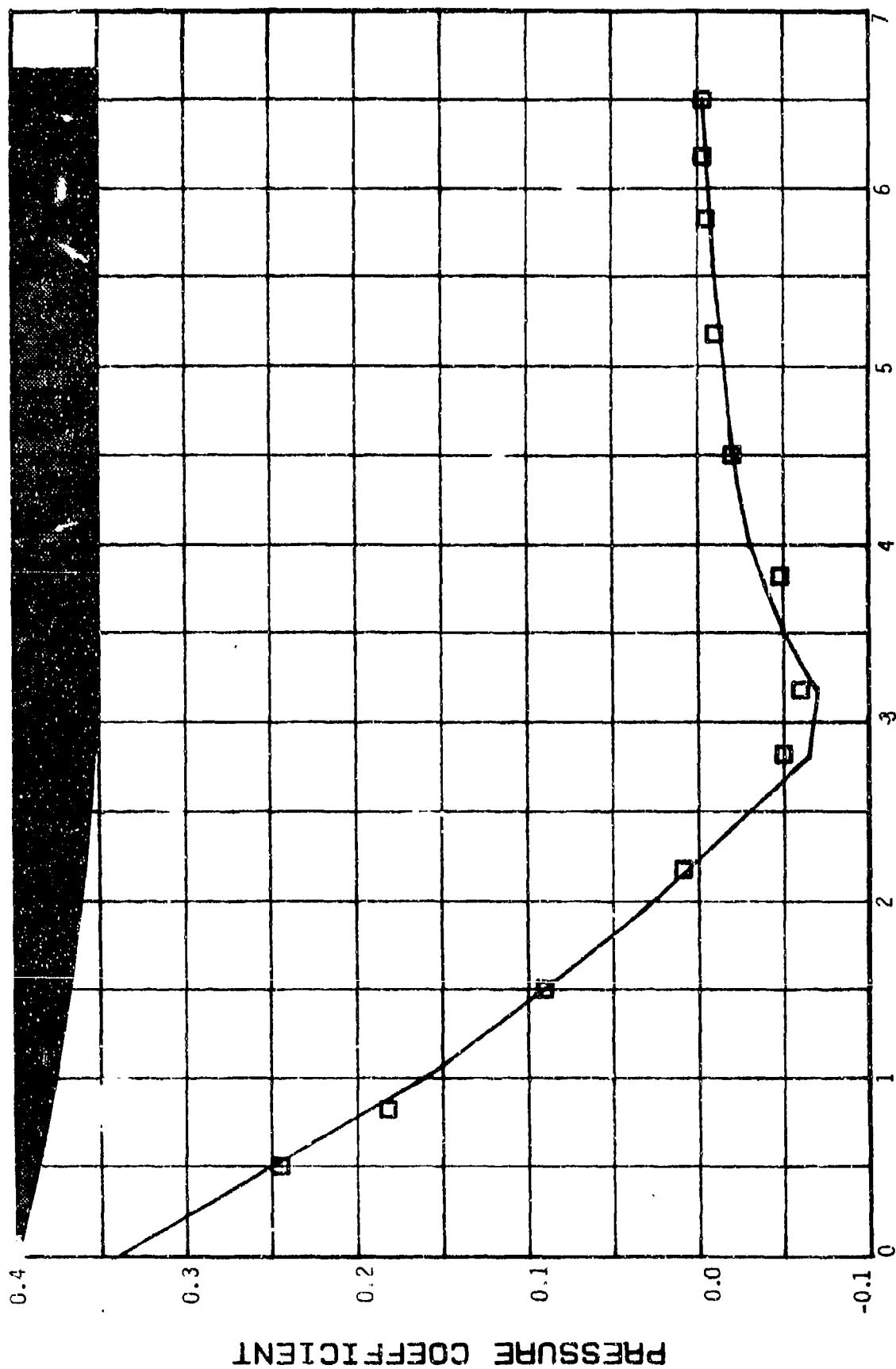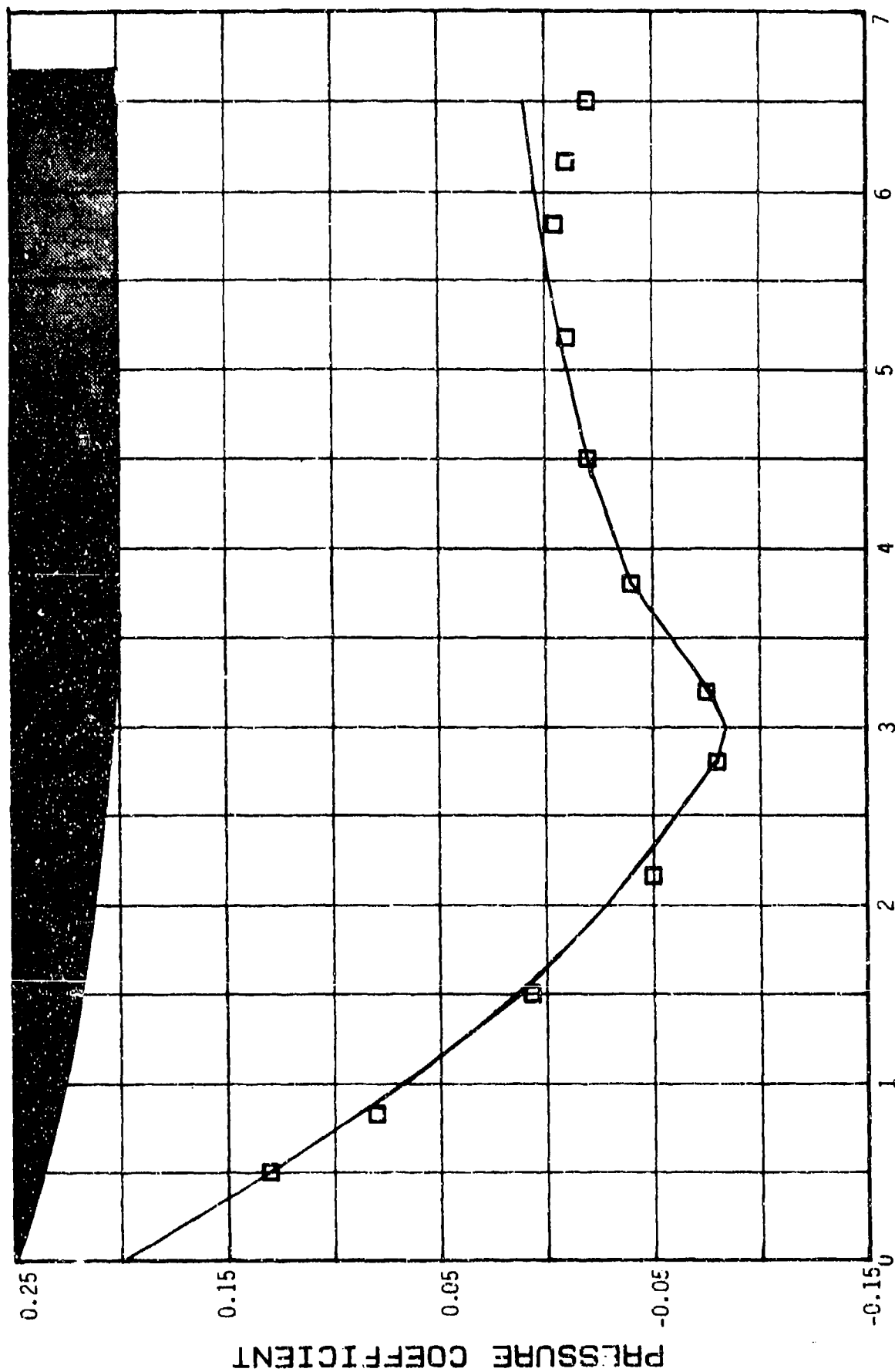
LONGITUDINAL STATION

FIGURE 21 SOSE PRESSURE COEFFICIENT DISTRIBUTION OVER A BLUNTED OGIVE CYLINDER AT ANGLE OF ATTACK

38

MACH 1.6 ALPHA=8.0 PHI=0.

LONGITUDINAL STATION

PRESSURE COEFFICIENT

FIGURE 22 SOSE PRESSURE COEFFICIENTS FOR A CIRCULAR-ARC-CIRCULAR-ARC

39

MACH=4.63 ALPHA=8.0 PHI=0.

PRESSURE COEFFICIENT DISTRIBUTION OVER AN OGIVE-CYLINDER-BOATTAIL

FIGURE 23 SOSE PRESSURE COEFFICIENT DISTRIBUTION OVER AN OGIVE-CYLINDER-BOATTAIL

LONGITUDINAL STATION

PRESSURE COEFFICIENT

MACH=1.6 ALPHA=8.0 PHI=0.

FIGURE 24 SOSE PRESSURE COEFFICIENT DISTRIBUTION OVER A CIRCULAR-ARC-CIRCULAR-ARC-FLARE

PRESSURE COEFFICIENT

LONGITUDINAL STATION

41
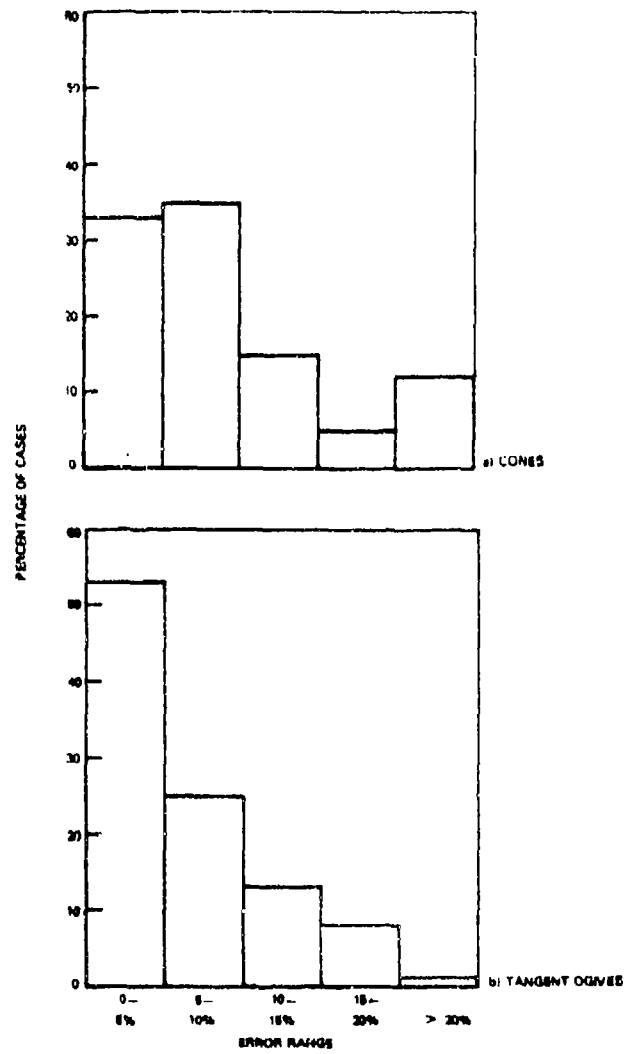
FIGURE 25   SOSE AVERAGE ERROR--NORMAL FORCE SLOPE
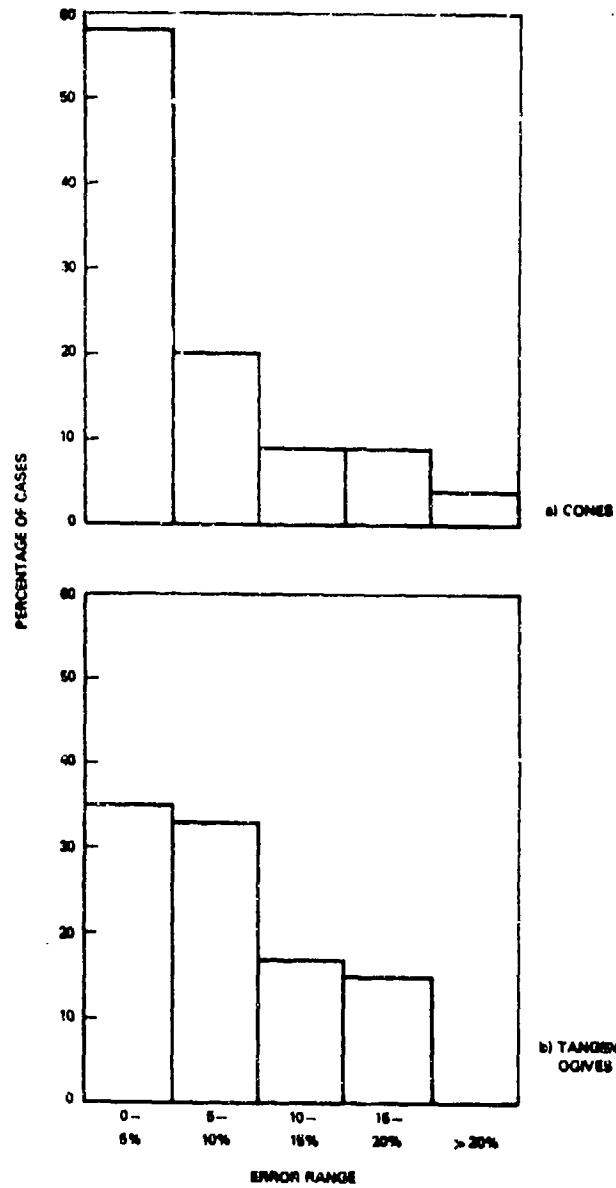
FIGURE 26   SOSE AVERAGE ERROR--PITCHING MOMENT SLOPE

CONFIGURATION	C_{N_α} AVERAGE ERROR	C_{M_α} AVERAGE ERROR
SHARP CONE-CYLINDER	9.2%	6.4%
SHARP TANGENT OGIVE-CYLINDER	6.2	7.6

FIGURE 27 PREDICTION ERROR OF POTENTIAL SLOPES USING SOSE

CONFIGURATION SELECTION CRITERIA	AVERAGE ERROR
$\beta/f_N < 0.4$	7.7%
$M < 2.0$	7.0%
$f_A = 0.$	8.4%
$M \geq 2, \ f_A > 0.$	5.0%

FIGURE 28 PREDICTION ERROR FOR TANGENT OGIVE-CYLINDER CONFIGURATIONS, C_{N_α}

The same data base was used to demonstrate the accuracy of the Hybrid Theory. As shown in Figure 29, the Hybrid Theory was shown to be approximately twice as accurate as SOSE. Because of the increased accuracy of this method, it was advantageous to include it; its retention also provided a solution to the wave drag problem experienced with SOSE at lower supersonic speeds (see Figure 12).

The subsonic/transonic incremental normal force slope for a flare is assumed by the selected method to be dependent upon the cylinder diameter to flare base diameter ratio, and is insensitive to a flare angle for angles up to ten degrees (Reference 13). This theory gives acceptable results for preliminary designs as shown in Figure 30. No systematic trend in the experimental data could be found which would allow a more accurate method to be developed, nor were data for higher flare angles found in the open literature. Hence, the selected method appears to be the best available for the range of configurations anticipated. However, a better technique should be sought which includes the effect of larger flare angles and the influence of centerbody length since these are significant effects.

3.1.2.2 **Viscous Normal Force and Pitching Moment** - The effect of angle of attack is modeled by assuming that the drag of an infinite cylinder normal to the flow can be linearily superimposed upon the configuration potential normal force or pitching moment. Since there are at least nine different cross flow drag models available, it is necessary to pair the potential model with its corresponding viscous model to obtain a correct method. This "pairing" is required since an empirically derived correction factor is applied to the viscous model in the subsonic/transonic Mach regime. The correction factor, is the cross flow drag proportionality factor; it specifies how two-dimensional the flow around the body becomes.

The choices for cross flow drag were reduced to the three shown in Figure 31. The Jorgensen model is, perhaps, the most "empirically correct" of the three, since two-dimensional cylinder cross flow data was used and not data "corrected" to match the potential model employed. Jorgenson used a
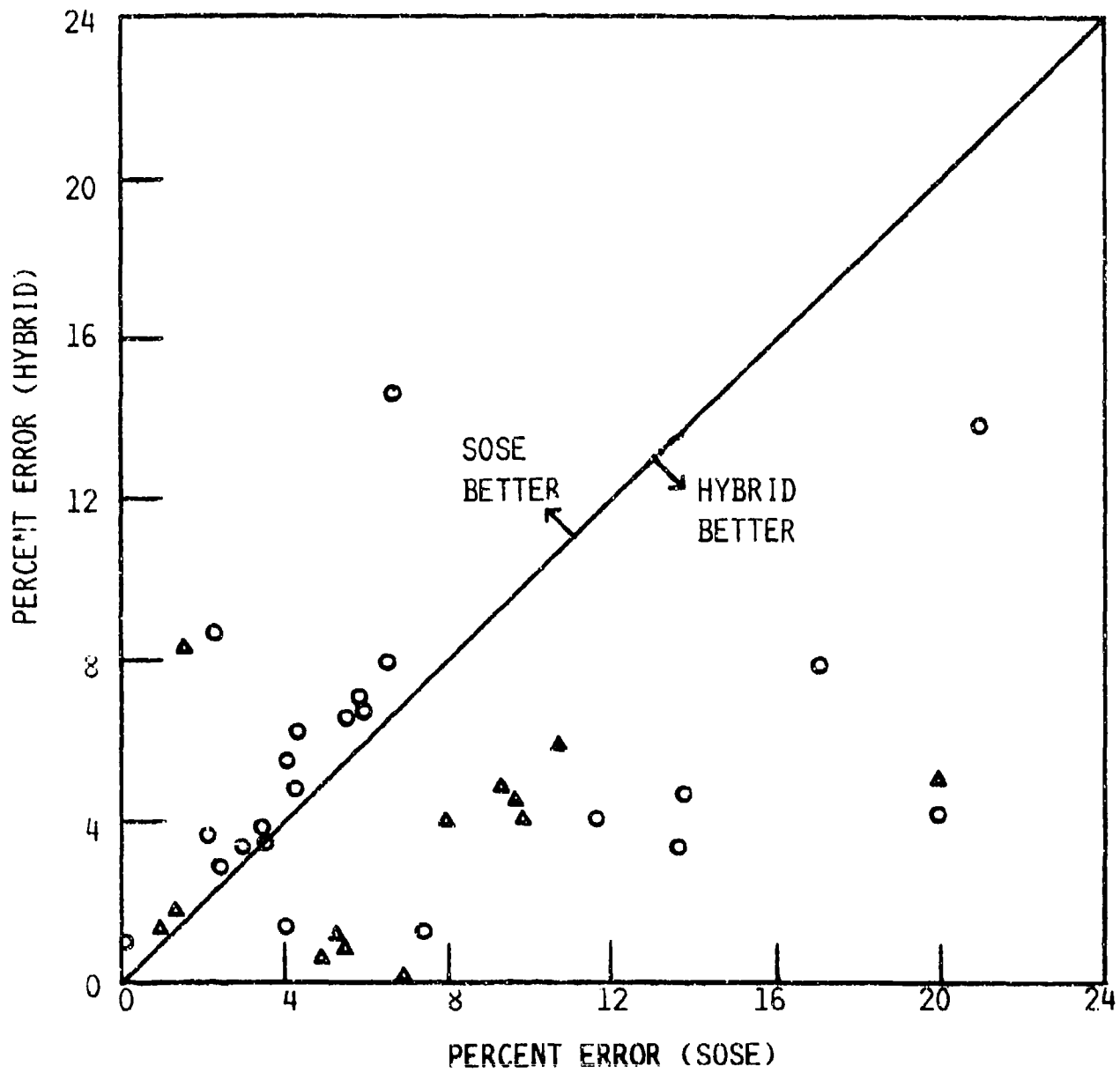
FIGURE 29 HYBRID VERSUS SOSE PREDICTIVE ERROR--C_{M_α}
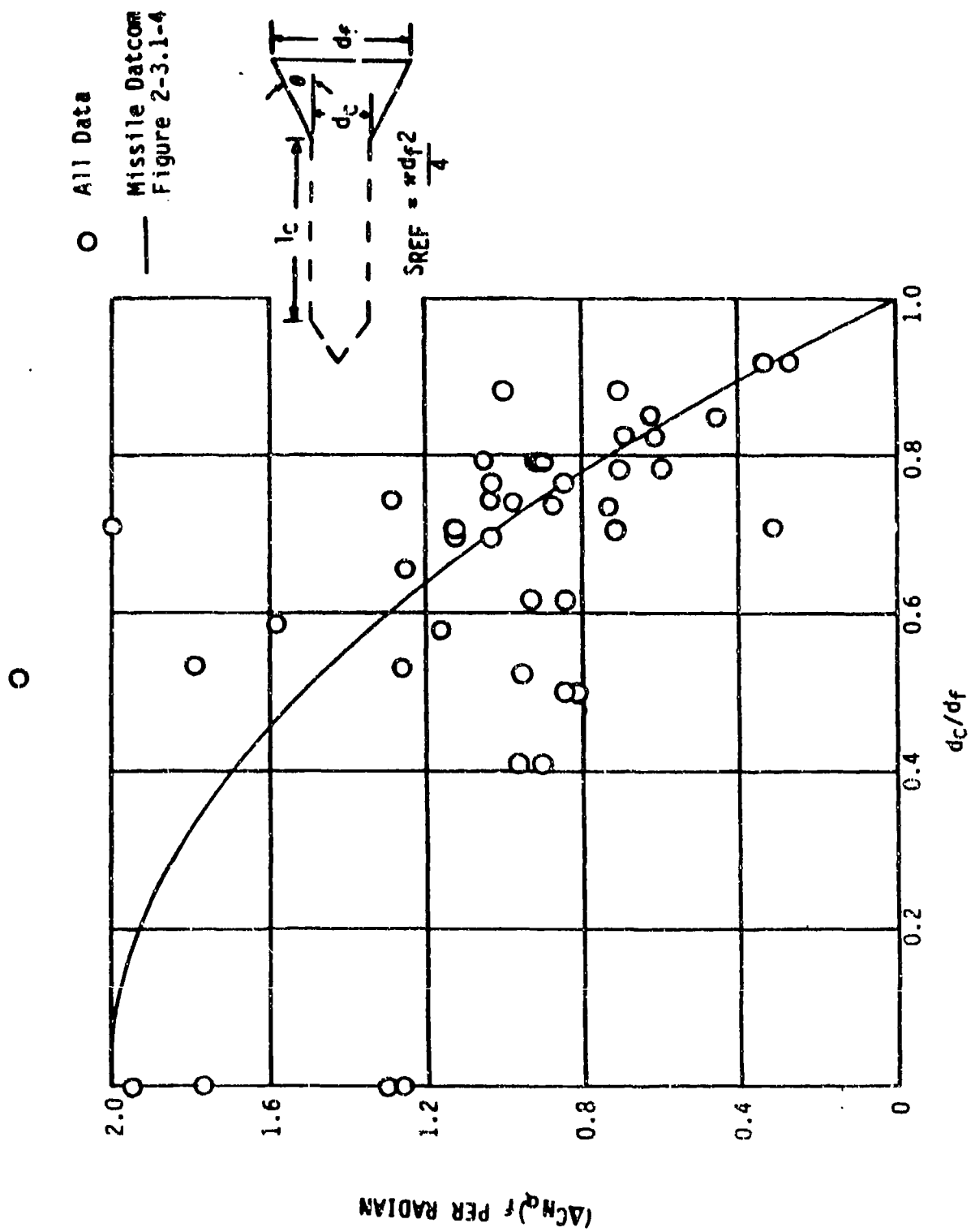
FIGURE 30 SUBSONIC/TRANSONIC FLARE METHOD VERIFICATION
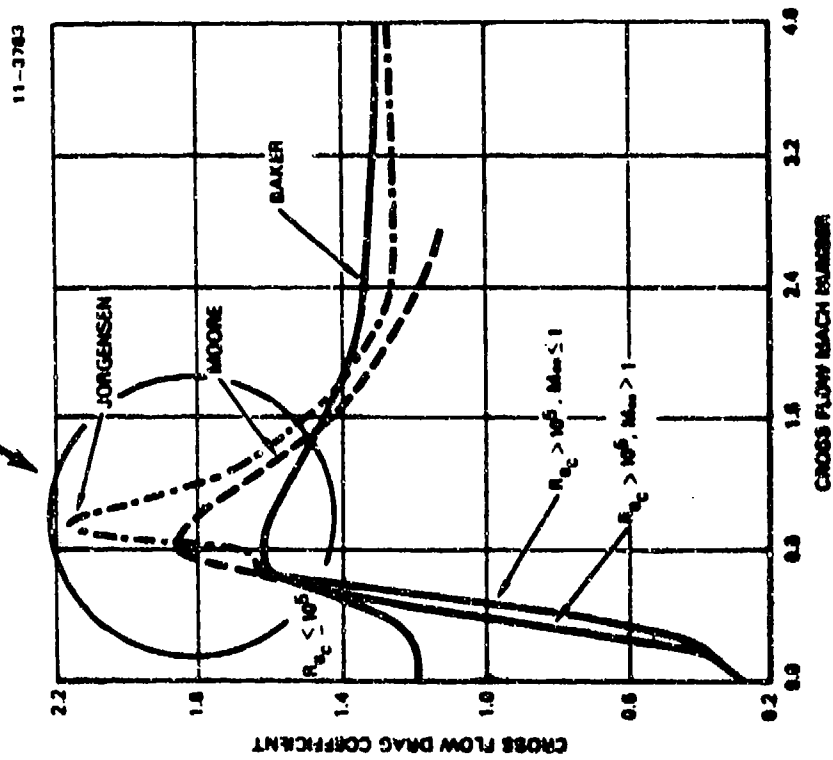
FIGURE 31 COMPARISON OF CROSS-FLOW DRAG MODELS AVAILABLE

48

nose-cylinder normal force coefficient slope of two per radian to derive his cross flow drag coefficient. Moore and Baker relied on experimental nose cylinder normal force coefficient slope to define the cross flow drag coefficient as a function of cross flow Mach number.

In Figure 32, experimental data for the cross flow drag coefficient of infinte cylinders as a function of cross flow Mach number is shown. This data was then used to compute the viscous normal force and pitching moment coefficient. The dotted line labeled "old fairing" is the cross flow drag coefficient variation first assumed. Extensive correlations with experimental data showed that this model tended to overpredict C_N from 10 to 20 percent for typical missile angles of attack and Mach number ranges. By adjusting the cross flow drag coefficient variation to the curve labeled "new fairing" the error in most predictions was held to 10 percent or less. This modification is a methods calibration. A different choice of a normal force coefficient slope prediction method would probably not yield the accuracy level observed with the current method.

Calibrating the method does not violate any method derivation assumptions or theoretical base. The assumption that the normal force and pitching moment can be estimated by summing potential and viscous contributions is based on the assumption that the longitudinal and normal force vectors can be vectorally summed. This is a basic assumption of linearity for a physical phenomenon which is not completely accurate, but is a reasonable approximation to a complex analysis.

3.1.3 Lateral-Directional Coefficients

The methods described in Section 3.1.2 for normal force and pitching moment are directly applicable to side force and yawing moment. The angle of attack used by those methods is really the total body angle-of-attack. Any directional effect arises from the axis system employed, ignoring the effect of asymmetric vortex shedding. If C_N' and C_m' represent the body normal force and pitching moment coefficients, respectively, as a function of total
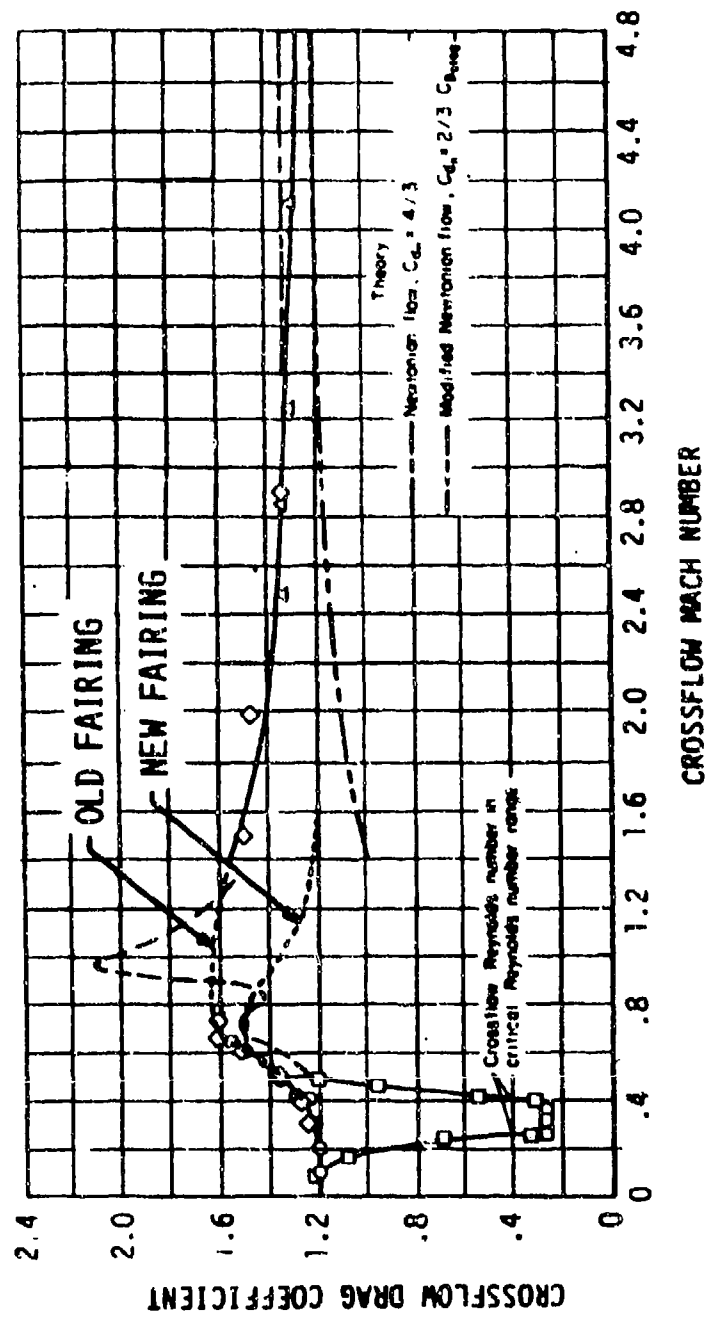
FIGURE 32 MODIFICATION OF CROSS-FLOW DRAG

50

angle-of-attack, then the body axis normal force, side force, pitching moment, and yawing moment are respectively:

$$C_N = C_N' \cos(\phi')$$

$$C_Y = -C_N' \sin(\phi')$$

$$C_m = C_m' \cos(\phi')$$

$$C_n = -C_m' \sin(\phi')$$

where,

$$\phi' = \tan^{-1}(\tan \beta / \tan \alpha)$$

Methods for estimating the effect of "phantom yaw" or asymmetric vortex shedding have not been included into the handbook or the code due to the complexity of the solution and the uncertainty of such flow parameters as Mach number, Reynolds number, and angle of attack.

3.2 BODIES WITH NONCIRCULAR CROSS SECTIONS

The methods for noncircular bodies are variants of the circular body methods. Not only are these types of methods commonly used to estimate the aerodynamics of noncircular bodies but they are, for the most part, the only easy to apply techniques available.

At subsonic speeds one could model noncircular bodies using a potential code, where the geometry is modeled as a matrix of sources and sinks; 3-D Neumann (Reference 16) is an example of such an approach. However, the costs for such a solution are extremely high, and the setup time to prepare the inputs are highly labor intensive. Both of these disadvantages make their use in the preliminary design envirnoment questionable, and perhaps unnecessary if a "simple" approach produces results of sufficient accuracy.

51

At transonic speeds, the accurate prediction of aerodynamics for noncircular bodies must rely on very complex codes, such as the implementation of a Navier-Stokes solution. These types of analyses are inappropiate for preliminary design.

At high supersonic speeds, the Supersonic/Hypersonic Arbitrary Body (S/HABP) code (Reference 17) is a reasonable alternative for noncircular bodies due to the less complicated analyses performed. Although this approach was selected to model airbreathing inlets, the complexity of user preparation was extensive. Results using the Jorgensen approach, which modifies the potential and viscous components of normal force and pitching moment, was found to be highly successful for elliptically shaped geometries, making the use of a S/HABP analysis unnecessary. An extension of slender body theory using apparent area calculations was found to be useful in predicting the longitudinal aerodynamics of bodies with many arbitrary cross sections. While the method implemented can handle bodies not normally thought of as slender it does have serious limitations. These are discussed in Section 3.2.2.

The following paragraphs summarize the method changes applied to the circular body methods, described in Section 3.1, for application to bodies whose cross section can be represented by an ellipse. Following the description of the elliptic body methods are paragraphs describing the arbitrary cross section methods used.

3.2.1 Bodies with Elliptic Cross Sections

3.2.1.1 Axial Force Coefficient - The methods selected for computing the axial force of bodies with noncircular cross sections are those selected for circular bodies, as described in Section 3.1.1. The complexity of the flow field makes accurate solutions extremely costly due to the complex analysis codes required. Hence, the use of circular body methods, with appropiate corrections to account for cross section shape, is the most economical approach. The methods and cross section correction factors are described below.

3.2.1.1.1 Skin Friction - The method described in Section 3.1.1.1 is used for noncircular bodies. Even though the local skin friction coefficient could approach flat plate values over some portions of the configuration, the three-dimensional correction to flat plate friction is used to approximate the skin friction over the whole wetted surface of the geometry.

3.2.1.1.2 Subsonic Pressure Drag - Subsonic pressure drag for circular bodies is computed using the drag due to skin friction and a "form factor" adjustment. This "form factor" was empirically derived and is a function of body fineness ratio. It is assumed that the noncircular body fineness ratio (based upon an equivalent circular body diameter) can be used to estimate the pressure drag of noncircular bodies. This approximation is adequate for preliminary design.

3.2.1.1.3 Transonic Pressure/Wave Drag - Estimating the transonic drag characteristics of circular bodies is extremely difficult since the methods available are limited to a small number of geometries. The prediction of noncircular bodies is even more uncertain. It is assumed that the pressure/wave drag characteristics would be the same as those for a circular body with the same longitudinal cross-sectional area distribution.

3.2.1.1.4 Supersonic Wave Drag - This is the only component of axial force for which a method specifically intended for elliptical bodies exists. The method derived by Van Dyke using second-order slender body theory, does not predict a significant variation in wave drag for typical major to minor axis ratios, as shown in Figure 33. The Van Dyke method is complex, and the effect of cross section shape on wave drag can be assumed to be second order in preliminary design, and is ignored in Missile DATCOM's elliptic body methods.

3.2.1.1.5 Boattail Pressure/Wave Drag - It is assumed that the influence of boattails are similar to those for circular bodies. An equivalent circular body has been assumed.
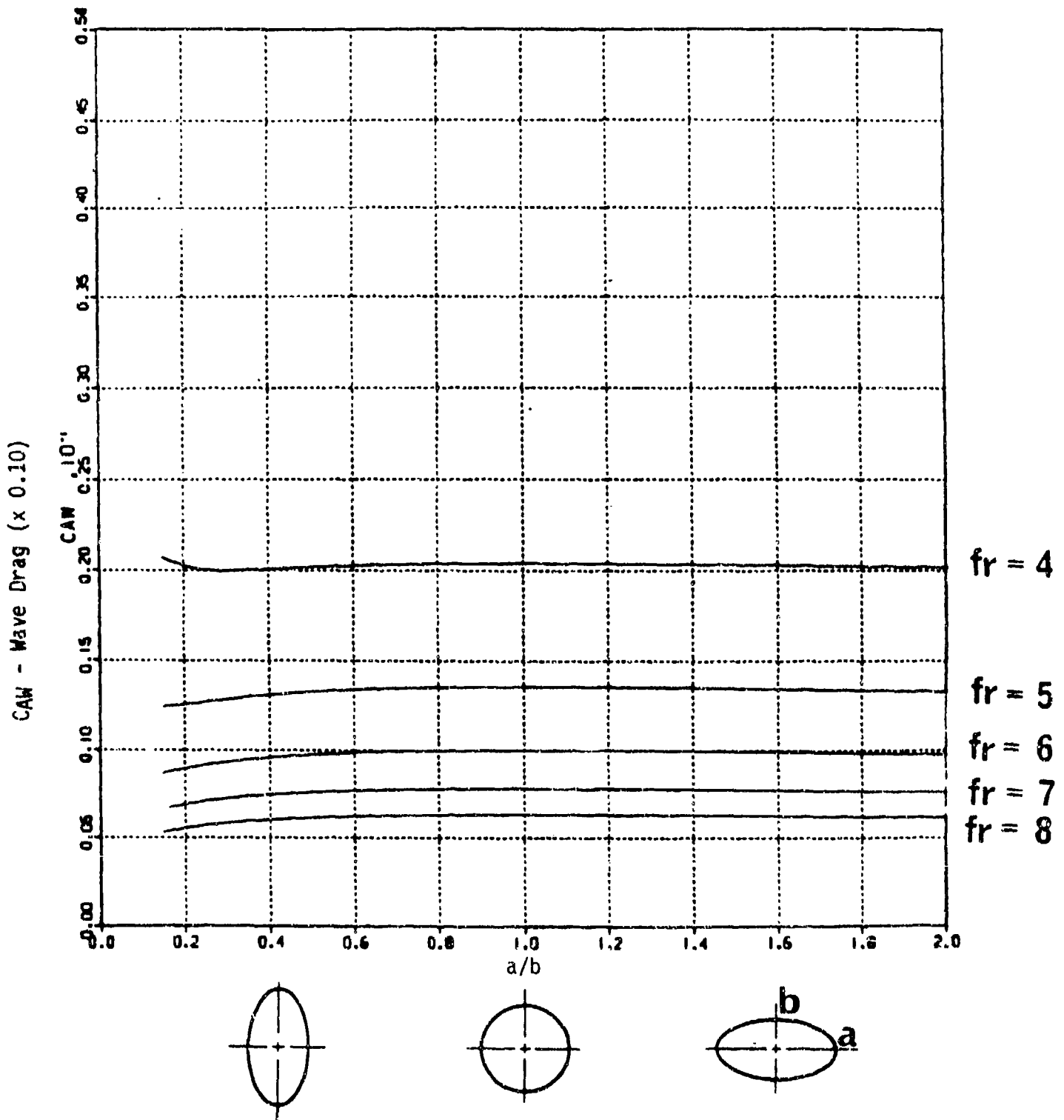
FIGURE 33 C_{AW} VS ECCENTRICITY (A/B) FOR VARYING FINENESS RATIOS

54

3.2.1.1.6 Flare Pressure/Wave Drag - It is assumed that the influence of flares are similar to those for circular bodies. An equivalent circular body has been assumed.

3.2.1.1.7 General Nose Shape Pressure/Wave Drag - As described in Section 3.1.1.7, few easy to apply methods exist for predicting the effect of arbitrary longitudinal variation in the nose shapes of circular bodies. Being able to analyze non-circular bodies is more difficult. The methods implemented are described in Section 3.2.4.

3.2.1.1.8 Base Drag - Refer to Section 3.1.1.8 for the circular body methods since they are applied to noncircular geometries.

3.2.1.1.9 Angle of Attack Effect - The methods for circular bodies, described in Section 3.1.1.10, are assumed to be applicable to noncircular geometries.

3.2.1.2 Normal Force and Pitching Moment Coefficient - The circular body methods described in Section 3.1.2 are assumed to be applicable to noncircular geometries, provided that the effect of cross section is accounted for using correction factors:

$$c_N = \left(\frac{c_N}{c_{N_o}}\right)_{SB} c_{N_p} + \left(\frac{c_N}{c_{N_o}}\right)_{NT} c_{N_V}$$

$$c_m = \left(\frac{c_m}{c_{m_o}}\right)_{SB} c_{m_p} + \left(\frac{c_m}{c_{m_o}}\right)_{NT} c_{m_V}$$

A slender body theory (SB) correction is made to the potential component of each coefficient, and a Newtonian theory (NT) correction is made to the viscous component. For bodies whose cross section shape varies along its

length, the constants can be replaced with integrals along the body length. It is this form of the equations which are referred to as the Jorgensen method in this report.

The Newtonian correction factor is only valid in the Hypersonic Mach regime. Some limited empirical results, ratioed to Newtonian values, are available and plotted in Figure 34. This ratio, K_n, is included as a multiplier to the viscous component of both the normal force and pitching moment coefficients. The accuracy of this correction factor is demonstrated in Figure 35. The dashed lines represent the use of the integral form of the equations, given above; the solid lines represent the same predictions with the correction term added to correct the Newtonian theory. The latter method is demonstrated to be superior.

3.2.1.3 Lateral-Directional Coefficients - Since the Jorgensen method is used for predicting C_N and C_m, the same approach was selected for C_Y and C_n. The slender body and Newtonian theory correction terms become roll dependent. Hence, the selection of the proper roll attitude and axis system is required to obtain the correct coefficients.

3.2.2 Arbitrary Bodies with Nonelliptic Cross Sections

The capability to predict the linear portion of the longitudinal stability coefficients of bodies with arbitrary cross sections has been included in the code. The methods selected for predicting normal force and pitching moment curve slopes are based on slender body theory since it allows for rapid predictions without requiring the user to panel the configuration. Slender body theory also has the versatility of being Mach number independent. To predict the pressure drag of arbitrary bodies, a panel model of the body is created from the user inputs. The code employed is based on the Supersonic/Hypersonic Arbitrary Body Program (S/HABP).

56
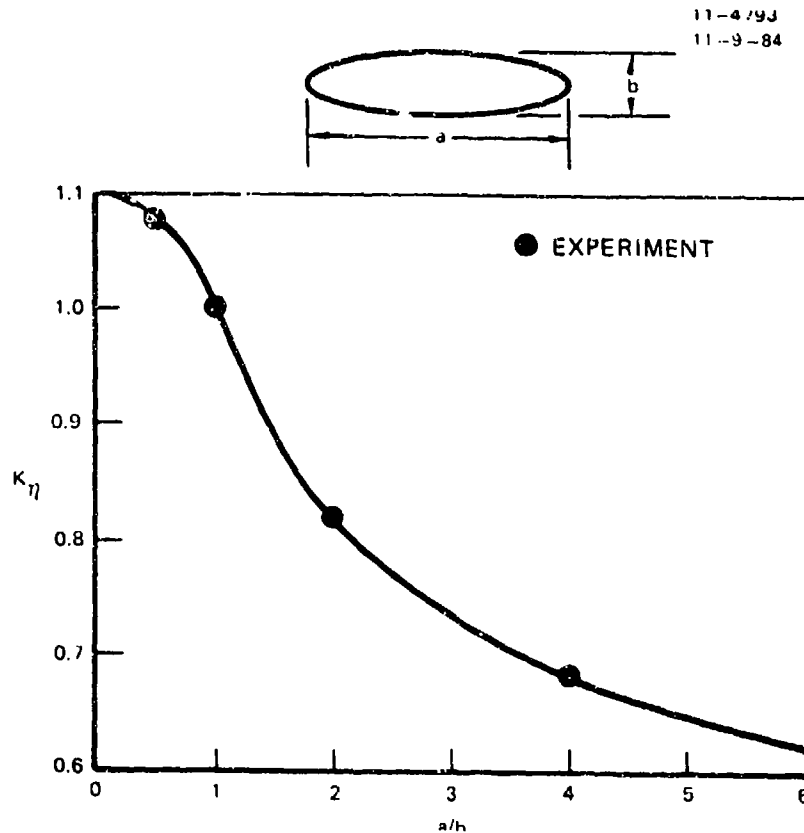
FIGURE 34 CORRECTION OF VISCOUS CROSS-FLOW FOR
ELLIPTICAL CROSS-SECTIONS IN SUBCRITICAL FLOW
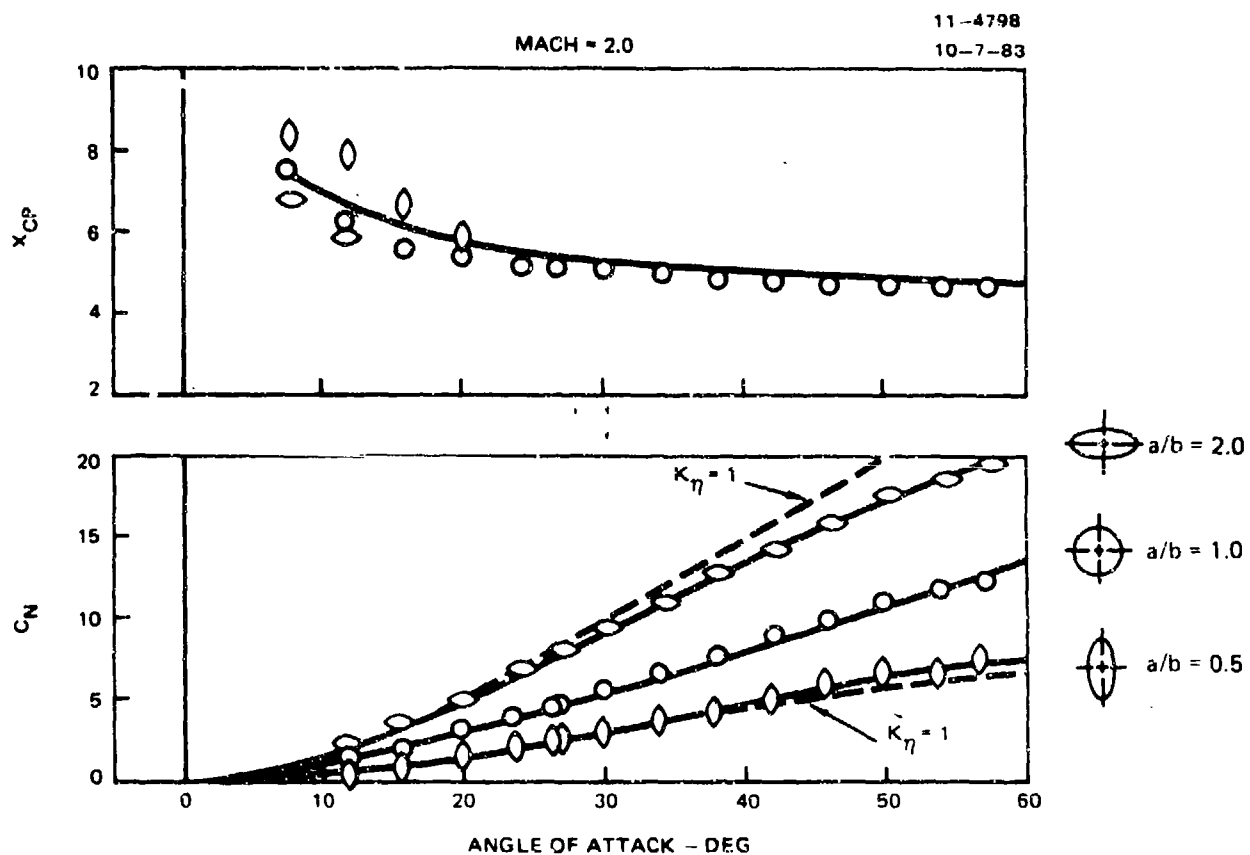
FIGURE 35 EFFECT OF K_η ON CONSTANT ELLIPTICITY BODY PREDICTIONS

57

Even though the approach selected did allow for the analysis of a wide array of body cross sections, the basis in slender body theory resulted in some limitations on the types of geometries which could be accurately analyzed. It was found that the nose finess ratio had to be greater than five. The body base cross-sectional aspect ratio had to be less than five. The base cross-sectional apect ratio was defined as the base width squared and divided by the base area. The final restriction is that the bodies can not be boattailed or flared.

The following sections describe the methods used to predict the individual coefficients. Currently methods are available to predict C_N, C_m, C_Y, C_n and $C_{A\alpha}$. Notably no simple methods such as those described in previous sections have been found for estimating the values of C_{No}, C_{Mo}, C_{Yo}, $C_{A\alpha}$.

3.2.2.1 <u>Axial Force</u> - The axial force methods implemented in the code vary with the free stream Mach numbers being evaluated. There is one combir-tion of methods for the subsonic/transonic regime and another combinati of methods for the supersonic regime. The C_A predictions are limited to zero degrees angle of attack and consist of a skin friction and a pressure drag component:

$$C_{Ao} = C_{Af} + C_{AP}$$

The C_{Af} term is the skin friction component which is proportional to the wetted area. The pressure term is proportional to the body fineness ratio.

3.2.2.1.1 Skin Friction - The skin friction portion of the axial force coefficient is computed using the circular body skin friction methods. These methods compute the flat plate skin friction coefficient for the free stream Reynolds number. The flat plate skin friction coefficient is then corrected for curvature and non-dimensionalized by the ratio of the wetted area divided by the reference area.

Quadralaterals are computed using the S/HABP geometry package to approximate the surface. The wetted area is the sum of the area of the quadralaterals.

3.2.2.1.2 Pressure/Wave Drag - At a free stream Mach numbers of less than 1.4, a subsonic/transonic pressure drag method is used. This method uses the simple expression for three-dimensional pressure drag presented in the feasibility study.

$$C_{A_p} = 7(t/C)^3 \, C_f \, \frac{Sc}{S_{Ref}}$$

where: t   - body's equivalent axisymmetric diameter

C   - body's length

Cf   - skin friction coefficient

Sc   - cross sectional area

S_{Ref} - reference area

The accuracy of this method has not been checked for a wide range of configurations. It was developed for ellipsoid type bodies which as a class of shapes which have low cross sectional aspect ratios. The small number of comparisons is due to a lack of subsonic arbitrary body data. The lack of data may, however, reflect a lack of interest in arbitrarily shaped subsonic configurations. Further method validation and development is necessary.

For free stream Mach numbers greater than 1.4, the pressure drag is computed using S/HABP methods. The nose, which is described by the user using the nose tip and base cross section shapes, is broken up into quadralaterals. The pressure coefficients on each of these panels is computed using the ACM empirical equations for leeside panels and the Dahlem-Buck equations for windward panels (Reference 18). The pressure force on each panel is then computed and resolved into the axial force direction. The resulting axial force is then nondimensionalized to compute the portion of the axial force coefficient which results from the pressure forces.

The pressure forces are computed only for the nose in the arbitrary body methods. This is because the body is assumed to be at zero degrees angle of attack. Since the centerbody sides are parallel to the centerline, it will not contribute pressure forces in the axial direction.

Comparison of the axial force coefficient results obtained using this method with data showed an overprediction trend. The median of the predicted values was found to be 25 percent above the data (Figure 36). Therefore, a correction factor was applied to reduce the predicted axial force by 25 percent.

3.2.2.2 **Normal Force Coefficient** - The methods coded to predict the normal force coefficients (C_N) of arbitrary cross section shaped bodies are based on slender body theory. Methods have been coded to predict only the normal force coefficient slope. The normal force at zero-angle-of-attack is not currently computed. Currently no methods are included to predict the viscous contribution to normal force coefficient.

The accuracy of the selected method is based on the ability to accurately evaluate the apparent area of the cross section at the base of the nose. A modified method of Hess and Smith, (Reference 19) was used to calculate apparent area. The nose cross section is divided into 100 segments, each with a distributed source strength. The results of this method have been checked against analytical solutions. With 100 test points the numerical results were within three percent of the analytical results for all cross sections except thin vertical shapes. Figure 37 shows comparisons of the method used to the analytical closed form solutions for rounded shapes, and Figure 38 shows the same comparisons for flat sided shapes.

Once the apparent area of the cross section has been computed, the normal force coefficient is computed from the equation:

$$C_{N_\alpha} = \frac{2 \ A'}{S_{Ref}}$$

where: A'   - apparent area of base cross section of the nose
        S_{Ref} - reference area

60
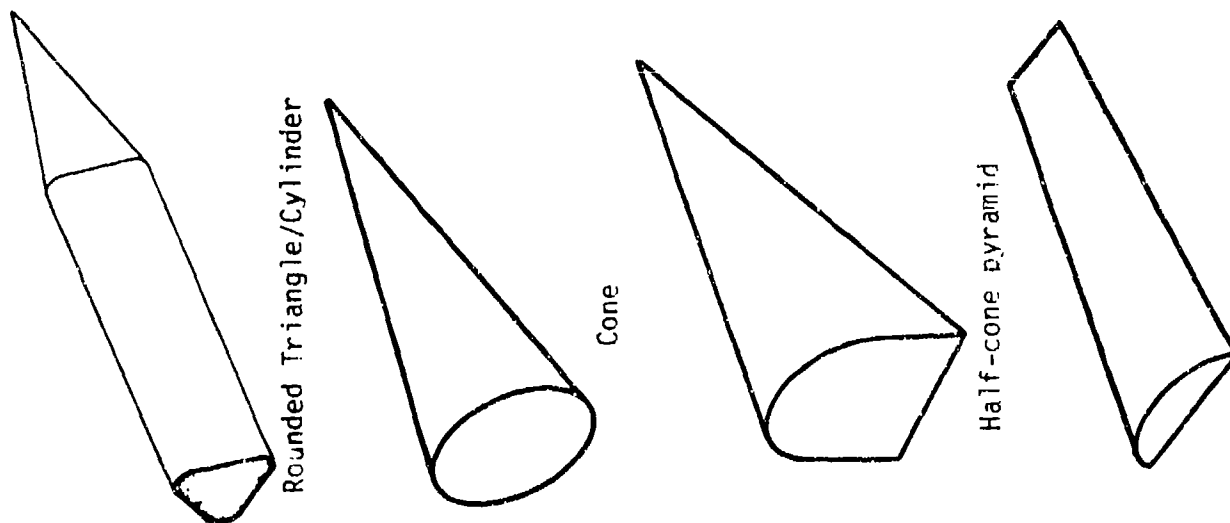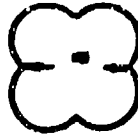
MACH NUMBER	$C_{A_{W_{calc}}}$	$C_{A_{W_{exp}}}$	% ERROR	$C_{A_{calc}}$	$C_{A_{exp}}$	% ERROR
2.5	.09015	.0357	152.5	.16251	.145	12.1
1.9	.01829	.013	406.9	.02696	.0217	24.2
2.86	.01633	.0107	526.2	.02381	.0182	30.8
3.96	.01441	.0104	385.8	.02079	.0168	23.8
4.63	.01352	.0137	-1.3	.01837	.0195	-5.8
6.83	.00993	.0035	183.7	.01748	.011	58.9
5.04				.00764	.0075	1.9

Rounded Triangle/Cylinder

Cone

Half-cone pyramid
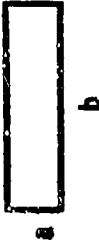
Spatualar

Figure 36   Comparison of Wave/Pressure Drag and Axial Force for Various Configurations

61

SHAPE	EQUATION	ANALYTICAL	COMPUTED	% ERROR
	$A_{11} = \pi r^2$	3.142	3.184	+1.337
	$A_{22} = \pi r^2$	3.142	3.184	+1.337
	$A_{11} = \pi b^2/4$	12.566	12.735	+1.345
	$A_{22} = \pi a^2/4$	3.142	3.184	+1.337
	$A_{11} = 2\pi r^2(\pi^2/3 - 1)$	14.388	15.163	+5.386
	$A_{22} = 2\pi r^2(\pi^2/6 - 1)$	4.052	4.146	+2.320
	$A_{11} = \pi a^2 k^2 - a^2(2 + \pi)$	5.658	5.687	+ .513
	$A_{22} = \pi a^2 k^2 - a^2(2 + \pi)$	5.658	5.687	+ .513

NOTE: $K = 1.8541$, THE COMPLETE ELLIPTIC INTEGRAL OF MODULUS $\sqrt{.5}$

FIGURE 37 COMPARISON OF ADDED MASS VALUES FOR VARIOUS ROUNDED CROSS SECTIONS

62

SHAPE	EQUATION	ANALYTICAL	COMPUTED	% ERROR
	$A_{11} = 0.654\pi r^2$ $A_{22} = 0.654\pi r^2$	2.055 2.055	2.054 2.054	- .049 - .049
	$A_{11} = 0.757\pi r^2$ $A_{22} = 0.757\pi r^2$	2.377 2.377	2.378 2.378	+ .042 + .042
	$A_{11} = 0.500\pi a^2$ $A_{22} = 0.323\pi b^2$	0.141 1.013	0.131 1.005	-7.092 - .790
	$A_{11} = \dfrac{\pi \theta_1 s^2}{[\Gamma(1 - \theta_1/2\pi)\Gamma(1 - \theta_2/2\pi)]^2} - \sin\theta_1$	0.132	0.132	0.000
	$A_{22} = \dfrac{\pi \theta_2 s^2}{[\Gamma(1 - \theta_1/2\pi)\Gamma(1 - \theta_2/2\pi)]^2} - \sin\theta_2$	2.659	2.659	0.000

NOTE: $\Gamma(x)$ IS THE GAMMA FUNCTION OF X.

FIGURE 38 COMPARISON OF ADDED MASS VALUES FOR VARIOUS FLAT SIDED CROSS SECTIONS

63

The simplicity of this equation means that the value of normal force coefficient is Mach number independent and only a function of the nose base cross section. However, there are some limitations placed on the configurations for which accurate results can be obtained due to the methods basis in slender body theory. Comparison with data have shown that the fineness ratio of the nose should be greater than five. The aspect ratio of the cross section:

$$AR_{C.S.} = \frac{WIDTH^2}{BASE\ AREA}$$

must be less than five. These two limiations keep the configuration from becoming too blunt or flat.

To calculate the contribution of the centerbody which includes the pressure carryover from the nose an equivalent circular body method has been employed. An equivalent axisymmetric body radius is computed based on the maximum arbitrary body cross section. The relationship used is:

$$S_{REF} = \pi r_{eq}^2$$

Using the value of r_{eq}, the $C_{N\alpha}$ of a circular cone-cylinder configuration with the same nose and centerbody fineness ratios as the arbitrary body is computed using the Missile Datcom axisymmetric body methods. This process is outlined in Figure 39 for a rounded triangular body. After the equivalent cone-cylinder $C_{N\alpha}$ is computed, it is scaled based on the ratio of the apparent areas of the arbitrary body to that of a cone. The equation that results is:

$$C_{N\alpha}ARB.BODY = \frac{A'\ ARB.BODY}{A'\ CONE}\ C_{N\alpha}\ CONE/CYL$$

The results of this method have been checked against data and the results of a comparison with one extensive data base are presented in Figure 40. The configurations in this data base were tested at five Mach numbers from 2.5 to 4.5. Figure 40 presents the error in the prediction of C_N for each

64
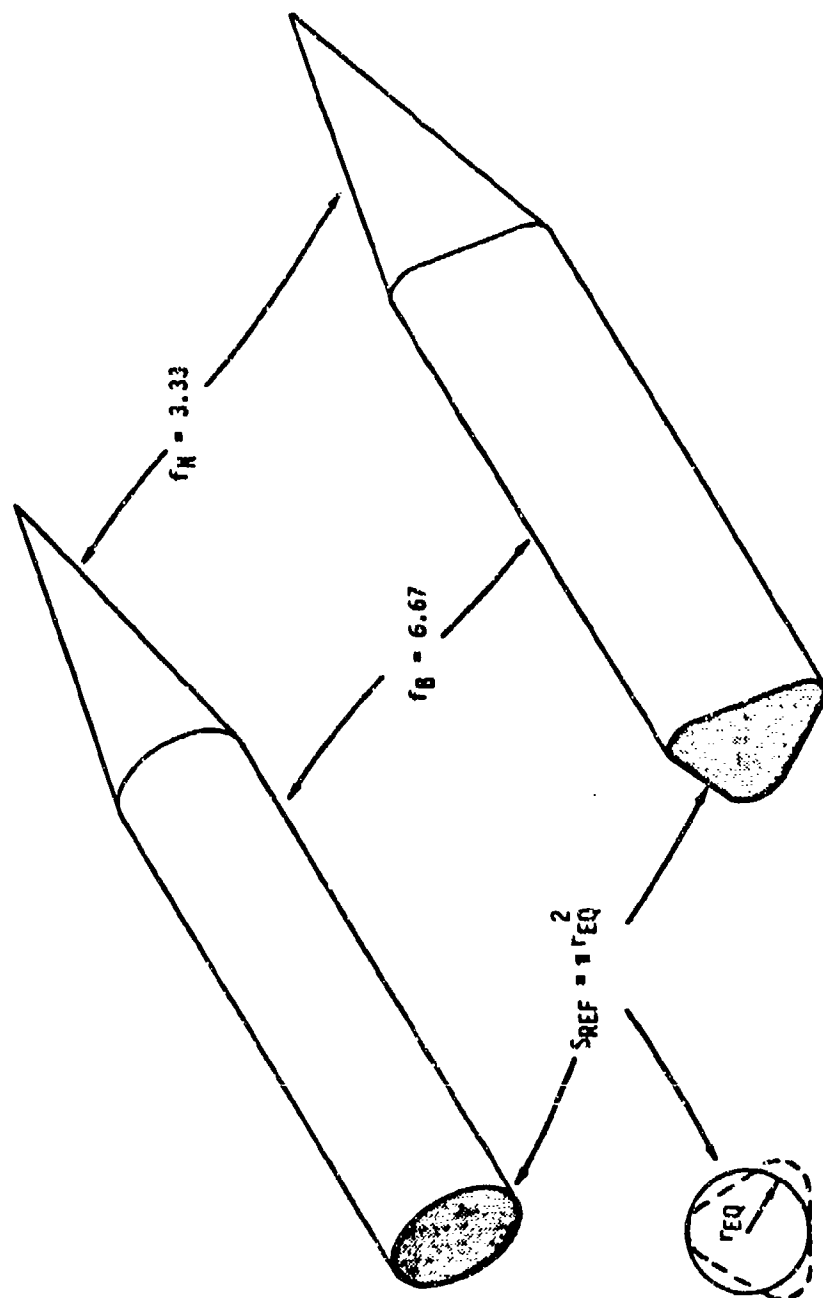
$$CN_{\alpha ARB.BODY} = A'_{ARB.NOSE} \cdot \frac{CN_{\alpha CONE/CYL.}}{A'_{CONE}}$$

FIGURE 39 EXTENSION OF SLENDER BODY THEORY FOR NOSE/CENTERBODY CONFIGURATIONS USING THE EQUIVALENT RADIUS

65
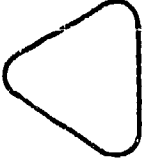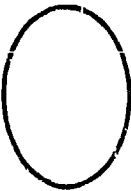
	EXP.	CALC	% ERROR
	3.95	3.73	- 5.6
	4.13	4.73	+14.5
	5.44	6.32	+16.2
	1.80	1.58	-12.2
	10.3	9.45	- 8.3
	10.3	9.45	- 8.3

FIGURE 40 COMPARISON OF C_N DATA FOR VARIOUS NOSE/CENTERBODY CONFIGURATIONS OF FINENESS RATIO=10

configuration tested at a Mach number of 2.5. The worst case is the 2.5 to 1 horizontal ellipse with an error of 16.2 percent. From this figure it can be seen that the accuracy is acceptable for preliminary design.

This method is considered conducive to preliminary design since it is both quick running and allows for the body cross sections to be changed easily. These features allow for the types of parametric studies commonly performed in the preliminary design environment.

3.2.2.3 Pitching Moment Coefficient

As with the normal force, only the linear component of the pitching moment is computed. There are no methods are included for computing either zero angle of attack pitching moment or the nonlinear component.

The method incorporated into the code for computing $C_{m\alpha}$ is based on the apparent area, A', calculation used to compute $C_{N\alpha}$. Using slender body theory the value of $C_{m\alpha}$ is found from the integral equation.

$$C_{m\alpha} = \int_{nose}^{base} \frac{2}{S_{Ref}L_{Ref}} \cdot X \cdot dA'$$

were $C_{M\alpha}$ is measured about the nose tip.

This equation is automated by breaking the nose up into nine longitudinal stations for which the apparent corss-sectional areas are computed. The $C_{m\alpha}$ contribution of each segment is computed using the equation:

$$C_{m\alpha_i} = \frac{2}{S_{Ref}L_{Ref}} (X_{cg} - X_i)(A_i' - A_{i-1}')$$

67

where: A'_i – apparent area of segments base cross section

A'_{i-1} – apparent area of segments front cross section

L_{Ref} – reference length (usually base diameter)

S_{Ref} – reference area (usually base area)

X_{CG} – longitudinal center of gravity position

X_i – centroid of ith segment

The contributions of each segment to the nose $C_{m\alpha}$ is then summed.

  The pitching moment curve slope value that is computed for the nose is corrected to include the effect of an afterbody by using a method analogous to the normal force curve slope correction. The method employed uses the computation of an equivalent axisymmetric body $C_{m\alpha}$ to provide the nose to afterbody ratio of $C_{m\alpha}$ effects. Data comparisons of nose alone results have shown sufficient accuracy for preliminary design analysis.

4.0 FIN ALONE METHOD SELECTIONS

The method summary for fin alone aerodynamics is shown in Figure 41. Unlike the method selected for body alone aerodynamics, most of the subsonic/transonic methods are theoretical or semiempirical. These types of methods maximize the panel shapes that can be addressed.

Table 2 summarizes the methods selected compared to those recommended in the Feasibility Study. Note that most of the methods implemented are those recommended during the Feasibility Study. The three methods changed were due to ease of use, extended capability, or additional accuracy through use of a theoretical method.

Figure 42 indicates those fin method application areas as a function of Mach regime and panel shape. Note that the area with the most questionable or limited application is that of non-straight tapered fins. Although airfoil section results are not generally available at supersonic speeds, this is not a major problem area since the methods at these speeds assumed that the fins are thin. Supersonic fins usually are thin to minimize drag.

The following paragraphs describe the method selections for straight tapered and nonstraight tapered fin panels.

4.1 FINS WITH STRAIGHT TAPER

There are far more methods for predicting the aerodynamics of straight tapered fins than there are for other panel shapes. This is particularly true at transonic and supersonic speeds. In fact, there are more theoretical methods for fins than for any other component of the configuration, and this is probably due to the amount of work performed to analyze airplanes, particularly commercial aircraft.

	SUBSONIC $M \leq 0.6$	TRANSONIC $0.6 < M \leq 1.4$	SUPERSONIC $M > 1.4$
AIRFOIL SECTION AERODYNAMICS	WEBER ANALYSIS (CONFORMAL MAPPING) ARC R & M 2918, ARC R&M 3026 (33,34)		(NOT REQUIRED)
C_{N_α}	DATCOM 4.1.3.2 (30)	R.A.S. DATA SHEETS (32)	DATCOM 4.1.3.2 (30)
C_{m_α}	DATCOM 4.1.4.2 (30)		
$C_{N_{\alpha\alpha}}$	DATCOM 4.1.3.3, 4.1.3.4 (30)		
$C_m(\alpha)$	ENGINEERING METHOD (NONLINEAR AT PLANFORM CENTROID) (35)		
SKIN FRICTION	BLASIUS + TRANSITION▲ + VAN DRIEST II (4,5,3)		
PRESSURE DRAG	"FLUID DYNAMIC DRAG" (HOERNER) (6)		(NOT APPLICABLE)
WAVE DRAG	(NOT APPLICABLE)	LINEAR FAIRING FROM M = 1.05 (29)	NWL TR-3018 (USED TO M = 1.05) (29)
LEADING EDGE BLUNTNESS DRAG	DATCOM 4.1.5.1▲ (30)		
TRAILING EDGE DRAG	NWL TR-2796▲ (36)		
$C_A(\alpha)$	DATCOM 4.1.5.2 (30)		(INVARIANT)

▲ EMPIRICAL METHOD
( ) REF. NUMBER

FIGURE 41   FIN ALONE METHOD SUMMARY

TABLE 2 FIN ALONE METHODS

	FEASIBILITY STUDY	SELECTED METHOD	REASON FOR CHANGE
C_{A_p}	Datcom (Hoerner)(Ref. 20, 6)	Datcom (Hoerner)	(No change)
C_{A_W}	Datcom (Ref. 30)	NSWC (Ref. 36)	Theoretical method; more accurate
$C_{A_{LE}}$	Datcom	Datcom/NSWC (Ref. 30, 24)	Expanded capability
$C_{A_{TE}}$	NSWC (Ref. 31)	NSWC	(No change)
$C_A(\alpha)$	Datcom	Datcom	(No change)
$C_{N_\alpha}, C_{m_\alpha}$ (subsonic)	Datcom	Datcom	(No change)
$C_{N_\alpha}, C_{m_\alpha}$ (transonic)	Datcom	R.A.S. Data Sheets (Ref. 32)	Ease of use
$C_{N_\alpha}, C_{m_\alpha}$	Datcom	Datcom	(No change)
$C_N(\alpha), C_m(\alpha)$	Datcom	Datcom	(No change)

71

Fin Alone

	SUBSONIC $M \leqslant 0.8$	TRANSONIC $0.8 \leqslant M \leqslant 1.4$	SUPERSONIC $M > 1.4$
PLANFORM			
TRAPEZOIDAL	\	\	\
DOUBLE DELTA/CRANKED	\	.	.
OTHER	?	X	X
TAPER RATIO			
$0 \leqslant \lambda \leqslant 1$	\	\	\
ASPECT RATIO			
$0.5 \leqslant A \leqslant 4$	\	\	\
AIRFOIL SECTION			
SUPERSONIC	\	\	\
NACA	\	\	X
OTHER	\	\	X
SPHERICALLY BLUNTED L.E.	√	√	√
NON-SHARP T.E.	\	\	\
ANGLE OF ATTACK			
$0 \leqslant a \leqslant 60$	√	√	√

√ APPLICATION SUITABLE
? APPLICATION QUESTIONABLE/LIMITED
X DOES NOT APPLY

FIGURE 42   COMPONENT BUILD-UP APPLICABILITY

The following paragraphs describe the methods selected for straight taper-ed fins, typical of those used on conventional missile configurations. Note that methods were selected which were applicable to panels with aspect ratios from 0.5 to 4. Although panel aspect ratios greater than 4 have been predict-ed with the selected methods yielding excellent results, they have not been verified for a wide variety of panels. Therefore, these methods can not be used with a high degree of confidence for high aspect ratio panels.

4.1.1 Axial Force Coefficient

As with bodies alone, the axial force of a fin is assumed to be comprised of a zero-lift component and a component due to angle of attack. However fins can be cambered, which can result in the zero-lift component of axial force not occuring at zero angle of attack. Therefore, the methods for fin alone aerodynamics are more complex, and often require a method change as a function of Mach number and angle of attack.

Figure 43 illustrates the variation in fin drag (or axial force) at zero-lift. The subsonic pressure drag method assumes that it is almost invariant to a Mach number of 1.05, and then linearily decreases to zero at Mach 1.2. Wave drag is assumed to begin at Mach 0.8, when local shocks first appear in the flow, increasing to a maximum near Mach 1.05, where the flow is all supersonic. Leading edge bluntness drag varies nearly monotonically across the Mach spectrum.

4.1.1.1 <u>Skin Friction</u> - The skin friction of fins can be calculated using the method described for body alone, except that a two-dimensional to three-dimen-sional correction factor to account for surface shape is not used. This is due to the fact that the skin friction methods are based upon flat plate data correlations and theory. Although experimental data for skin friction is dif-ficult to obtain, the accuracy of the method used has been implied from numer-ous correlations with axial force data across the Mach regime.
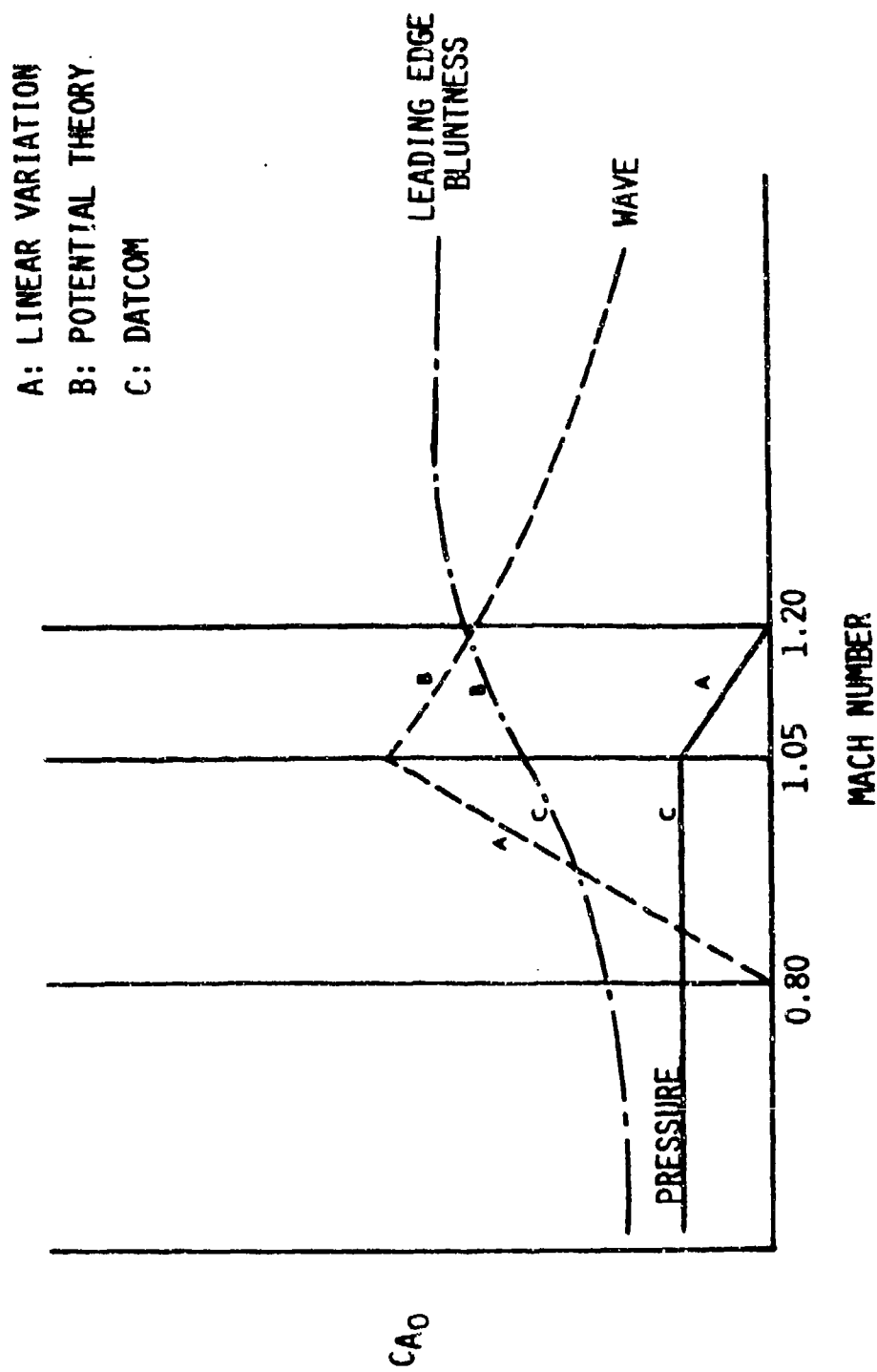
FIGURE 43 FIN DRAG METHODS

A: LINEAR VARIATION
B: POTENTIAL THEORY
C: DATCOM

LEADING EDGE BLUNTNESS

WAVE

PRESSURE

CA_0

MACH NUMBER

0.80   1.05 1.20

74

4.1.1.2 <u>Subsonic Pressure Drag</u> - The subsonic assumption implies that no shocks are present in the flow field region being analyzed. In the transonic flow, a particular fin panel can have both subsonic and supersonic flow occurring simultaneously over different portions of the panel. For bodies, it was assumed the subsonic pressure drag was a function of the body length to diameter ratio, and was correlated to the configuration skin friction coefficient. This scheme is used for fins as well, except that the correlation is not based upon overall length, but rather the thickness to chord ratio.

4.1.1.3 <u>Transonic Pressure/Wave Drag</u> - This nomenclature is used for that portion of fin drag which exists due to presence of shocklets in the flow field. This occurs near Mach 0.8 and increases until the fin flow is entirely supersonic (except perhaps blunted leading edges where shocklets may be present at lower Mach numbers). The method used is a potential flow method, (Reference 6), and is solved by calculating the potential flow about the fin at Mach 1.05, and then linearily reducing that value as a function of Mach number to zero at Mach 0.8. Although this approach is approximate, the results have been observed to give accuracies consistent with preliminary design.

4.1.1.4 <u>Supersonic Wave Drag</u> - The methods available for calculating fin supersonic wave drag have been developed for thin airfoil sections. Corrections are available to extrapolate the method to surfaces with small to moderate thickness to chord ratios. The extrapolation is developed primarily from experimental observations. The method selected was developed for the NSWC Aeroprediction code (Reference 29), where the surface of the fin is transformed into a computational grid, and a potential flow solution is applied. This method is very powerful, and permits the accurate calculation of the drag characteristics of straight-tapered surfaces, but has the disadvantage that no source or sink line placed on the airfoil surface can be swept forward; this condition is easily violated if the surface has a forward swept trailing edge. Hence, both this method, and that from the U. S. Air

Force DATCOM (Reference 30) which allows for swept forward trailing edges, are incorporated into the computer code. The potential flow method is more accurate than the DATCOM method.

4.1.1.5 **Leading Edge Bluntness Drag** - The supersonic source/sink method described in Section 4.1.1.4 has the capability to compute the effect of spherically blunted leading and trailing edges on fin panels. At subsonic and transonic speeds, however, there is no easy-to-apply accurate method available. Hence, the empirical correlation from the U.S. Air Force DATCOM, which is a function of leading edge projected area, Mach number, and leading edge sweepback was selected. There was insufficient data to completely evaluate the accuracy of the technique, but it is believed to be sufficiently accurate for missile preliminary design.

4.1.1.6 **Base Drag** - The method selected for fin base drag is based on two-dimensional base drag data. This method could not be totally validated since the base drag of fins is normally such a small contribution to total drag. However, the data used in deriving the method is believed to be accurate and since this component is small, it does not warrent a high degree of validation.

4.1.1.7 **Angle-of-Attack Effect** - As mentioned earlier, the drag of a fin at angle of attack has been extensively studied, both theoretically and empirically, for aircraft configurations. The method selected for Missile DATCOM is that of the U. S. Air Force DATCOM. The plot of drag versus lift is assumed to have a parabolic shape and to be dependent of fin panel lift, airfoil section shape, and aspect ratio efficiency (Oswald's efficiency). Results computed using this method have agreed quite well with experiment for a wide variety of missile configurations. However, the method seems to fail when the angle of attack approaches 30 degrees; the drag due to lift curve shape departs significantly from the parabolic shape. This method discrepancy becomes more noticeable for missiles, where the required angle-of-attack range is much higher than for airplanes. It is recommended that a new method be developed which addresses the higher angle-of-attack requirements of missiles.

4.1.2 Normal Force and Pitching Moment Coefficient

Figure 44 illustrates the method used to compute fin normal force as a function of angle of attack and Mach number. The normal force is, analagous to that for bodies alone. It is assumed to be comprised of a potential and a nonlinear contribution:

$$C_N = C_{NP} + C_{NN}$$

where,

$$C_{NP} = C_{N\alpha} \sin(\alpha)$$

and

$$C_{NN} = C_{N\alpha\alpha} \sin^2(\alpha)$$

The potential normal force is computed from the fin panel $C_{N\alpha}$, which is Mach dependent. The nonlinear effect is analagous to the viscous effect for bodies, except that it is assumed to be a stall or post stall effect. An alternate method considered uses a "true" viscous model where the effect of angle-of-attack is assumed to be is obtained at 90 degrees angle of attack, adjusting for cross flow Mach number. This idea was not implemented since it ignores the effect of stall.

A key input into the angle-of-attack analysis is the angle of attack for stall and shock detachment. As shown in Figure 44, the method used is dependent on Mach number, angle-of-attack, the airfoil's thickness to chord ratio, and lift.

4.1.2.1 **Airfoil Section Characteristics** – At subsonic and transonic speeds, the airfoil section characteristics are required in order to accurately model fin panel lift and drag. The method selected for incorporation into the computer code is the Airfoil Section Module from the Digital DATCOM computer code, which is used for the prediction of aircraft aerodynamics. It has been validated for a wide variety of airfoil shapes and is a relatively simple

77

SUBSONIC (M < 0.8)

C_N

STALL CONDITIONS FROM
EMPIRICAL CORRELATIONS

$C_{N_{\alpha\alpha}}$ FROM EMPIRICAL
CORRELATIONS

C_{N_α} FROM LOWRY-POLHAMUS

ANGLE OF ATTACK

TRANSONIC (0.8 < M < 1.4)

C_N

FAIRED BETWEEN STALL
AND SHOCK DETACHMENT CONDITIONS

$C_{N_{\alpha\alpha}}$ FAIRED BETWEEN
M = 0.8 AND M = 1.4 RESULTS

C_{N_α} FROM R.A.S. DATA SHEETS

ANGLE OF ATTACK

SUPERSONIC (M ≥ 1.4)

C_N

SHOCK DETACHMENT FROM
NACA 1135

$C_{N_{\alpha\alpha}}$ FROM EMPIRICAL
CORRELATIONS

C_{N_α} FROM SUPERSONIC WING THEORY

ANGLE OF ATTACK

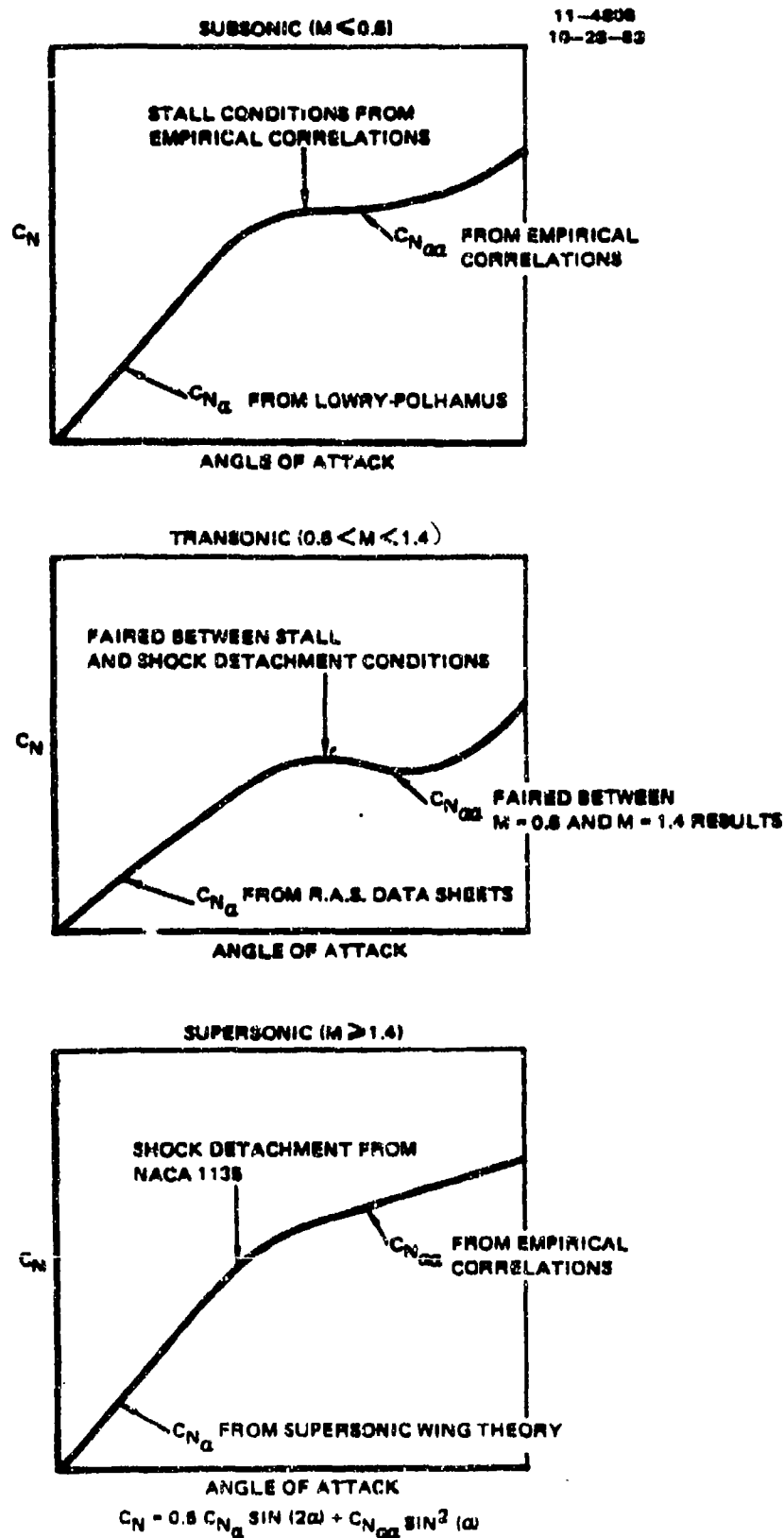$$C_N = 0.5\,C_{N_\alpha} \sin(2\alpha) + C_{N_{\alpha\alpha}} \sin^2(\alpha)$$

FIGURE 44   FIN ALONE NORMAL FORCE METHODS

78

technique to apply. However, it is not amenable to hand calculation, and the Handbook user must rely upon data from an airfoil section handbook to obtain the airfoil's aerodynamic characteristics. The airfoil section characteristics of the fins are not required at supersonic speeds, since those methods assume thin airfoils, and a limited correction for thickness to chord ratio is used.

4.1.2.2 <u>Potential Normal Force and Pitching Moment Coefficient</u> - Since the potential pitching moment coefficient is computed using the potential normal force coefficient, it is important that the potential normal force be as accurate as possible. In order to insure accuracy over the greatest range of planform shapes, results from theoretical methods were selected if possible at all Mach numbers. At subsonic speeds, the most reliable method is the Lowry-Polhamus correlation for straight tapered surfaces (Reference 31). It is a theoretical method which had been adjusted to correlate with experimental data. It has been validated over a wide range of panel aspect ratios, down to an aspect ratio of one half. Its accuracy is unknown for aspect ratios smaller than 0.5; no upper limit has been noted in the method validation.

At transonic speeds, the only theoretical results available are those from the R.A.S. data sheets (Reference 32). The curves from the R.A.S. compendium represent results for panels with aspect ratios that cannot be accurately evaluated in the transonic regime, but are "best" estimates based upon experimental data results. To use a true theoretical method at transonic speeds would be cost prohibitive, hence an interpolation of this data base is the best compromise of cost and accuracy. The predictions coincide with theoretical results at both subsonic and supersonic speeds for method compatibility.

At supersonic speeds, supersonic wing theory was selected. The results have been shown to be accurate for a wide range of thin wings which makes the method a powerful missile aerodynamic prediction tool.

4.1.2.3 **Nonlinear Normal Force and Pitching Moment Coefficient** - The non-linear variation in normal force is based upon the method of the U.S. Air Force DATCOM. The method is an empirical correlation for wing normal force coefficient with angle-of-attack for a wide variety of wing shapes. Although the form of the method is the same at all speeds, the phenomena modeled are quite different. At subsonic speeds, the wing stall angle of attack and wing maximum lift coefficient (at stall) are required; these are obtained using the U.S. Air Force DATCOM methods as well. The stall characteristics dominate the post stall behavior of the wing lift coefficient. Since this post stall behavior is based upon empirical data correlations for "typical" subsonic airfoils, the characteristic shape of the wing stall will not necessarily be that experienced for thin, missile airfoils. Since no other method is readily available, this method was selected. Beyond stall, the wing lift for missile wings closely follows results typical of aircraft.

At supersonic speeds, the concept of stall is not directly applicable. Instead, the wing lift will vary almost linearily until the angle-of-attack is great enough for the leading edge shock to become detached. The shock detachment angle of attack is a function of the Mach number and the semi-apex angle of the airfoil leading edge. Above shock detachment, the U.S. Air Force DAT-COM methods for wing lift variation is used. The shock detachment angle is determined using the DATCOM method.

At transonic speeds there is no suitable method for determining the angle of attack for which wing lift no longer remains linear. An approximate method was implemented. It assumes that the maximum lift angle of attack in shock-free flow (subsonic speeds) and the shock detachment angle of attack (at supersonic speeds) can be linearily interpolated as a function of Mach number at transonic speeds. Results obtained using this procedure have been found to have adequate accuracy for preliminary design.

Figure 45 presents the range of planform shapes and Mach numbers used in the validation of fin alone normal force methods. The aspect ratios investigated where from 0.5 to 4.0, the taper ratios from 0.0 to 1.0, and the Mach
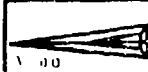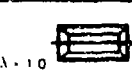
FIGURE 45 ASPECT RATIO/TAPER RATIO MATRIX OF MACH NUMBERS
FOR WHICH FIN ALONE C_N PREDICTIONS WERE EVALUATED

numbers from 0.80 to 4.60. Typical results are shown in Figure 46 for an as-
pect ratio 0.5 panel with a nonswept trailing edge. The four Mach numbers
shown include a subsonic/transonic, a low supersonic, and two supersonic con-
ditions. Up to 30° angle of attack, the prediction method follows the ex-
perimental data closely. Similar results were obtained for all of the fin
panels illustrated in Figure 45.

The potential pitching moment is computed using the linear center of pres-
sure, which was obtained using theoretical methods similar to those used for
normal force coefficient. The nonlinear center of pressure was assumed to be
at the panel area centroid at 90° angle of attack for all speeds. The
center of pressure was assumed to vary linearily as a function of angle-of-
attack from the linear center of pressure at zero angle of attack to the area
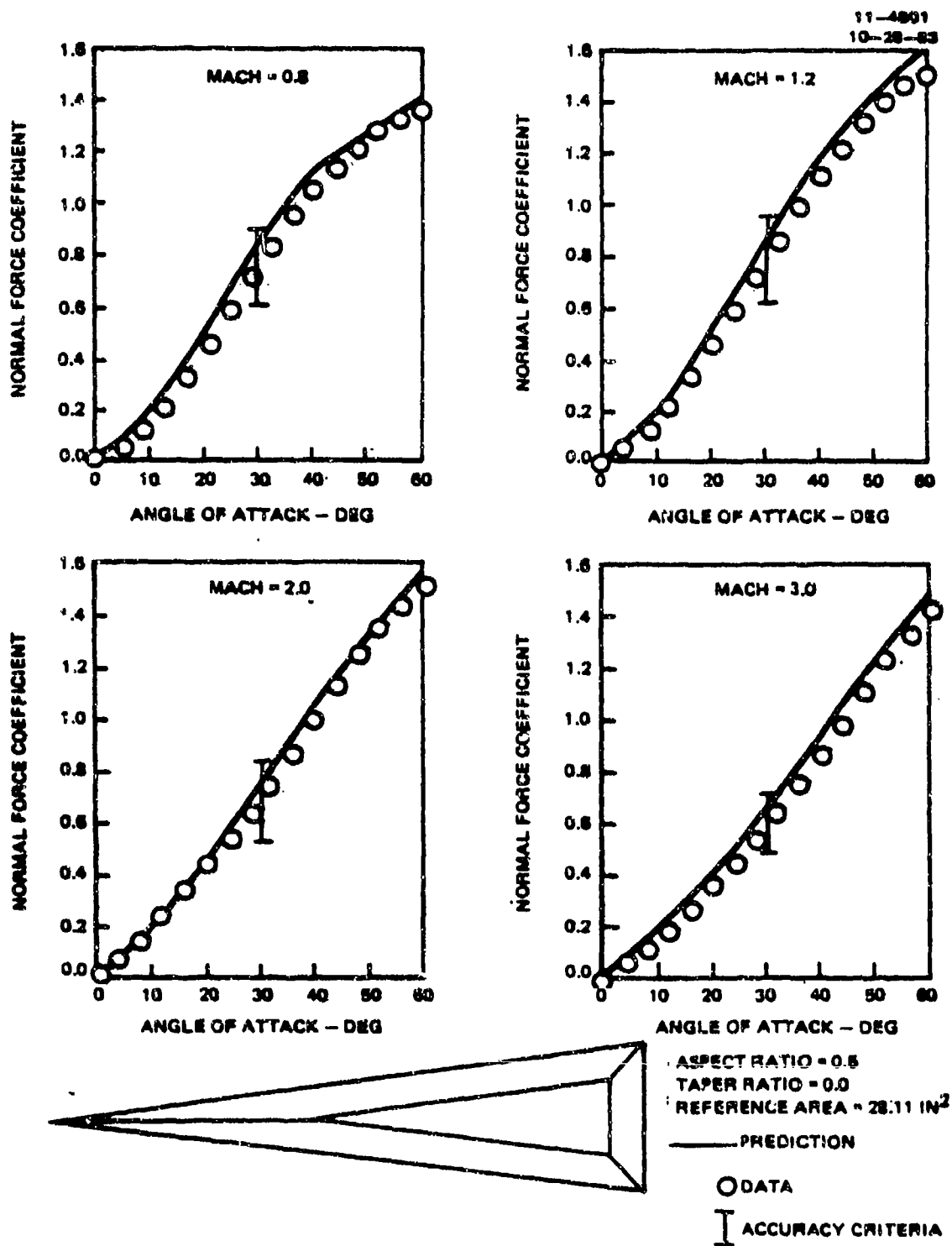
FIGURE 46 FIN ALONE C_N DATA COMPARISON FOR AN ASPECT RATIO 0.5 FIN

centroid at 90° angle of attack. This method is an engineering approximation since no theoretical method which can be easily applied is available.

4.1.3 Lateral-Directional Coefficients

Specific methods for computing the lateral-directional characteristics of fin panels alone were not selected for application in Missile DATCOM. The lateral-directional coefficients are computed for complete configurations using a concept called the "equivalent angle-of-attack" method which uses the panel normal force and center of pressure normal to the panel. This is adjusted to account for panel deflection and roll angle about the fuselage. This method yields the panel loads normal to the panels which are then resolved into body axis components. Therefore, in the calculation of configuration normal force and pitching moment, the loads for computing side force, yawing moment, and rolling moment are directly available. This method, does not require another method dedicated to the calculation of lateral-directional coefficients.

4.2 FINS WITH NON-STRAIGHT TAPER

The methods for non-straight tapered fins are essentially those for straight tapered fins. The exceptions are the calcuation of normal force coefficient and aerodynamic center.

For normal force and normal-force-curve slope, an effective straight tapered panel is computed. This effective panel has the same aspect ratio and taper ratio as the nonstraight panel but uses an effective h 'f-chord sweep angle. This angle is computed as:

$$\cos(\Lambda_c/2)_{eff} = \frac{1}{S} \sum_{i=1}^{n} \cos(\Lambda_c/2)_i \; S_{F_i}$$

83

where   N   is the number of panel segments

        S_F is the total panel area

        $(\Lambda c/2)_i$ is the half-chord sweep angle of each panel segment

        S_{Fi} is the area of each panel segment

Normal force and normal-force-curve slope coefficients are then computed using this effective straight-tapered panel.

To compute the panel aerodynamic center for nonstraight tapered fins, the fin is divided into two fin panels. The individual lift and aerodynamic center for each panel are then used to establish the aerodynamic center for the complete fins.

5.0 INLET METHODS

The inlet methods incorporated into Missile DATCOM are designed to provide the capability to analyze the external aerodynamics of general inlet geometries without the need for complex inputs. This capability had been developed in a pilot program written by Krieger, Williams and Hood (Reference 37).

The pilot program was restricted to the analysis of axisymmetric and 2-D inlets operating on vehicles flying at supersonic speeds. Only the external forces on the inlet are predicted and the assumption is made that the inlet is operating at its design mass flow. No spill drag or body inlet interference effects were included in the methods.

This pilot program was used as the basis for the Missile DATCOM methods. No methods were identified that provided accurate subsonic or transonic predictions. As a result, no capability to analyze inlets operating in subsonic or transonic flow was incorporated into Missile DATCOM.

The contributions of the inlets to the full configuration aerodynamics are treated as incremental additions. Up to four axisymmetric or 2-D inlets mounted on diverters can be positioned around the missile body at user-defined roll angles. The contribution of the body surface covered by the diverter is subtracted from the body coefficients in which it had been included. Both the skin friction and pressure forces are accounted for on the surfaces of the inlet. No other body-inlet interference effects are included.

5.1 METHODOLOGY USED

The inlet and diverter geometries are input separately in a coordinate system attached to the inlet. This process is shown as steps 1 and 2 of Figure 47. Figure 47 describes the process by which the inlet model is constructed and then its position is located relative to the body.

ACTUAL CONFIGURATION
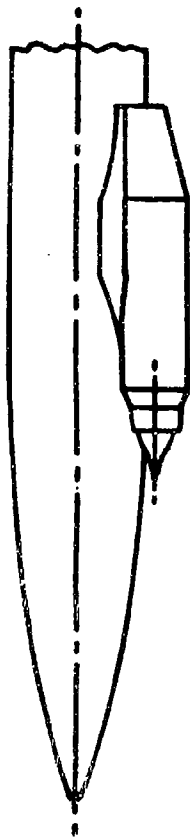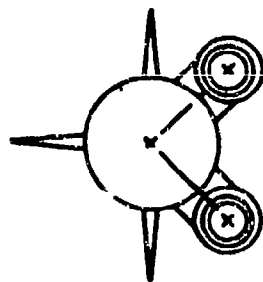
MISSILE DATCOM MODEL

1. SEPARATES MISSILE BODY, DIVERTER AND INLET
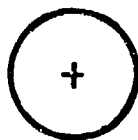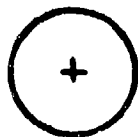
2. SETS UP COORDINATES WITH INPUTS

3. COMBINES INLET WITH BODY IN HORIZONTAL POSITION
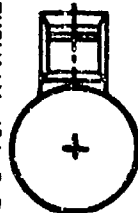
4. ROTATES TO PROPER ANGLE (PHI)
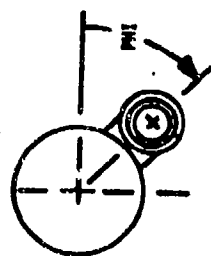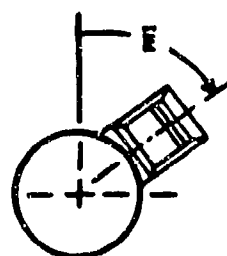
5. GENERATES A MIRROR IMAGE FOR TWIN INLET CONFIGURATIONS
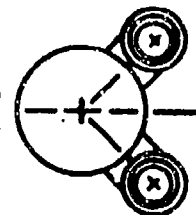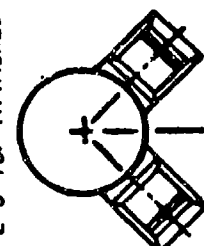
FIGURE 47   GEOMETRY CONSTRUCTION PROCEDURE

86

Once the inlet and diverter geometries have been described, a panel model of them is created. This model consists of S/HABP quadralaterals constructed by geometry package described in Reference 37. The corner points of the quadrilaterals are defined using the inlet diverter inputs. A description of these inputs and assumptions made by the code are included in Volume 1 of the Misile DATCOM User's Manual. The paneled geometries are shown in Figure 48. The axisymmetric inlets are paneled circumferentially while the 2-D inlets are constructed of longitudinal panels. Both are attached to a diverter which is attached to the missile body.

The coefficient contributions resulting from the surfaces of the diverter that attach to either the inlet or the missile body are subtracted out of the aerodynamic calculations when the inlet increments are computed. This is done to negate the contributions computed for the hidden surfaces of the inlet and body.

A single inlet is constructed in the horizontal position then transformed into the body axis system. This process includes the rotation of the inlet about the body centerline and the reflection of the inlet through the vertical plane if twin inlets have been prescribed. Special consideration is given to twin inlets that are input at a rotated position of 90 degrees. For this configuration, the two inlets are placed on the top and bottom of the body.

After the quadrilaterals are transformed, their outward normals are computed. The angle between the outward normals and the free stream velocity vector is determined. This is used to compute the impact angle of the free stream velocity on each panel. The pressure coefficient is then computed for each panel individually based on the impact angle. For windward impact angles the Dahlem-Buck equation is used, while for leeward panels the ACM empirical equation is used. These two equations are described in Reference 18 including a plot of their values with variation in impact angle. The pressure forces on the inlets are computed by multiplying the area, the pressure coefficient and the unit vector of each quadrilateral then adding the product to obtain the total aerodynamic coefficient. The panel moment arm about its reference center of gravity is included in the product for pitching moment coefficient.
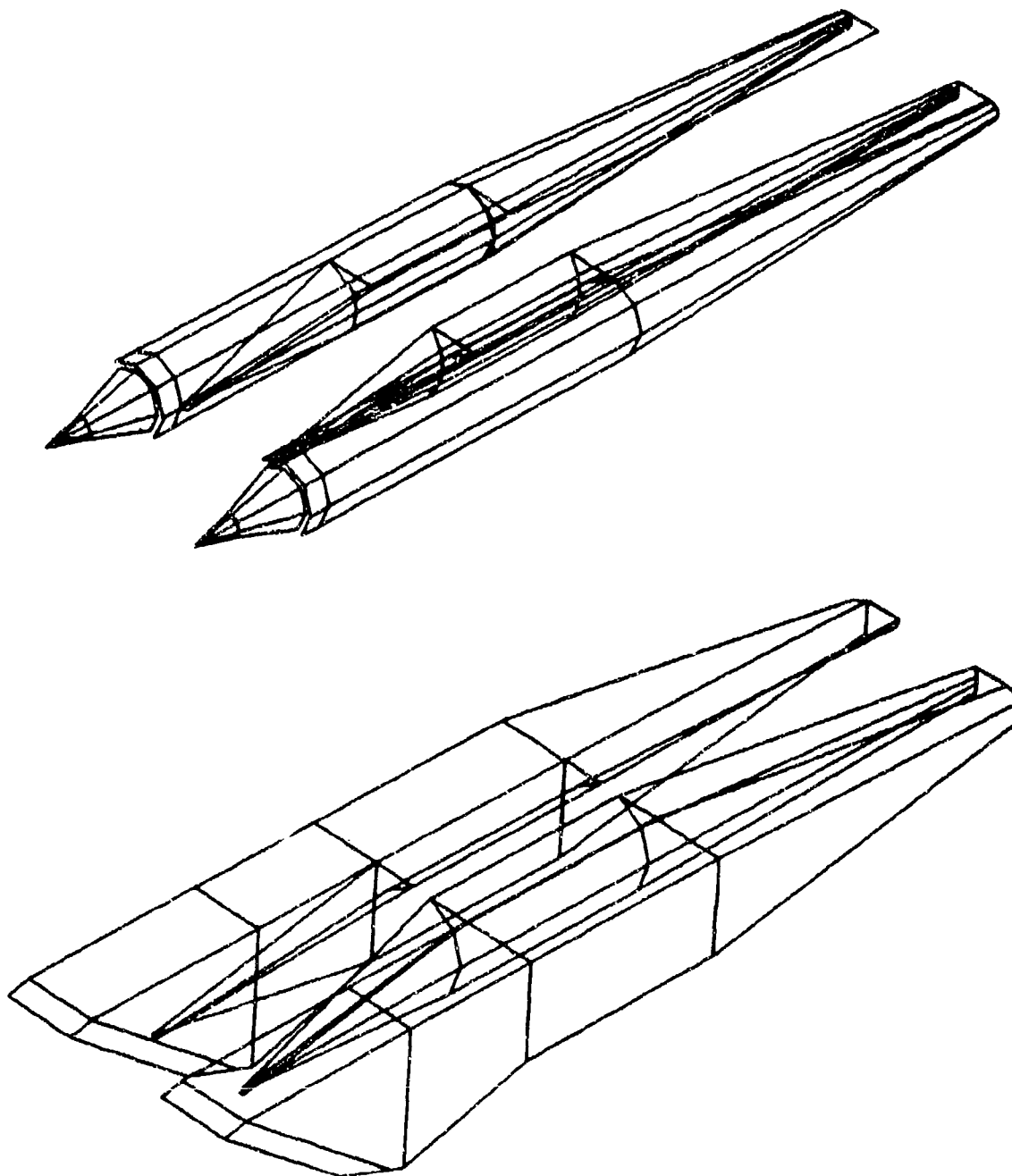
FIGURE 48   INLET CONFIGURATION MODELS SHOWING QUADRALATERAL MODELING

The skin friction component of the inlet forces is accounted for by computing the average skin friction coefficient for an equivalent flat plate having equal length and area of the inlet. The method of Van Driest II is used for the skin friction coefficient. The resulting shear force is then corrected for three dimensional effects. Skin friction effects are only included in the axial force coefficients.

5.2 RESULTS AND IMPROVEMENTS

The inlet method's prediction capabilities were checked against a data base which includes four axisymmetric inlet configurations and four two-dimensional inlet configurations. This data base is documented in References 38 and 39. Comparisons were made for all eight configurations at flight Mach numbers of 2.5 and 3.95. The inlets were designed to operate at a Mach number of 3.00. An oil flow analysis of the inlets, reported in Reference 40, concluded that the axisymmetric inlet was unstarted at Mach 2.5 which agrees with the design operation conditions.

The C_N comparisons showed good agreement at both Mach numbers and for all configurations. Figure 49 shows a representative data comparison. It presents the comparisons for the twin axisymmetric configuration at Mach 2.5. The C_{Ao} values were found to be acceptable for the higher Mach numbers and most lower Mach numbers, but the change in C_A with angle of attack was underpredicted for most cases. The pitching moment prediction accuracy was found to be very dependent on Mach number. The higher Mach number comparisons were good (Table 3). However, at the lower Mach number of 2.5 the predictions were very poor. Figure 49 shows a comparison with data that fails to match both the magnitude and trend of the data.

The results of these data comparisons indicate that the inlet methods are acceptable for supersonic Mach numbers but only marginally for low supersonic Mach numbers. The poor predictions at the low Mach numbers are explainable by the fact that the inlet methods do not include shocks, vortices or the effects of the body flow field. The poor pitching moment comparisons combined with the good normal force predictions indicated a local pressure distribution problem. A need for improved inlet methods is evident.
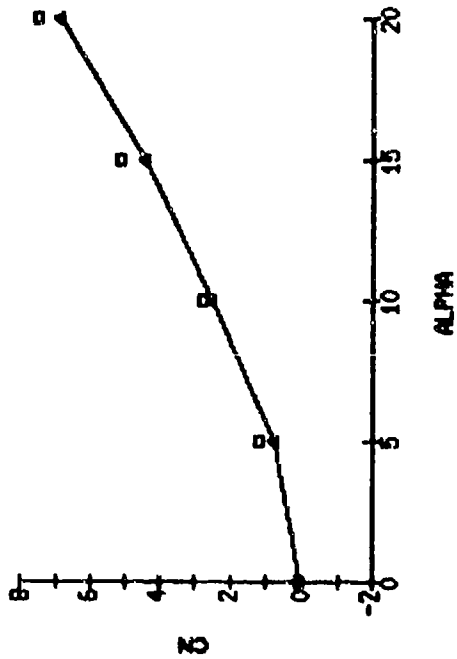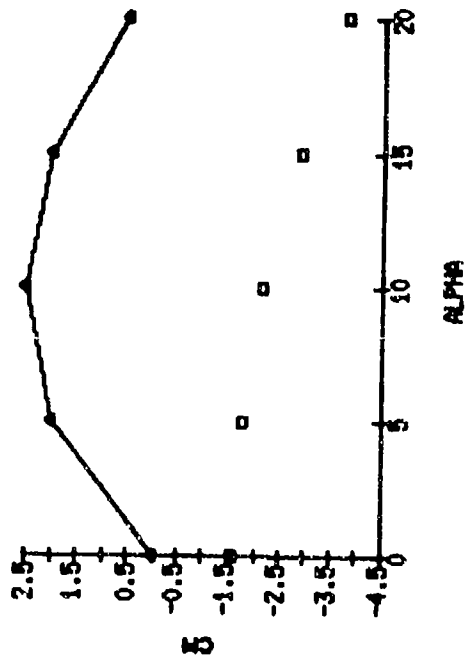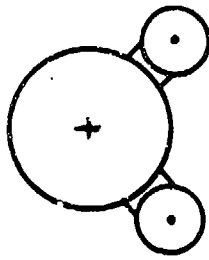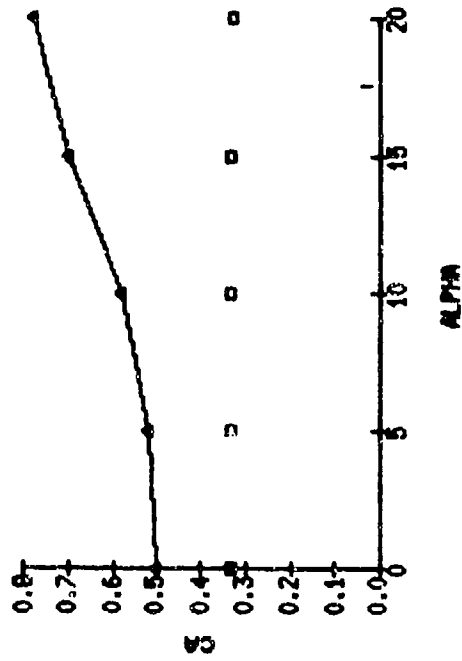
FIGURE 49 MISSILE DATCOM INLET PREDICTIONS COMPARED TO NASA TN 84558 DATA

MACH = 2.5

90

TABLE 3 COMPARISON OF STATIC COEFFICIENTS FOR BODY WITH
2-D INLET AT MACH = 3.95

| | CN | | CM | | CA | |
ALPHA	EXPERIMENTAL	MISSILE DATCOM	EXPERIMENTAL	MISSILE DATCOM	EXPERIMENTAL	MISSILE DATCOM
0	0.0	-0.088	-0.2	-1.544	.29	0.213
5	0.4	0.360	0.6	0.072	.31	0.208
10	1.4	1.378	1.4	1.327	.40	0.204
15	2.5	2.489	2.1	2.658	.51	0.205
20	3.8	3.780	3.5	3.830	.60	0.204

6.0 CONFIGURATION SYNTHESIS

The purpose of configuration synthesis is to take the body and fin alone aerodynamic characteristics and combine them to obtain the total configuration aerodynamic characteristics. There are many ways to synthesize a configuration. The most common approach is to take the panel alone normal force coefficient, multiply it by a carryover interference factor, obtained using slender body theory, and then add the result to the body alone normal force. This can be represented mathematically, for a fin-body configuration, as:

$$C_{NFB} = C_{NB} + [K_{F(B)} + K_{B(F)}]C_{NF}$$

The disadvantage of this method is that it assumes that the angle of attack range to be analyzed is within the linear lift range and that the panels are in the planar (or +) orientation. It has been customarily used at angles of attack where nonlinear lift effects occur. But with a significant overprediction of the total configuration characteristics. Hence, it is not completely suitable for missile applications where the angle of attack regime required is above 20°.

An alternative approach, and that selected for use in Missile DATCOM, is the "equivalent angle of attack method" developed by Nielsen, et al (Reference 43). This method assumes that the panel loading for a given panel angle-of-attack is unique. With this method the panel angle of attack is computed including the effect of panel roll orientation with respect to the free stream velocity vector, panel proximity to the fuselage or to other panels, and external vortex flow field effects. Then the isolated panel characteristics are interpolated at the panel equivalent angle of attack to yield the panel load when mounted on a body in combination with other surfaces.

This concept works extremely well. It inherently includes the nonlinear panel loading with angle-of-attack, from the isolated panel characteristics and makes the synthesis of the complete configuration aerodynamics an easy to

apply process. The difficult task is the computation of the panel equivalent angle-of-attack, but this is greatly simplified since most of the methodology is directly derived from the original method described above.

Figures 50 and 51 illustrate the relative importance of component interference on total configuration aerodynamics. These figures demonstrate that the body, lifting surfaces, and carryover interference effects (neglecting the influence of vortices) tend to overpredict configuration normal force by 15 percent. The effect of body and wing vortices on the tail surfaces are to reduce total normal force, since they decrease the tail surface local angle-of-attack.

Figure 52 summarizes the methods selected for configuration synthesis of missile configurations. Note that only the body vortex strength and tracking methods are empirically based; this is due to the complexity of this phenomenon and the ready availability of data correlations for a wide range of missile body shapes. Table 4 summarizes the method differences between those selected from the Feasibility Study and those eventually incorporated into the methods compendium, and Figure 53 illustrates the applicability of the component build up methods. The carryover interference method originally selected were those documented in NACA 1307 (Reference 44); they were replaced by the AIAA Journal methods (References 45-47) since they are (1) closed form solutions as a function of afterbody length (which was not included in the original reference) and (2) adjusted to account for panel trailing-edge sweep (which the original method did not address). The panel-panel interference correlation developed by Nielsen was retained for use, but is limited to planar or cruciform fin panels; it is not applicable to multi-paneled shapes or for fin sets where the fins are not 90° or 180° apart. The multi-fin method proposed by Darling (Reference 48) is not appropiate for the "equivalent angle of attack method" and was not incorporated. Instead Nielsen's method has been extended to fin sets with three or more fins by mapping the fins adjacent to the panel being analyzed into a four fin geometry.

94
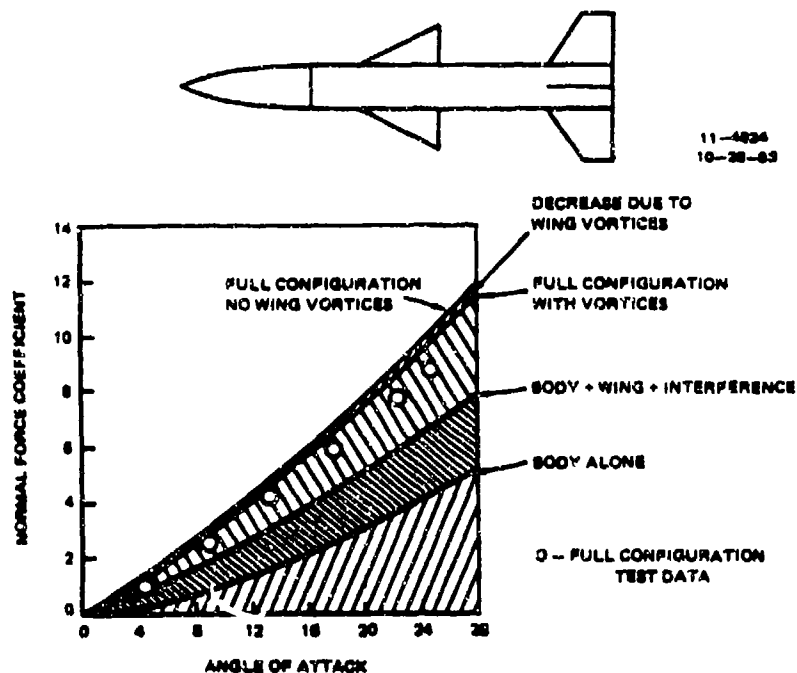
FIGURE 50 RELATIVE IMPORTANCE OF THE WING VORTEX CONTRIBUTION TO A
CRUCIFORM "+" MISSILE CONFIGURATION
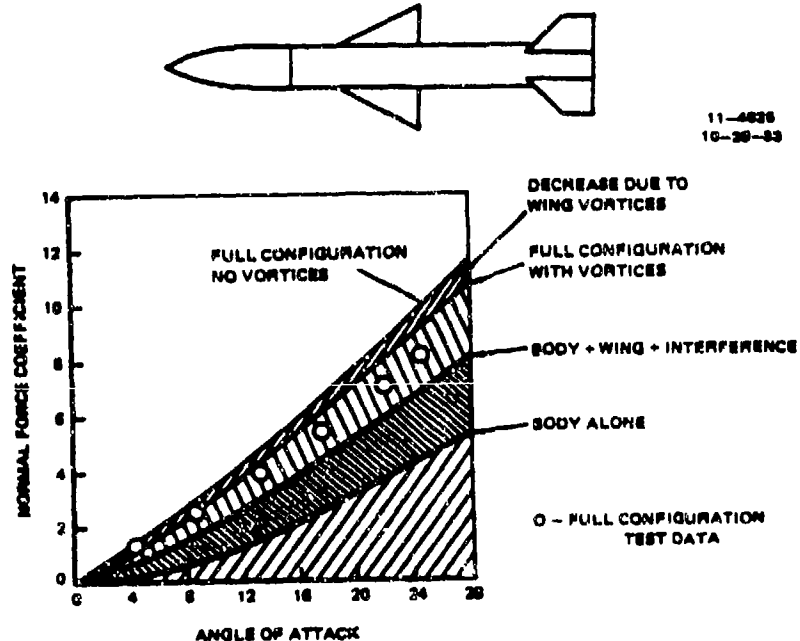
FIGURE 51 RELATIVE IMPORTANCE OF THE WING VORTEX CONTRIBUTION TO A
CRUCIFORM "X" MISSILE CONFIGURATION

	SUBSONIC	TRANSONIC	SUPERSONIC
	M < 0.8	0.8 ≤ M ≤ 1.2	M > 1.2
CARRY-OVER INTERFERENCE	NACA 1307 (44)	AIAA JOURNAL, JUN/AUG 1982 (45,46,47)	
BODY VORTICES STRENGTH/TRACKING	NWC TP-5761▲ (51)		
WING VORTICES STRENGTH/TRACKING	NACA 1307 (44)		
PANEL LOADS	AIAA PAPER 77 1153 (43)		

▲ EMPIRICAL METHOD

( ) REF. NUMBER

FIGURE 52   CONFIGURATION SYNTHESIS METHODS

TABLE 4 SYNTHESIS METHODS

	FEASIBILITY STUDY	SELECTED METHOD	REASON FOR CHANGE
K,k	NACA 1307	NACA 1307/AIAA J. (Ref. 44-47)	Enhanced method
Panel/Panel	Nielsen (Ref. 52)	Nielsen	(No change)
Multi-fin	Darling (Ref. 48)	(None)	Not appropriate for α_{eq}
Fin gaps	(None)	(None)	(No change)
Body shape	Krieger (Ref. 35)	(New method)(Ref. 53)	Method developed for better accuracy Too limited in scope
Body vortices	Nielsen (Ref. 52)	Nielsen	(No change)
Fin vortices	NACA-1307	NACA-1307/modified	Add "viscous core" model
Synthesis approach	α_{eq}/Nielsen (Ref. 43)	α_{eq}/New (Ref. 51)	Better accuracy by not using empirical data for fin loads

97

	SUBSONIC $M \leqslant 0.8$	TRANSONIC $0.8 < M \leqslant 1.4$	SUPERSONIC $M \geqslant 1.4$
PANEL COMBINATION			
PLANAR	＼	＼′	＼′
CRUCIFORM	＼	＼′	＼′
OTHER	?	?	?
WING-TAIL ORIENTATION			
IN-LINE	＼	＼′	＼′
INTERDIGITATED	＼	＼′	＼
OFFSET	?	?	?
OTHER	?	?	?

＼ APPLICATION SUITABLE
? APPLICATION QUESTIONABLE, LIMITED

FIGURE 53 COMPONENT BUILD-UP APPLICABILITY

No methods were selected for the effect of fin gaps since those influences have been demonstrated to be small. Some available experimental data indi-cates that the resulting error is less than 10 percent of the configuration normal force coefficient. There are currently no methods that enable the cu-lation of this effect for a wide range of fin panels; the limited empirical data correlations cannot be extended to handle a wide variety of fin-body com-binations that one would experience in the missile design environment. There-fore, no method is included to predict the effect of fin panel "unporting" although a methods development task should be undertaken to correct this de-ficiency.

The accuracy of the methods implemented were demonstrated by comparison to the configurations shown in Figure 54. As shown in Figures 55 and 56, the predictive accuracy of the methods is excellent. Note that predictive accu-racy was determined by comparing the prediction to test data and then applying the accuracy criteria defined in Figure 5.

98
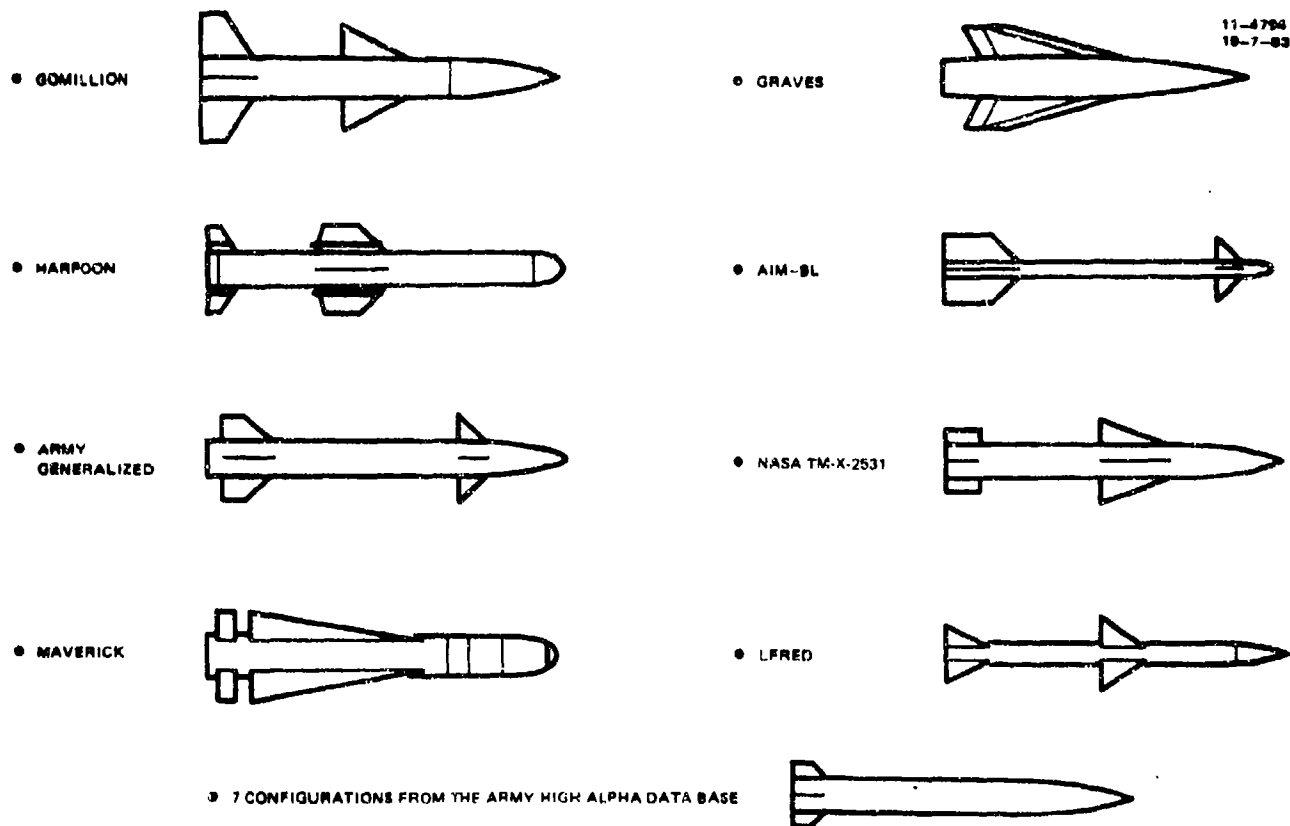
FIGURE 54   AXISYMMETRIC BODY CONFIGURATIONS INVESTIGATED

6.1   EQUIVALENT ANGLE OF ATTACK

The advantage of the equivalent angle-of-attack method is that the aero-dynamics for isolated fin panels, including any nonlinearities, are used in the prediction of total configuration aerodynamics. The isolated fin panel data is interpolated using the fin local, or equivalent angle-of-attack. This angle-of-attack includes the effect of fin deflection, presence of a body, presence of adjacent fin panels, fin roll angle position about the body, and any external vortices. The accuracy of this method is illustrated in Figure 57. The panel loads for a fin are plotted versus roll angle (measured from top vertical enter) at two angles of attack. These plots show excellent pre-dictions even in the transonic regime using the equivalent angle of attack method.

CONFIGURATION	NUMBER COMPARISONS	WITHIN ACCURACY
FIN ALONE	78	91%
HARPOON	14	71%
ARMY GENERALIZED	6	83%
NASA TMX–2531	3	100%
AIM–9L	10	100%
LFRED	43	69%
MAVERICK	7	43%
HIGH-ALPHA B·T	84	95%
GOMILLION	111	86%
TOTAL/AVERAGE	356	86%

FIGURE 55 LONGITUDINAL AERODYNAMICS PREDICTIVE ACCURACY
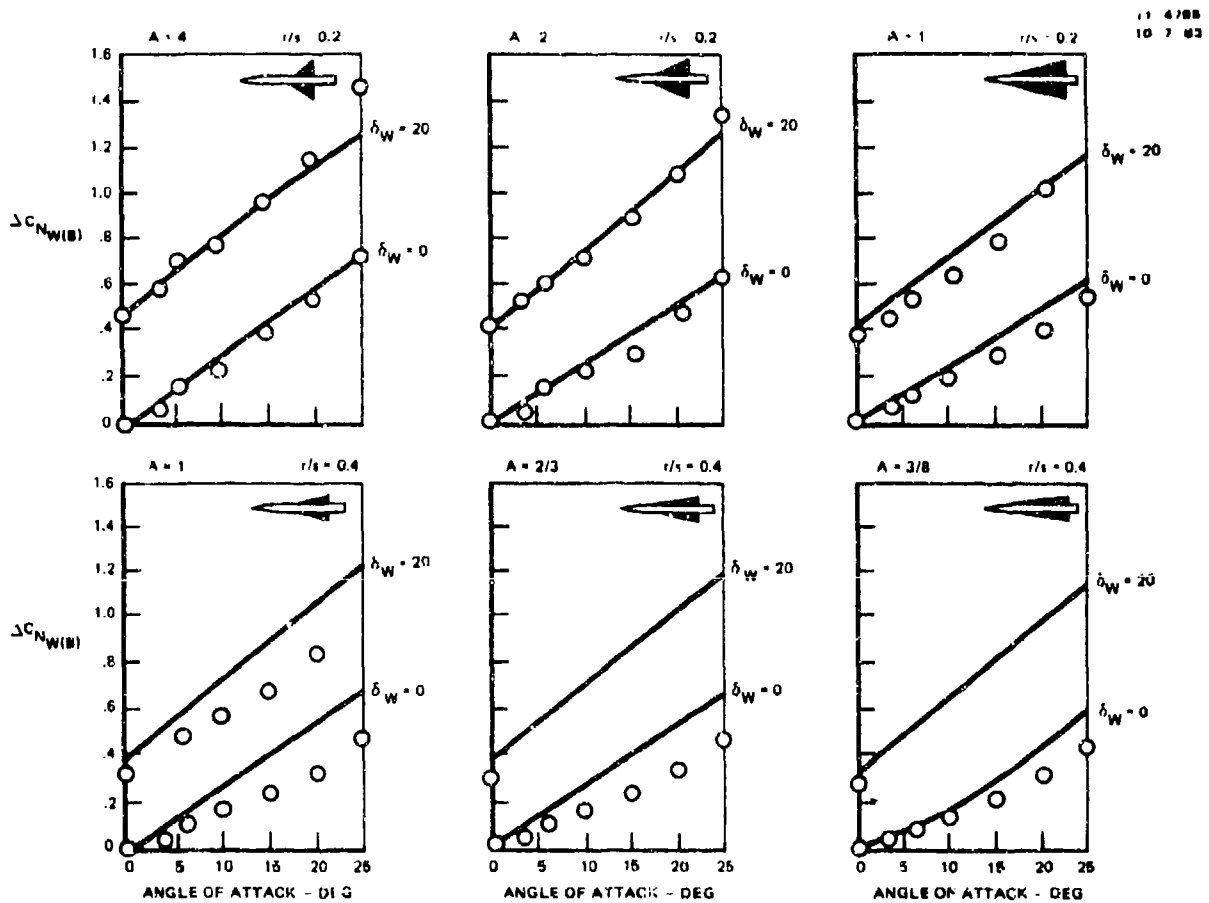
FIGURE 56 COMPARISON OF WING IN PRESENCE OF THE BODY
PREDICTIONS WITH EXPERIMENT AT MACH 3.36
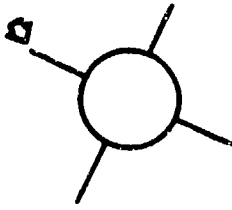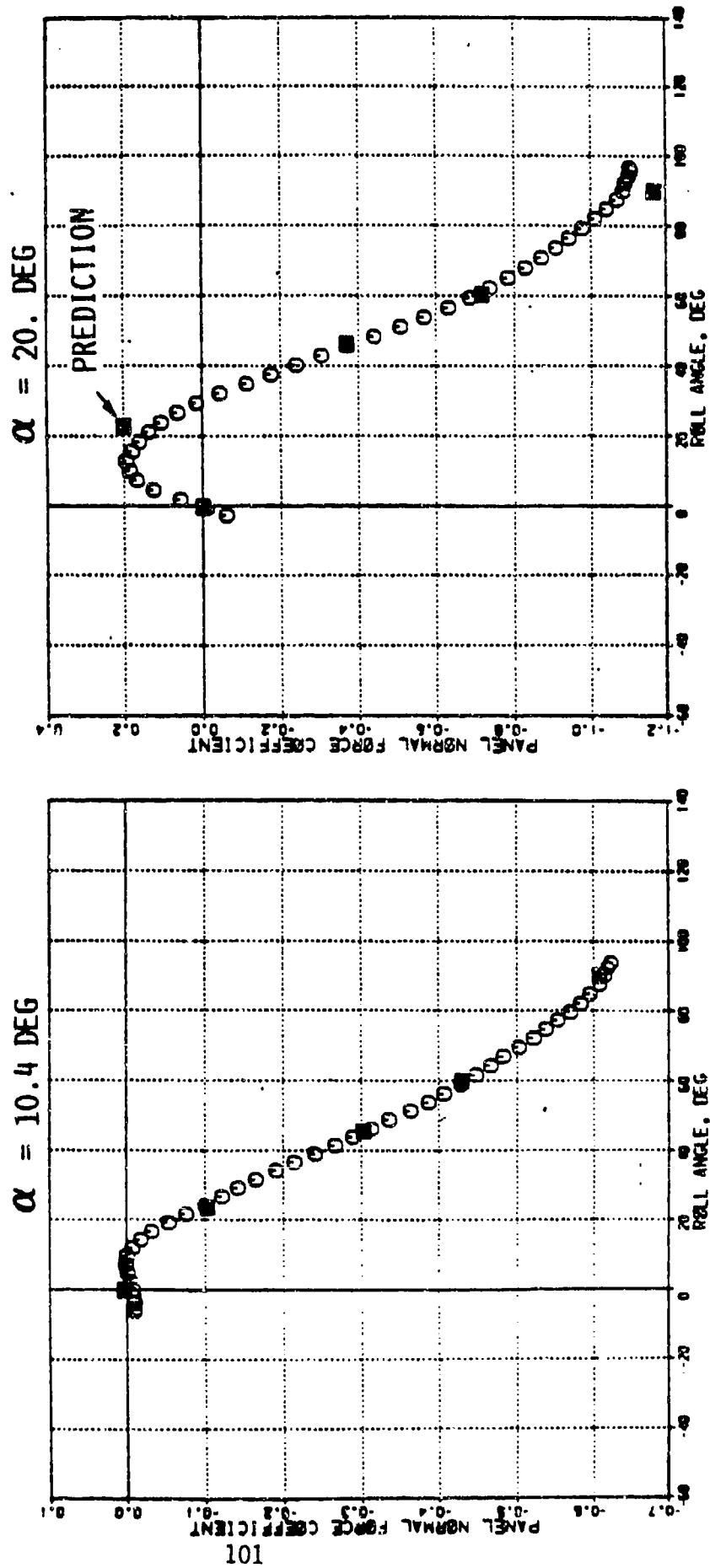
FIGURE 57 TRANSONIC PANEL LOAD PREDICTIONS GOOD

6.2 CARRYOVER INTERFERENCE

Carryover interference accounts for the change in panel angle of attack due to the presence of a body, since the body produces a flow field which varies across the fin span. The method selected for Missile DATCOM are those developed in NACA 1307 (Reference 44). They have been modified to reflect empirical corrections due to fin trailing-edge sweep, since the NACA 1307 methods are for nonswept trailing-edge panels. The carryover interference due to angle-of-attack method employed at supersonic speeds are those developed by Fan and Vira, Reference 46. They include the effect of fin afterbody length. The methods are a collection of closed-form equations which reproduce the NACA 1307 results for no afterbody and full afterbody.

The effect of panel incidence on carryover interference are exactly those developed in NACA 1307. No other method was found that enables the prediction of this effect other than empirical data correlations.

The effect of roll angle (combined pitch and yaw angle-of-attack) are computed using the method developed by Nielsen (Reference 43) from slender body theory. Unfortunately, the method addresses only planar or cruciform fin panels. Although one could interpolate between the planar and cruciform results to model equally spaced triform fin arrangements, other fin combinations are not addressed. A method should be developed to accommodate these types of general fin arrangements.

There is need for further method development of an angle-of-attack correction to body-wing carry-over for geometries where the body is dominant (Reference 50). This is illustrated in Figure 57 which shows normal force coefficient in presence of the body versus angle-of-attack for various aspect ratios and body radius to span ratios (Reference 50). This figure illustrates that the error increases with a decrease in aspect ratio, and decreases with a decrease in body radius to span ratio.

6.3 VORTEX TRACKING AND STRENGTH

Two vortex sources are included in the Missile Datcom analysis of the complete configuration aerodynamics. These are (1) vortices which are shed from the body nose, and (2) vortices that are shed from any forward lifting surfaces. Methods for vortices which originate from the afterbody have not been included. This was done to simplify the analysis since complex flow calculations are required to adequately model these vortices. The influence of these vortices on aft mounted fin panels are minor and can be ignored in preliminary missile design. It is hoped that an easy to apply technique will be developed to completely model the vortices remaining in the flow field.

6.3.1 Body Vortices

The body vortices are tracked using a method developed by Nielsen, et.al. (Reference 51). It relies upon an extensive empirical correlation, and has been observed to be adequate for preliminary design. The strength of the vortices are computed using the lift generated by the body.

6.3.2 Lifting Surface Vortices

The fin vortices are computed using the methods outlined in the U.S. Air Force DATCOM. The vortices are tracked assumming that they follow the path of the free stream velocity vector. This technique showed good predictions except when the vortex core generated by a forward fin impinged upon an aft fin. A new model was developed which established a vortex core radius of .255 of the fin span generating the vortex. The vortex is then tracked along the free stream unless it impinges on a trailing fin in which case it is offset by the core radius. Figure 58 shows the improvement of this method over the original method. The vortex strength is computed from the fin lift. Note that fin lift is dependent upon panel local angle of attack, which in turn is dependent upon any external vortices. Hence, in order to accurately compute

panel lift, and, vortex strength, the panel loads for each panel on the configuration must be calculated starting from the nose of the vehicle and working aft. Therefore, the effect of vortices originating ahead of a fin set is included in the calculation of that fin set's equivalent angle of attack.

GOMILLION B-W-T. 'X' CONFIGURATION
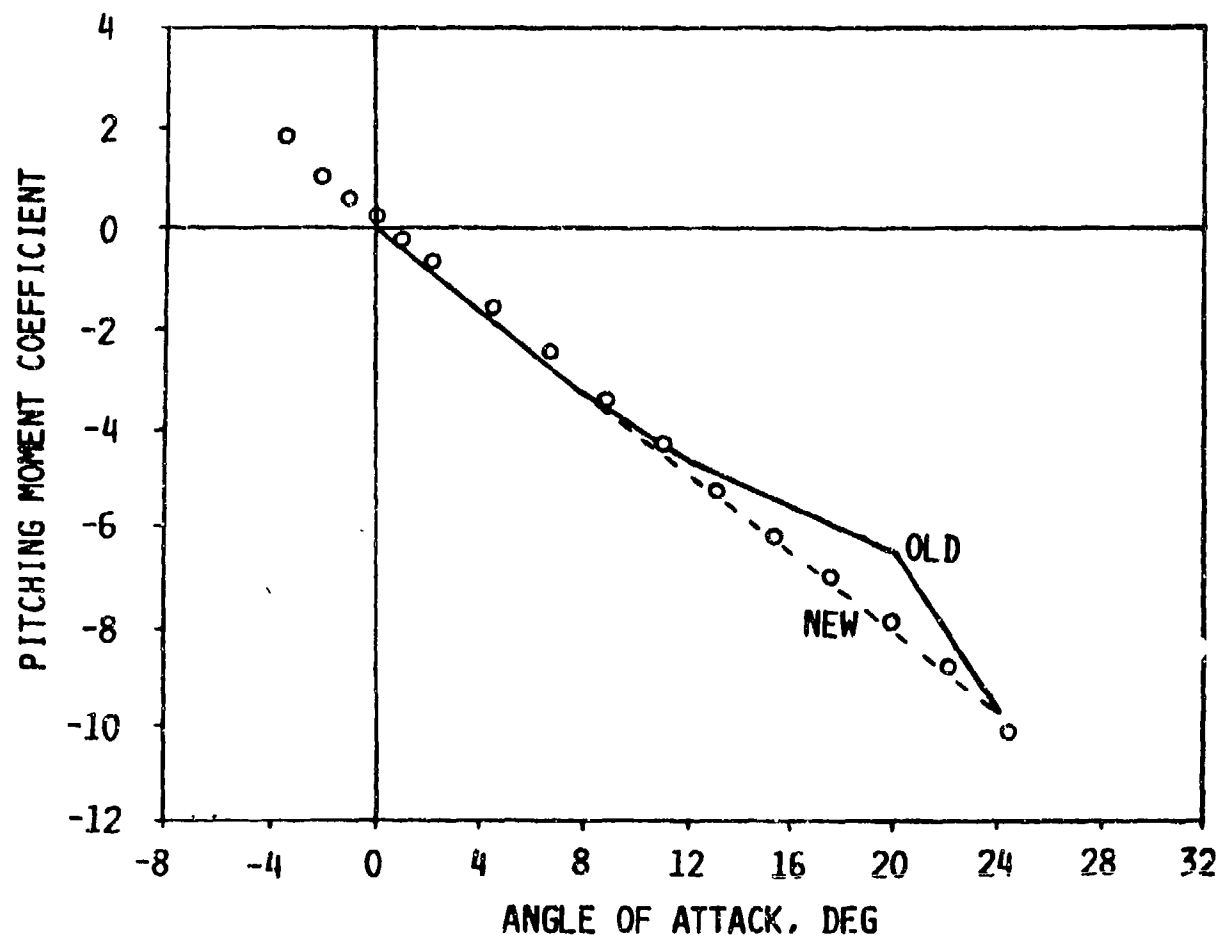
FIGURE 58   EFFECT OF NEW VORTEX CORE MODEL

7.0 DYNAMIC DERIVATIVE METHOD SELECTION

This section summarizes the methods selected for dynamic derivatives. It is divided into three parts: body alone methods, fin alone methods and configuration synthesis. Each section is further subdivided by coefficient.

The available methodologies are for conventional missile shapes at low angle of attack. The methods were not as numerous as those for the static coefficients, and no methods were found that specifically address the effect of body incidence. Longitudinal dynamic derivative methods for both body- and fin-alone, and Magnus coefficient methods for body alone were selected. Figure 59 summarizes the methods selected.

7.1 BODY ALONE

The available body-alone methodology suitable for preliminary design is derived from slender body theory, or correlations of large amounts of test data. The large effects of viscosity over slender bodies at anything but small angles of attack make slender body results applicable only in the linear angle-of-attack range. Although viscous effects such as boundary layer transition have been shown to have significant effects on dynamic stability, the mathematical complexity involved in these solutions renders them unsuitable for preliminary design.

7.1.1 Normal Force Due to Pitch Rate

The method selected is that of the United States Air Force Stability and Control DATCOM. The method used subsonically, transonically and supersonically were derived from slender body theory. Also there is a hypersonic method derived from simple Newtonian theory.

METHOD

DERIVATIVE	BODY			FIN			CONFIGURATION SYNTHESIS
	SUBSONIC	TRANSONIC	SUPERSONIC	SUBSONIC	TRANSONIC	SUPERSONIC	
C_{N_q}	DATCOM[1]	DATCOM	DATCOM	DATCOM	DATCOM	DATCOM	$C_{N_q} = (C_{N_q})_{BODY} +$ $[K_{B(W)}+K_{W(B)}](C_{N_q})_{FIN}$
C_{m_q}	DATCOM	DATCOM	DATCOM	DATCOM	DATCOM	DATCOM	
$C_{N_{\dot\alpha}}$	ERICSSON	ERICSSON	ERICSSON	DATCOM	DATCOM	DATCOM[3]	$C_{N_{\dot\alpha}} = (C_{N_{\dot\alpha}})_{BODY} +$ $[K_{B(W)}+K_{W(B)}](C_{N_{\dot\alpha}})_{FIN}$
$C_{m_{\dot\alpha}}$				DATCOM	DATCOM	DATCOM[3]	$C_{m_{\dot\alpha}} = (C_{m_{\dot\alpha}})_{BODY} +$ $[K_{B(W)}+K_{W(B)}](C_{m_{\dot\alpha}})_{FIN}$
$C_{m_q}+C_{m_{\dot\alpha}}$				$C_{m_q}+C_{m_{\dot\alpha}}$	$C_{m_q}+C_{m_{\dot\alpha}}$	$C_{m_q}+C_{m_{\dot\alpha}}$	
C_{Y_p}	SPINNER[2]	SPINNER	SPINNER				
$C_{n_p}/\sin\alpha$	SPINNER	SPINNER	SPINNER				
C_{l_p}	SPINNER	SPINNER	SPINNER				

1. USAF STABILITY AND CONTROL DATCOM, REFERENCE 30
2. ARDC SPINNER CODE, REFERENCE 56
3. USES TABLE LOOK UP FOR SUPERSONIC LEADING EDGES

FIGURE 59 SUMMARY OF DYNAMIC DERIVATIVE METHODOLOGY

7.1.2 Pitching Moment Due to Pitch Rate

As recommended in the Missile DATCOM Feasibility Report, the method of Ericsson was chosen (Reference 54). Ericsson extended the simple slender body theory and Newtonian theory to more properly account for Mach number. The method computes the total damping in pitch derivative $C_{m_q} + C_{m_{\dot{\alpha}}}$. These two are computed as their sum in both the handbook and the computer code. Figure 60 shows good comparisons for body alone pitch damping. For the handbook a less mathematically intensive method than that of Reference 55 was chosen to compute C_{m_q} supersonically. The method is that of DATCOM for supersonic body alone C_{m_q}. If C_{m_q} alone and not the total pitch damping derivative is desired the method of DATCOM may be used in all Mach regimes. For hypersonic Mach numbers, the method of DATCOM was selected which applies simple Newtonian theory to calculate C_{m_q} of cones with or without spherical nose caps and conic frustums.

7.1.3 Normal Force Due to Rate of Change of Angle of Attack

The method chosen is that of DATCOM which was derived using slender body theory. This method is applicable to all Mach regimes.

7.1.4 Pitching Moment Due to Rate of Change of Angle of Attack

As mentioned in Section 7.1.2, the method selected is that of Ericsson which gives the total damping in pitch derivative $C_{m_q} + C_{m_{\dot{\alpha}}}$. For the handbook, a different method was selected for Mach numbers gr iter than one, which is better suited for hand calculations. The method is that of DATCOM for body alone $C_{m_{\dot{\alpha}}}$. If $C_{m_{\dot{\alpha}}}$ alone is desired and not the total pitch damping derivative the method of DATCOM may be used in all Mach regimes.

7.1.5 Side force Due to Roll Rate

An empirical method was selected from Reference 56. The method is derived from wind tunnel and ballistic range test on spin stabilized projectiles.
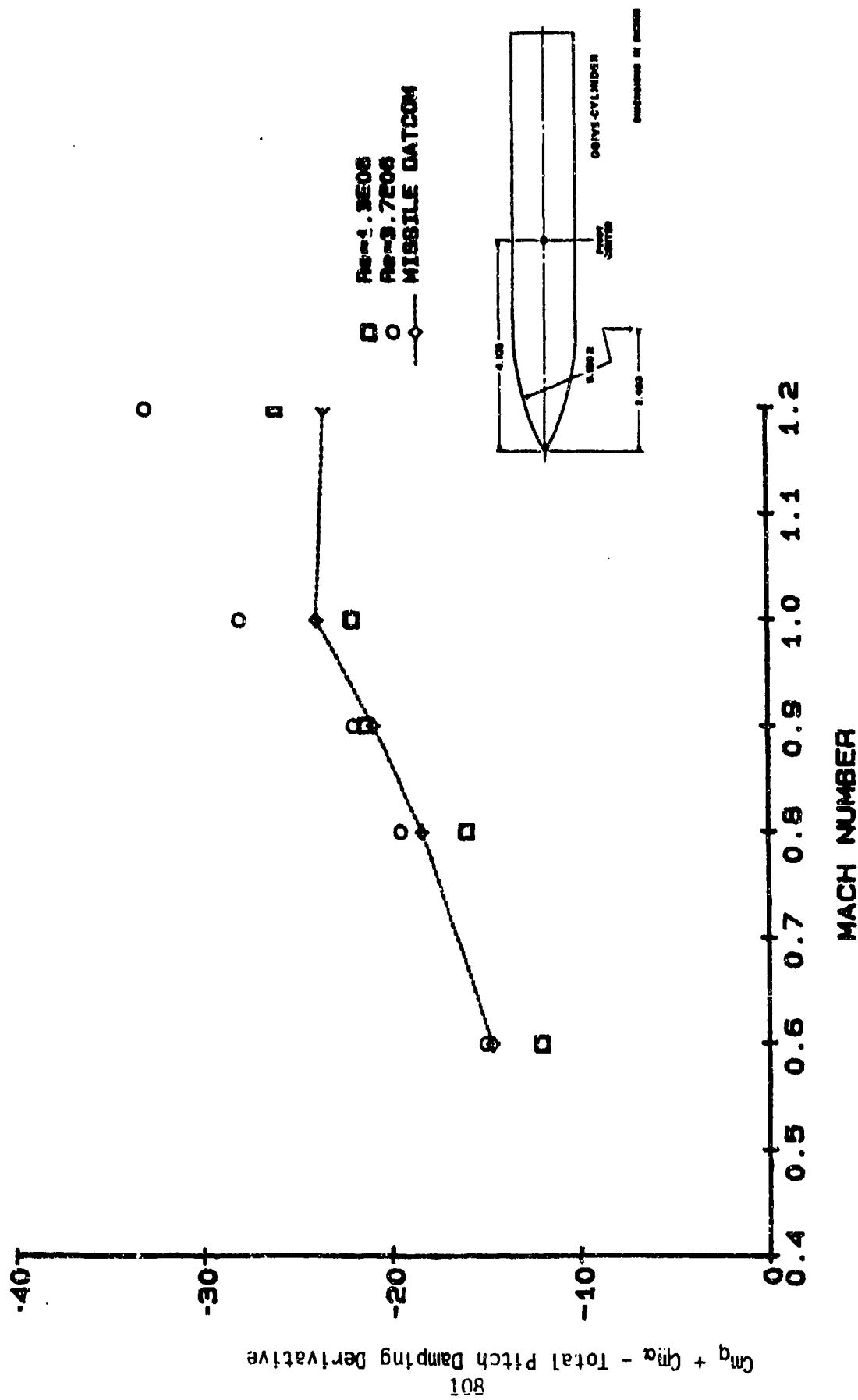
FIGURE 60 BODY ALONE PITCH DAMPING COMPARISON

MACH NUMBER

$Cm_q + Cm_\alpha$ - Total Pitch Damping Derivative

This method is good for bodies whose length is between 2.5 and 10 calibers, whose nose length is between 1.2 to 5.5 calibers and whose boattail length is between 0 to 1 caliber.

7.1.6 Yawing Moment Due to Roll Rate

The method selected, which gives $C_{np}/\sin\alpha$, is an empirical method based on wind tunnel and ballistic range test of spin stabilized projectiles (Reference 56). Caution should be taken using this method since $C_{np} \cdot \sin\alpha$ versus $\sin\alpha$ does not continue to behave in polynominal fashion at higher angles of attack (see Figure 61). This method should not be applied beyond the second positive maximum (counting the one at $\alpha=0$ as the first). Additional limitations on this method are listed in Section 7.1.5.

7.1.7 Rolling Moment Due to Roll Rate

The roll damping derivative method selected is that of Reference 57. The method is empirical and was derived from correlations of wind tunnel and ballistic range test. Limitations on this method are listed in Section 7.1.5.

FIGURE 61 LIMIT OF YAWING MOMENT DUE TO ROLL RATE METHOD

7.2 FIN ALONE

The only available methods suitable for use in Missile DATCOM to compute fin alone dynamic derivatives are the methods of the United States Air Force Stability and Control DATCOM. The methods are based on lifting surface theory for subsonic speeds and on linearized theory for supersonic speeds. The methods are thus limited to conditions for which the flow is attached over the surface of the fin, i.e., the linear lift range. Thes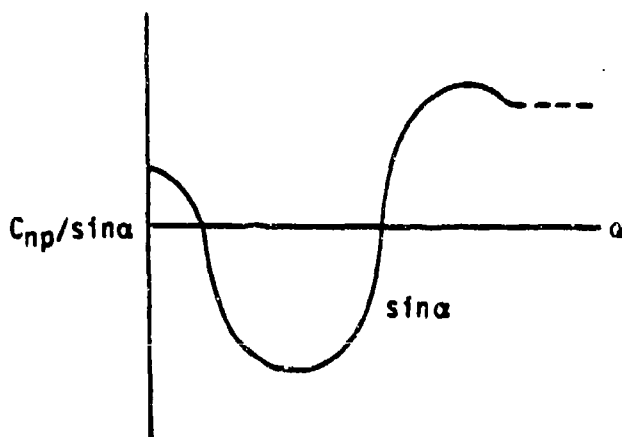e methods were developed for airplanes which generally have larger aspect ratio lifting surfaces. There are some limits on AR (where is the Mach similarity factor) for the supersonic methods. In the supersonic regime the methods were developed for beta times aspect ratio greater than four. For typical missile aspect ratios at low supersonic Mach numbers beta times aspect ratio is commonly less than four. For sample cases, however, the trends beyond this limit look reasonable. However the accuracy of this method for lower aspect ratios cannot be determined because only a small amount of experimental data is available, and that data is for subsonic Mach numbers.

7.2.1 Normal Force and Pitching Moment Due to Pitch Rate

The methods selected are from DATCOM. The method used depends upon Mach regime and planform geometry. In the transonic regime a linear fairing is used between the value of the coefficient at Mach equal to 0.8 and 1.2. Supersonically, when the leading edge is subsonic, there are methods for fins with taper ratio of 0 or taper ration between 0.25 and 1, there are no methods for taper ratio between 0 and 0.25. In the computer code a linear fairing is used between the value of the coefficient at a taper ratio of 0 and of 0.25. There are separate methods for subsonic and supersonic leading edges. During the method change over when the leading edge is sonic or slightly higher the methods do not match, and the supersonic leading edge method yields unrealistic results.

7.2.2 Normal Force and Pitching Moment Due to Rate of Change of Angle of Attack

The methods selected are from DATCOM. The subsonic method is applicable to fins with triangular planforms. Supersonically, when the fin has a subsonic leading edge, there are no methods for taper ratio between 0 and 0.25; methods are available for a taper ratio of 0 and taper ratios between 0.25 and 1. Supersonically when the fin has a supersonic leading edge, the computer code uses a table look-up on design charts to compute these coefficients.

7.3 CONFIGURATION SYNTHESIS

Configuration synthesis is done by determining the contribution of each component using the body alone and fin-alone methods previously discussed. The contribution of each fin to a fin set is determined by taking into account the fin's position on the body. The contribution of each fin is then summed to compute the contribution of a fin set. Body on fin and fin on body interference factors are computed using slender body theory. Then the coefficient for the total configuration is the body contribution plus the product of the interference factor and the fin set contribution.

Figures 62 and 63 show comparisons of two configurations. The Sidewinder comparisons (Figure 62) for the body-canard-tail in "+" configuration show errors between 19 and 27 percent. Both the body tail configurations (Finner and Sidewinder) over predict damping n pitch. The error for the sidewinder body-tail configuration ranges from 8.6 to 20 percent.
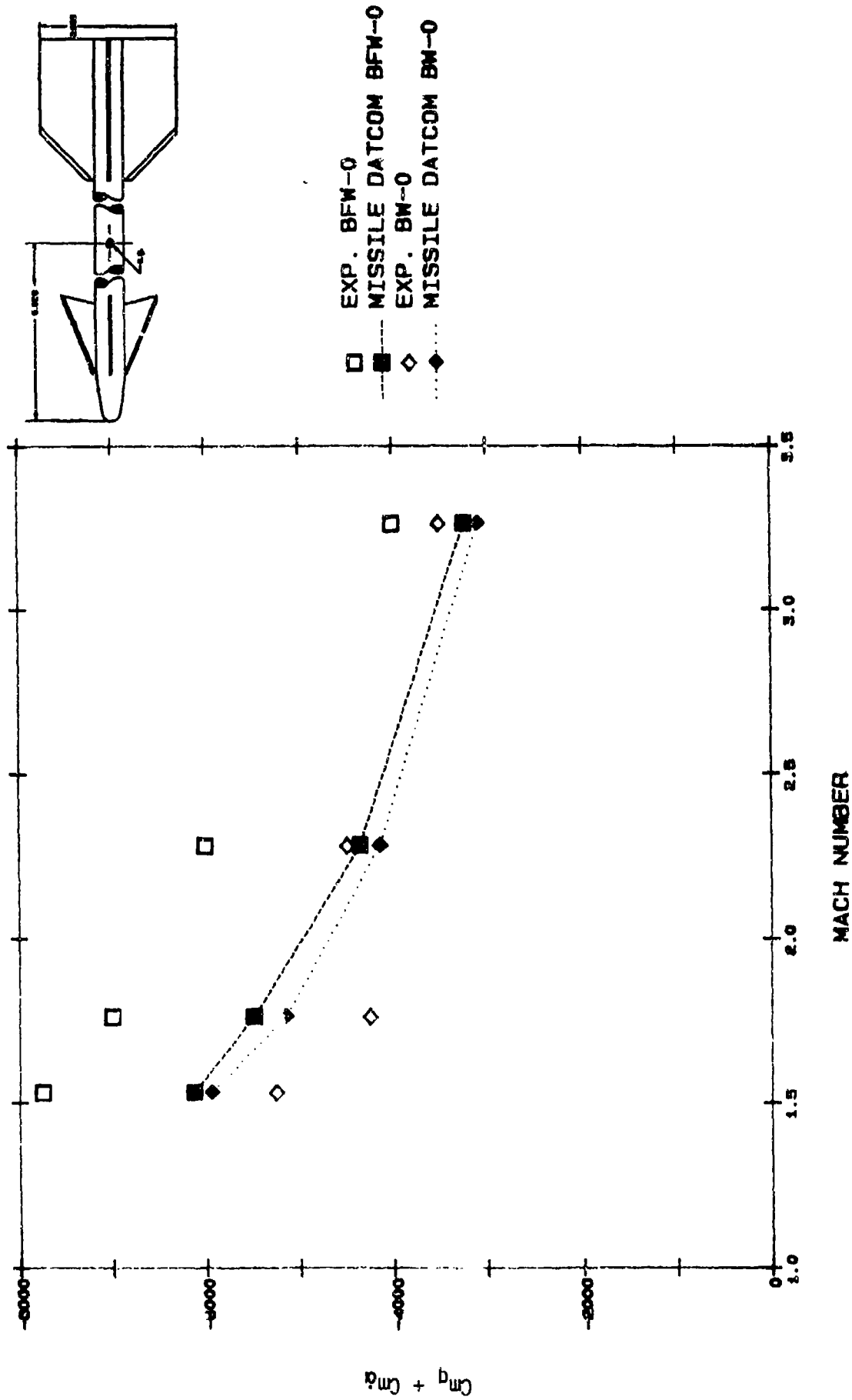
FIGURE 62 MISSILE DATCOM COMPARISONS OF PITCH DAMPING WITH SIDEWINDER MISSILE
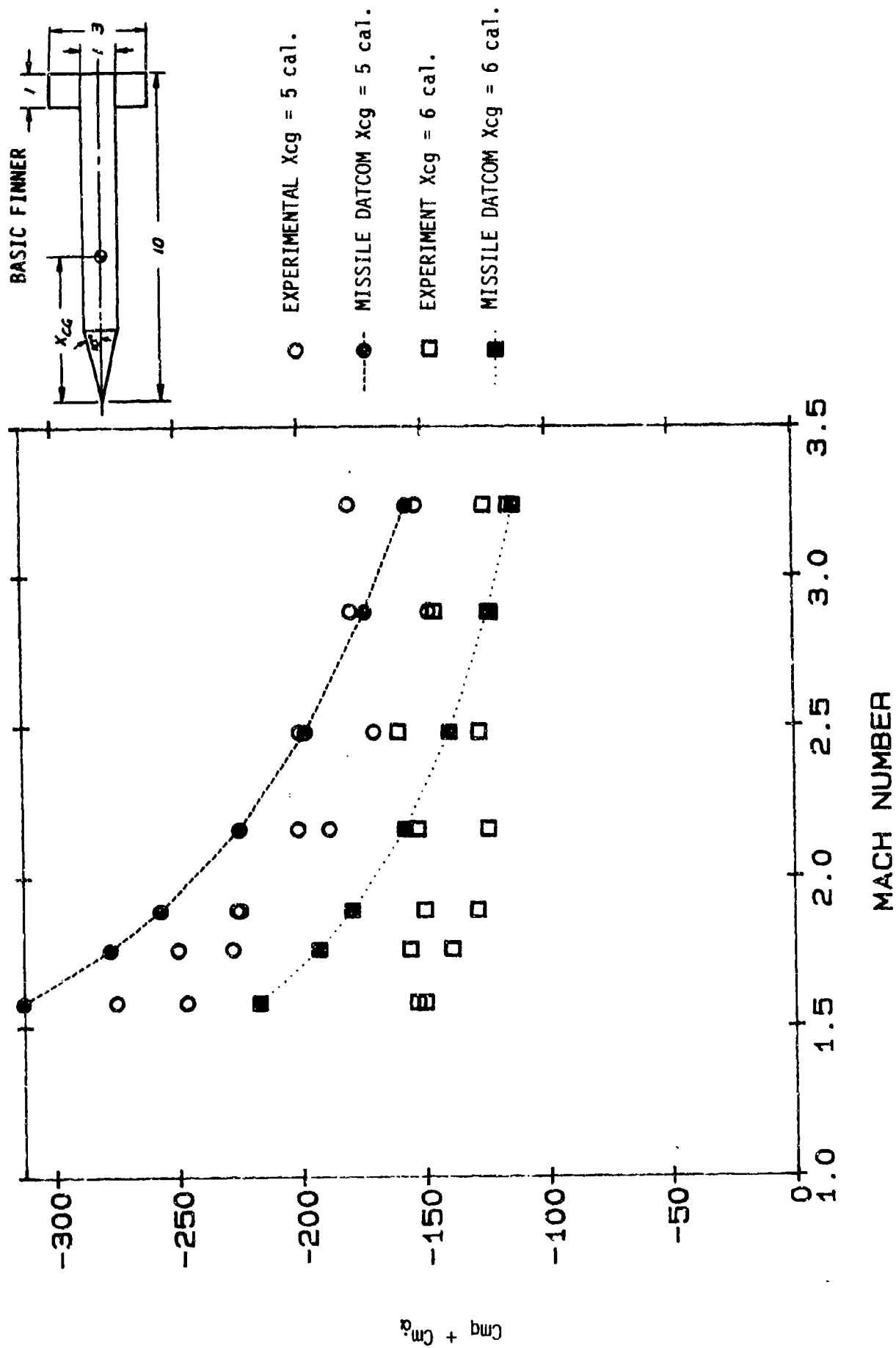BODY-CANARD-TAIL AND BODY-TAIL "+" CONFIGURATION

FIGURE 63 CONE-CYLINDER TAIL PITCH DAMPING COMPARISON

113

8.0 COMPUTER PROGRAM

The Missile DATCOM computer code was written in ANSI FORTRAN using structured programming techniques including in-code documentation. Input to the code is accomplished by namelist inputs and control cards that are read by a namelist emulator which is part of the code. The namelist, emulator was developed because not all machines have FORTRAN namelist and the code is not easily converted to fixed field inputs. Once read, the inputs are checked for valid variables and major errors. If an input error is found, a diagnostic message is written to the output file describing what the error is and where it is.

The computer code can be run either in "un-overlayed" or in "overlayed" mode. In "un-overlayed" mode, the required core memory is approximately 277,000 octal words on CDC machines. If the program is "overlayed" the core requirement on CDC machines is 76,000 octal words. On the virtual memory VAX machine the core requirement is 735,744 bytes. The code can be easily converted from FORTRAN IV to FORTRAN V. The user is referred to Volume 2 of the Program User's Guide for more details.

The computer code was developed in parallel with the handbooks. Most of the methods in the handbooks are incorporated into the computer code. In some instances a more accurate but mathematically more-intensive method was incorporated into the code.

The methods selected were coded into individual subroutines or in the case of complex methods into a group of subroutines called method modules. To replace a method, a new method is coded into a subroutine and inserted in place of the old subroutine. In the case of method modules the substitition is a little more complex but is still easily accomplished. Because the code was developed using top-down design, most of the control logic is in the upper level of the code and would not require a change.

The computer code also has two additional capabilities which allow for more detailed analysis of a configuration, experimental data substitution and configuration incrementing.

Experimental data substitution allows the user to input experimental data for any part of the configuration (body, fin set 1, etc.) or any partial configuration (body + 1 fin set, etc.). For example the user may input body alone experimental data and/or body + 1 fin set experimental data for a configuration having a body + 2 fin sets. The experimental data is substituted into the appropriate common block and replaces the computed theoretical coefficients. The substutited coefficients are then used in configuration synthesis.

Configuration incrementing allows the user to input experimental data for a configuration in the first case of a run and then vary some components of the configuration. In subsequent cases, correction factors are applied to the static aerodynamic coefficients. When incrementing all cases of a run must be for the same configuration (i.e., if the first case is a body + 1 fin set then the following case must also be a body + 1 fin set). In the first case, experimental data is substituted for the configuration being run. Comparisons are then made between the experimental and theoretical coefficients, and correction terms are calculated. In subsequent cases of that run, the correction factors are used to increment the theoretical coefficients of the configuration.

REFERENCES

1. Vukelich, S. R., "Development Feasibility of Missile Datcom,", AFWAL-TR-81-8130.

2. Krieger, R. J., and Williams, J. E., "Accuracy Criteria for Evaluating Supersonic Missile Aerodynamic Coefficient Predictions," AIAA Paper 81-1894, August 1981.

3. Van Driest, E. R., "Turbulent Boundary Layer in Compressible Fluids," J. Aero. Sci., Vol. 18, March 1951, pp 145-160.

4. Schlicting, H., "Boundary Layer Theory," McGraw-Hill Book Company, Inc.

5. Clutter, D. W., "Charts for Determining Skin Friction Coefficients on Smooth and Rough Flat Plates at Mach Numbers up to 5.0 With and Without Heat Transfer," DAC Report ES-29074, April 1959.

6. Hoerner, S. F., "Fluid Dynamic Drag," Published by Author, 1965.

7. Chaussee, D. S., "Improved Transonic Nose Drag Estimates for the NSWC Missile Aerodynamic Computer Program," NSWC/DL TR-3830, April 1978.

8. Devan, L., "Aerodynamics of Tactical Weapons to Mach Number 8 and Angle of Attack of 180°," NSWC TR-80-346, October 1980.

9. DeJarnette, F. R., Ford, C. P., and Young, D. E., "Calculations of Pressures on Bodies at Low Angles of Attack in Supersonic Flow," AIAA Journal, Vol. 17, No. 6, pp 526-536.

10. Van Dyke, M. D., "First and Second Order Theory of Supersonic Flow Post Bodies of Revolution," JAS, Vol. 18, No. 3, pp 161-169.

11. Payne, P. R., Hartley, R. M., and Taylor, R. M., "Afterbody Drag," DTNSRDC/ASED-80/10, May 1980.

12. Keller, J. D., and South, J. C., "RAXBOD: A FORTRAN Program for Inviscid Transonic Flow over Axisymmetric Bodies," NASA TMX-72331, 1976.

13. Army Material Command, "Engineering Design Handbook: Design of Aerodynamically Stabilized Free Rockets," AMC Pamphlet 706-280, July 1968.

14. Stoney, W. E., "Collection of Zero-Lift Drag Data on Bodies of Revolution from Free-Flight Investigations," NASA TR-R-100, 1961.

15. Jorgensen, L. H., "Prediction of Static Aerodynamic Characteristics for Space-Shuttle-Like and Other Bodies for Angles of Attack from 0° to 180°," NASA TN-D-6996, 1973.

16. Smith, A. M. O., and Pierce, J., "Exact Solution of the Neumann Problem. Calculation of Non-Circulatory Plane and Axially Symmetric Flows About or Within Arbitrary Boundaries," DAC Rpt. E526988, 1958.

17. Gentry, A. E., Smyth, D. N., and Oliver, W. R., "The Mark IV Supersonic-Hypersonic Arbitrary Body Programs," AFFDL TR-73-159, 1973.

18. Gregoire, J. E., and Krieger, R. J., "Aerodynamic Prediction Rationale for Advanced Arbitrarily Shaped Missile Concepts," AIAA Paper 80-0256, January 1980.

19. Kuchemann, D., Progress in Aeronautical Sciences, Vol. 8, Pergamon Press, 1967.

20. Messerschmitt-Boelkow-Blohm GmbH, "Data Sheets for the Determination of Normal Force, Moment, and Tangential Force Characteristics of Slender Nose-Cylinder Configuration in the Transonic Speed Regime," MBB Reports TN WE 2-97/69 and TN WE 12-88/70, 1970.

21. Mason, L., Devan, L., Moore, F. G., and McMillan, D., "Aerodynamic Design Manual for Tactical Weapons," NSWC TR-81-156, July 1981.

22. Goldstein, S., (Editor), "Modern Developments in Fluid Dynamics," The Clarendon Press, Oxford, 1938.

23. Baker, W. B., "Static Aerodynamic Characteristics of a Series of Generalized Slender Bodies With and Without Fins at Mach Numbers 0.6 to 3.0," AEDC-TR-75-124, 1976.

24. MDAC-West, "Aerodynamic Design Handbook," M8.080-CD, 1972.

25. Syverston, C. A., and Dennis, D. H., "A Second Order Shock Expansion Method Applicable to Bodies of Revolution Near Zero Lift," NACA Report 1328, 1957.

26. Payne, P. R., Hartley, R. M., and Taylor, R. M., "Afterbody Drag," DTNSRDC/ASED-80/10, 1980, ASED-80/12, 1980.

27. Allen, H. J., and Perkins, E. W., "A Study of Effects of Viscosity on Flow over Slender Inclined Bodies of Revolution," NACA Report 1048, 1951.

28. Klopfer, G. H., and Chausee, D. S., "Numerical Solution of Three-Dimensional Transonic Flows Around Axisymmetric Bodies at Angle of Attack," NEAR TR-176, 1979.

29. Moore, F. G., "Aerodynamics of Guided and Unguided Weapons," NWL TR-3018, January 1975.

30. Hoak, D. E., et al, "USAF Stability and Control Datcom," AFWAL TR-83-3098, October 1960, Revised 1978.

31. Lowry, J. G., and Polhamus, E., "A Method for Predicting Lift Increments Due to Flap Deflection at Low Angles of Attack in Incompressible Flow," NACA TR 3911, 1957.

32 Royal Aeronautical Society, "Data Sheets," 1966.

33. Weber, J., "The Calculation of the Pressure Distribution ove the Surface of Two-Dimensional and Swept Wings with Summetrical Aerofoil Sections," ARC R&M 2918, 1953.

34. Weber, J., "The Calculation of the Pressure Distribution on the Surface of Thick Cambered Wings and the Design of Wings with Given Pressure Distribution," ARC R&M 3026, 1955.

35. Krieger, R. J., et al, "Aerodynamic Standard Routine Handbook," MDC Report E2630, January 1977, Revised March 1978.

36. Moore, F. G., "Body Alone Aerodynamics of Guided and Unguided Projectiles at Subsonic, Transonic and Supersonic Mach Numbers," NWL TR-2796, 1972.

37. Krieger, R. J., Williams, J. E., and Hood, R. F., "A Component Buildup Aerodynamic Prediction Approach for Airbreathing Missiles," AIAA-83-0461, January 1983.

38. Hayes, C., "Aerodynamic Characteristics of a Series of Single-Inlet Air-breathing Missile Configurations," NASA TM-84557, 1983.

39. Hayes, C., "Aerodynamic Characteristics of a Series of Twin-Inlet Air-breathing Missile Configurations: I - Axisymmetric Inlets at Supersonic Speeds," NASA TM-84558, 1983.

40. Stoy, S. L., Dillon, J. L., and Roman, A. P., "Correlation and Analysis of Oil Flow Data for an Airbreathing Missile Model," AIAA 85-0452, January 1985.

41. Hayes, C., "Aerodynamic Characteristics of a Series of Twin-Inlet Air-breathing Missile Configurations: II -- Two Dimensional Inlets at Super-sonic Speeds," NASA TM-84559, 1983.

42. Hayes, C., "Aerodynamic Characteristics of a Series of Twin-Inlet Air-breathing Missile Configurations: III - Axisymmetric and Two-Dimen-sional Inlets at Subsonic-Transonic Speeds," NASA TM-84560, 1983.

43. Hemsch, M. J., Nielsen, J. N., Smith, C. A., and Perkins, S. C., "Com-ponent Aerodynamic Characteristics of Banked Cruciform Missiles with Arbitrary Control Deflections," AIAA Paper 77-1153, January 1977.

44. Pitts, W., Nielsen, J., and Kaattari, G., "Lift and Center of Pressure of Wing-Body-Tail Combinations at Subsonic, Transonic and Supersonic Speeds," NACA Report 1307, 1957.

45. Vukelich, S. R., and Williams, J. E., "Wing-Body Carryover at Supersonic Speeds with Finite Afterbodie,", AIAA Journal, M?y 1981, pp 661-664.

46. Vira, N. R., and Fan, D., "Closed-Form Solutions of Supersonic Wing-Body Interference," AIAA Journal, June 1982, pp 855-857.

47. Vira, N. R., and Fan. D., "Supersonic Wing-Body Center of Pressure with Finite Afterbodies," AIAA Journal, August 1982, pp 1144-1146.

48. Darling, J. A., "Handbook of Blunt-Body Aerodynamics, Volume I, Static Stability," NOL-TR-73-225, 1973.

49. Hemsch, M. J., Nielson, J. N., and Dillenius, M. F. E., "Method for Calculating Induced Rolling Moments for Cruciform Canard Missiles at Angles of Attack up to 20 Deg," NWC TP 5761, May 1975.

50. Stoy, S. L., and Vukelich, S. R., "Extension of Equivalent Angle of Attack Prediction Method," AIAA-84-0311, 1984.

51. Hemsch, M. J., Nielsen, J. N., and Dillenius, M. F. E., "Method for Calculating Induced Rolling Moments for Cruciform Canard-Missiles at Angles of Attack up to 20 Deg.," NWC TP 5761, May 1985.

52. Nielsen, J. N., Hemsch, M. J., and Smith, Ca. A., "Preliminary Method for Calculating the Aerodynamic Characteristics of Cruciform Missiles to High Angles of Attack Including Effects of Roll Angle and Control Deflections," NEAR TR-152, 1977.

53. Vukelich, S. R., "Aerodynamic Prediction of Elliptically Shaped Missile Configuration Using Component Build-Up Methodology," AIAA-85-0271.

54. Ericsson, L. E., "Effect of Mach Number on Slender Vehicle Dynamics," AIAA Paper 80-0362, 1980.

55. Ericsson, L. E., "Modification of Aerodynamic Prediction of the Longitudinal Dynamics of Tactical Weapons," LMSC-D646354, 1979.

56. Whyte, R. H., "Spin-73 an Updated Version of the Spinner Computer Program," Technical Report 4588, 1973.

57. Whyte, R. H., "A Revised Cl_p Algorthim for Spin-73," December 1979.